Osteology of *Dashanpusaurus dongi* (Sauropoda: Macronaria) and new evolutionary evidence from Middle Jurassic Chinese sauropods

Xin-Xin Ren, Shan Jiang, Xu-Ri Wang, Guang-Zhao Peng, Yong Ye, Logan King & Hai-Lu You

View supplementary material ⌖

Published online: 18 Nov 2022.

Submit your article to this journal ⌖

View related articles ⌖

View Crossmark data ⌖

Taylor & Francis
Taylor & Francis Group

Check for updates

Osteology of Dashanpusaurus dongi (Sauropoda: Macronaria) and new evolutionary evidence from Middle Jurassic Chinese sauropods

Xin-Xin Ren[a], Shan Jiang[b,c,d] (iD), Xu-Ri Wang[a] (iD), Guang-Zhao Peng[b,c,d], Yong Ye[b,c,d],
Logan King[e] and Hai-Lu You[f,g,h]* (iD)

[a]Key Laboratory of Stratigraphy and Paleontology of the Ministry of Natural Resources, Institute of Geology, Chinese Academy of Geological Sciences, Beijing, 100037, China; [b]Zigong Dinosaur Museum, Zigong, 643013, China; [c]Research Center of the Jurassic Stratigraphy and Paleontology, Zigong Dinosaur Museum, Zigong, 643013, China; [d]Key Laboratory of Paleontology and Paleoenvironment Coevolution (Sichuan-Chongqing Joint Construction), Zigong, 643013, China; [e]School of Earth Sciences, University of Bristol, Queens Road, Bristol BS8 1RJ, UK; [f]Key Laboratory of Vertebrate Evolution and Human Origins, Institute of Vertebrate Paleontology and Paleoanthropology, Chinese Academy of Sciences, Beijing, 100044, China; [g]CAS Center for Excellence in Life and Paleoenvironment, Beijing, 100044, China; [h]College of Earth and Planetary Sciences, University of Chinese Academy of Sciences, Beijing, 100049, China

The Middle Jurassic lower Shaximiao Formation in Sichuan Province of south-western China has yielded a diverse terrestrial vertebrate fauna dominated by sauropod dinosaurs. However, many of these sauropods lack detailed descriptions or explicit phylogenetic diagnoses. Here, we present a comprehensive redescription of Dashanpusaurus dongi, a species of sauropod found only in the lower Shaximiao Formation. We define the revised autapomorphies of the species as follows: neural canals are sub-square in anterior dorsal vertebrae; the presence of a thin accessory lamina that contacts the prezygodiapophyseal and paradiapophyseal laminae of the middle dorsals, forming an angle of 75° to the horizontal; and four ridges on the anterodistal edge of the humerus. Often considered part of the epipophyseal-prezygapophyseal lamina, a strut invades the spinodiapophyseal fossa in the cervical and anterior dorsal vertebrae. Anatomical comparisons indicate that this feature was widespread among early-diverging Middle Jurassic eusauropod lineages. This comparative anatomical data provides an opportunity to revisit the phylogenetic position of Dashanpusaurus and the relationships of the neosauropod clade. Recovered as a macronarian, a better understanding of Dashanpusaurus dongi will allow for clarification of the origin, early evolution, and palaeogeographical distribution of neosauropods. This study also suggests that the diversity and dispersity of the neosauropod clade occurred much earlier than previously realized.

Keywords: Sauropoda; Neosauropoda; Macronaria; Dashanpusaurus dongi; Middle Jurassic; lower Shaximiao Formation

Introduction

The lower Shaximiao Formation of Sichuan Province, China, has yielded diverse faunas of terrestrial vertebrates, including pterosaurs; sauropod, theropod and ornithischian dinosaurs; crocodyliform archosaurs; and early mammals (e.g. Young 1939, 1958; Dong et al. 1983; Dong & Tang 1984, 1985; He et al. 1984, 1988; Zhou 1984; Ouyang 1989; Peng 1992; Tang et al. 2001; Kuang 2004; Barrett et al. 2005; Peng et al. 2005; Ye et al. 2005; Jiang et al. 2011; Peng et al. 2019; Dai et al. 2020; Li et al. 2021; Tan et al. 2021). The 'Dashanpu Dinosaurian Fauna' is one of the most famous Middle Jurassic dinosaur faunal assemblages from this unit (Peng et al. 2005). The horizon is situated at the base of the lower Shaximiao Formation and is biostratigraphically correlated to the Middle Jurassic based on the presence of invertebrate fossils (e.g. bivalves) (Yang 1987; Du & Wang 2009). Although some researchers have produced U-Pb radiometric evidence indicating a late Middle to early Late Jurassic (Callovian–Oxfordian) age for the lower Shaximiao Formation (e.g. Li et al. 2010; Luo et al. 2014; Qian et al. 2016; Wang et al. 2018; Zhou et al. 2021), these ages remain difficult to reconcile with biostratigraphic correlations suggesting a Middle Jurassic (Bajocian–Bathonian) age for this stratum (e.g. Zhang et al. 1976; Chen et al. 1982; Shen 2003, 2004, 2010; Liao et al. 2014). We consider the age of the lower Shaximiao Formation to be unresolved.

The most abundant vertebrate remains encountered in Dashanpu Dinosaurian Fauna are those of sauropod

---

*Corresponding author. Email: youhailu@ivpp.ac.cn

dinosaurs and range from isolated elements to complete, articulated skeletons with skulls (Dong et al. 1983; Dong & Tang 1984, 1985; He et al. 1984, 1988; Zhang 1988; Ouyang 1989; Gao 1993; Peng et al. 2005; Jiang et al. 2011). Since the discovery of Shunosaurus lii in the late 1970s, six sauropod genera have been reported from this area (Shunosaurus, Protognathus, Omeisaurus, Abrosaurus, Dashanpusaurus and Datousaurus) (Dong et al. 1983; Dong & Tang 1984; He et al. 1984; Zhang 1988; Ouyang 1989; Kuang 2004; Peng et al. 2005; Jiang et al. 2011).

Despite the quality and abundance of the lower Shaximiao materials and their relevance to questions of sauropod systematics, taxonomy and diversity, the locality has been severely neglected and has not been subjected to detailed scrutiny. Here we attempt to partially rectify this deficit by providing a detailed redescription of Dashanpusaurus dongi, based on new anatomical details not recorded by Peng et al. (2005), and provide a discussion regarding the validity and diagnosis of this taxon.

Dashanpusaurus dongi was first reported by Peng et al. (2005), based on two partial postcranial skeletons from Dashanpu, Zigong City, Sichuan, China (Fig. 1). The original specimens were collected from the lower section (near the bottom) of the lower Shaximiao Formation and are regarded as Middle Jurassic (early Bajocian) in age. This taxon is significant for several reasons: Dashanpusaurus potentially represents the earliest known macronarian sauropod in Asia and is potentially a camarasaurid (Peng et al. 2005); if so, it provides another glimpse of later-diverging sauropod evolution during the otherwise poorly represented Middle Jurassic – a period that documents the significant richness of sauropods in China (e.g. Young 1939; Dong et al. 1983; He et al.1988; Zhang 1988; Ouyang 1989; Pi et al. 1996; Fang et al. 2000; Peng et al. 2005; Xing et al. 2015a; Xu et al. 2018); and it potentially demonstrates that basal macronarian taxa coexisted in the Middle Jurassic with some early-diverging taxa such as Shunosaurus lii and Omeisaurus tianfuensis. Moreover, this represents the first in a series of papers in which we will redescribe specimens of early-diverging sauropods of China to gain a fuller understanding of these important animals and their relevance to sauropod phylogeny and biogeographic history.

Methods

Descriptions and comparisons
All descriptions were made directly from the holotype and paratype specimens of Dashanpusaurus dongi. Comparisons with other taxa in this article were made from direct observations of specimens or with published descriptions, illustrations and photographs. We marked the reconstructed portions of each element in all relevant figures. We use Romerian orientational descriptors (e.g. anterior, posterior) rather than standardized terms (e.g. cranial, caudal). We use the anatomical nomenclature of Wilson (1999, 2012) and Wilson et al. (2011) for vertebral fossae, laminae and the components of the sauropod sacrum.

Measurements
The transverse width of the bifurcated neural spine is the length between the lateral apexes of the two metapophyses; the length of the deltopectoral crest measures from the distal maximum curvature point of the deltopectoral crest to the proximal-most point.

Phylogenetic analysis
Phylogenetic analyses were carried out in TNT v. 1.5 (Goloboff et al. 2008). Equal weights parsimony (EWP) and extended implied weighting (EIW) analyses were employed in the phylogenetic analysis. We set a general RAM of 300 Mb and a maximum of 500,000 trees for EWP and EIW, and used a concavity constant (K) of 12 for EIW. Firstly, the New Technology Search was applied; 50 search replications were used as a starting point for each hit, and the consensus was stabilized 10 times, using random and constraint sectorial searches under default settings, five ratchet iterations, and five rounds of tree fusing per replicate ('xmult = replications 50 hits 10 css rss ratchet 5 fuse 5'). Then, the resulting most parsimonious trees (MPTs) were used as the starting trees for a Traditional Search using tree bisection reconnection (TBR). The support for each node in the trees was assessed in TNT using Group present/ Contradicted (GC) values generated via symmetric resampling, based on 5000 replicates (Goloboff et al. 2003). The latter analyses used the Traditional Search option with TBR. Character mapping was carried out in Mesquite v. 2.75 (Maddison & Maddison 2011).

Anatomical abbreviations
4th, fourth trochanter of femur; ACDL, anterior centrodiapophyseal lamina; acf, anconeal fossa; ac fo, acromial fossa; ACH, anterior centrum dorsoventral height; ACPL, anterior centroparapophyseal lamina; ac ri, acromial ridge; ACS, anterior cervical series; act, acetabulum; ACW, anterior centrum transversal width; ae, anterior extended portion of humeral distal articular surface; aEI, ratio of total centrum length to the average centrum height and width (see Chure et al. 2010);

Figure 1. Locality of Dashanpusaurus dongi. A, world map, demarcating Sichuan Province; B, close-up of Sichuan Province, highlighting the location of Zigong City; C, collection sites of Dashanpusaurus dongi.

AL, thin accessory lamina contacting the prezygodiapo-physeal lamina and paradiapophyseal lamina; amp, ambiens process; AP, accessory process; avc, anteroven-tral concavity of ilium; bde, bevelled distal end; ca, cor-acoid articular surface; cc, cnemial crest; Cd, caudal vertebra; CDF, centrodiapophyseal fossa; cf, coracoid foramen; CL, centrum length with the anterior condyle; CPOL, centropostzygapophyseal lamina; CPRL, centro-prezygapophyseal lamina; Cv, cervical vertebra; D, dor-sal vertebra; dac, distal anterior concavity; di, diapophysis; dpc, deltopectoral crest; EPRL, epipophy-seal-prezygapophyseal lamina; fc, fibular condyle;

fmr, median ridges on femoral anterior surface; gl, glenoid; hpo, hyposphene-hypantrum system; ia, ischial articulation; ICF, intracostal fenestra; IE, internal excavation; ila, iliac articulation; Lat. SPOL, lateral spinopostzygapophyseal lamina; lb, lateral bulge; lc, lateral condyle; ld, lateral depression; lm, lateral malleolus; lr, lateral ridge; mc, medial condyle; M. cor, tuberosity for attachment of M. coracobrachialis; MCS, middle cervical series; md, medial deflection; Med. SPOL, medial spinopostzygapophyseal lamina; mm, medial malleolus; mp, medial process; nc, neural canal; nsp, neural spine; os, anterodorsally oblique strut; pa, parapophysis; pc, proximal concavity of radius; PCDL, posterior centrodiapophyseal lamina; PCS, posterior cervical series; pf, lateral pneumatic fossa or foramen; pho, hyposphene-hypantrum system; pmcr, posteromedial convexity of lower part of radius; POCDF, postzygapophyseal centrodiapophyseal fossa; PODL, postzygodiapophyseal lamina; POSDF, postzygapophyseal spinodiapophyseal fossa; posta, postacetabular process; poz, postzygapophysis; pp, posterior process; PPDL, paradiapophyseal lamina; PRCDF, prezygapophyseal centrodiapophyseal fossa; PRDL, prezygodiapophyseal lamina; prea, preacetabular process; PRPL, prezygoparapophyseal lamina; PRSDF, prezygapophyseal spinodiapophyseal fossa; PRSL, prespinal lamina; prz, prezygapophysis; puf, pubic foramen; pup, pubic peduncle; S, sacral vertebra; SDF, spinodiapophyseal fossa; SPDL, spinodiapophyseal lamina; SPOL, spinopostzygapophyseal lamina; SPRL, spinoprezygapophyseal lamina; tc, tibial condyle; tfi, tuberculum fibularis; tp, transverse process; TPOL, intrapostzygapophyseal lamina; TPRL, intraprezygapophyseal lamina; vc, ventral concavity; vlr, ventrolateral ridge; yo, sacricostal yoke.

Institutional abbreviations
CQ208, HEGT Chongqing Laboratory of Geological Heritage Protection and Research, No. 208 Hydrogeological and Engineering Geological Team, Chongqing Bureau of Geological and Mineral Resource Exploration and Development Chongqing, Chongqing, China; IVPP, Institute of Vertebrate Paleontology and Paleoanthropology, Chinese Academy of Sciences, Beijing, China; ZDM, Zigong Dinosaur Museum, Zigong, Sichuan, China.

Other abbreviations
DFA, distance from anterior end of centrum to anterior margin of neural arch; DFP, distance from posterior end of centrum to posterior margin of neural arch; GC, Group present/Contradicted; HRI, the average of the greatest widths of the proximal end, midshaft, and the distal end of humerus/length of the humerus;

MPTs, most parsimonious trees; NAH, neural arch dorsoventral height (measured from dorsal margin of centrum up to the base of the postzygapophyses); NSH, neural spine dorsoventral height (measured from the base of postzygapophyses up to neural spine summit); NSL, neural spine maximum anteroposterior length (measured above SPOLs); NSW, neural spine maximum transverse width; OTU, operational taxonomic unit; PCH, posterior centrum dorsoventral height; PCW, posterior centrum transverse width; TBR, tree bisection reconnection; vEI, the anteroposterior length of the centrum divided by the midline height of the cotyle (see Wedel et al. 2000); Vn, number of vertebrae.

Systematic palaeontology

Dinosauria Owen, 1842
Saurischia Seeley, 1887
Sauropodomorpha von Huene, 1932
Sauropoda Marsh, 1878
Neosauropoda Bonaparte, 1986a
Macronaria Wilson & Sereno, 1998
Dashanpusaurus Peng, Ye, Gao, Shu & Jiang, 2005

Type and only species. Dashanpusaurus dongi.

Diagnosis. As for the type and only known species (see below).

Dashanpusaurus dongi Peng, Ye, Gao, Shu & Jiang, 2005
(Figs 3–6, 7I, 8–25, 35A, B)

Holotype. ZDM 5028. Four cervical vertebrae, 13 dorsal vertebrae, five sacral vertebrae, 33 caudal vertebrae, left ulna, ilium, pubis, femur and tibia (Fig. 2).

Paratype. ZDM 5027. Four cervical vertebrae, 12 dorsal vertebrae, two caudal vertebrae, left scapula and coracoid, left humerus and radius, and some dorsal ribs.

Locality and horizon. The specimens were excavated in Dashanpu Town, Zigong City, Sichuan Province, in south-west China. Sauropod remains were found in purplish-red silty mudstones near the base of the lower Shaximiao Formation. Traditionally, a Bathonian–Callovian age was inferred for this unit (e.g. Deng et al. 2017; Huang 2019). A series of detrital zircon U-Pb dates for the lower Shaximiao Formation in the Sichuan Basin yielded a late Middle–early Late Jurassic age (Li et al. 2010; Luo et al. 2014; Qian et al. 2016; Wang et al. 2018). A new zircon U-Pb age from

Yunyang (Chongqing, north-west of Sichuan Basin) yielded a maximum depositional age of 166.0 ± 1.5 Ma (late Middle Jurassic) (Zhou et al. 2021). However, the invertebrate fossils and plant assemblage evidence indicate that the lower Shaximiao Formation is Middle Jurassic in age (potentially Bajocian–Bathonian) (Zhang et al. 1976; Chen et al. 1982; Shen 2003, 2004, 2010; Liao et al. 2014). More recently, detrital zircon U-Pb ages sampled in Dashanpu indicate that the bottom of the lower Shaximiao Formation possibly belongs to the earliest Bajocian (Tan et al. in prep.).

Remarks. Dashanpusaurus dongi was based on two partly articulated postcranial skeletons from the Dashanpu quarry. Unfortunately, the original excavation report is missing, so the quarry map and skeletal associations are unknown. Peng et al. (2005) assigned six middle and posterior cervical vertebrae; no cervical vertebrae are preserved from the paratype. However, four anterior cervical vertebrae were found during later observations at the Zigong Dinosaur Museum. According to the association of the anterior and posterior articular surfaces of centra, the features of the vertebrae, and the original storage records, these four anterior cervical vertebrae, and two anterior caudal vertebrae are from the paratype specimen (Figs 2, 3, 15). Additionally, the articular surfaces of the anterior cervical vertebrae from the paratype are transversely compressed, whereas the middle to posterior cervical vertebrae of the holotype are dorsoventrally compressed. Moreover, the features of these anterior cervicals are different from those of the other taxa from Dashanpu quarry (see Description, below) and the previous serial number of each vertebra suggests these four cervicals are isolated from the paratype, therefore we tentatively regard these cervicals as part of the paratype. The left ulna and ischium of the holotype are almost totally covered by plaster, making further anatomical descriptions impossible.

Emended diagnosis. Dashanpusaurus dongi is a macronarian sauropod with the following unique combination of character states (autapomorphies are marked by *): midline keels are present on the ventral surfaces of anterior cervical vertebrae; the centra of the anterior, middle and posterior dorsal vertebrae are opisthocoelous, amphiplatyan to amphicoelous, and amphicoelous, respectively; neural canals are sub-square in anterior dorsal vertebrae*; diapophyses of anterior to middle dorsal vertebrae project dorsolaterally; a thin AL contacts the PRDL and PPDL, forming an angle of approximately 75° to the horizontal in middle dorsal vertebrae*; an IE is situated below the diapophyses of dorsal vertebrae; anterior to middle dorsal neural spines are slightly bifurcated with transversely extended metapophyses;

neural spines have a slab-like morphology with expanded distal ends in posterior dorsal vertebrae; the medial spinopostzygapophyseal lamina (Med. SPOL) is prominent and robust and extends from the dorsal portion of the neural spine to the medial base of postzygapophysis on dorsal vertebrae; dorsal pneumatic fossae are large and simple without septa; four sacral vertebrae have completely fused centra; the anterior caudal vertebrae are amphicoelous; the ratio of maximum to minimum dorsoventral heights of the scapular blade is greater than two; there are four ridges on the anterodistal edge of the humerus*.

Comments. Peng et al. (2005) assigned this taxon to Camarasauridae. One previously identified character is retained as part of a unique combination of character states (midline keels weakly developed on ventral surfaces of cervical vertebrae). Six characters are revised and included in our new combination of character states: 'dorsal vertebrae are amphicoelous/amphiplatyan' was revised as 'the anterior dorsal vertebrae are opisthocoelous while the middle and posterior vertebrae are amphicoelous' (the anterior articular surfaces of the paratype's anterior dorsal vertebrae are flat or mildly concave); 'lateral excavations are well developed' was revised to 'dorsal pneumatic fossae are large and simple without septa'; 'the neural spines of the posterior cervical vertebrae and anterior dorsal vertebrae are shallowly bifurcated' was revised to 'the anterior to middle dorsal neural spines are slightly bifurcated with transversely extended metapophyses' (Peng et al. [2005] interpreted the holotype as including two posterior cervical vertebrae, but these are instead anterior dorsal vertebrae; the state of bifurcation in posterior cervical vertebrae is unknown); 'neural spines bear a slab-like morphology with expanded distal ends in middle and posterior dorsal vertebrae' was revised as 'neural spines bear a slab-like morphology with expanded distal ends in posterior dorsal vertebrae' (because many neural arches from middle dorsal vertebrate series are not preserved, we limited the state to the posterior dorsal vertebral series); 'four sacral vertebrae with completely fused centra' was revised as 'five sacral vertebrae with last four sacral centra completely fused' (the last dorsal vertebra was defined as the first sacral vertebra, as discussed below); and 'anterior caudal vertebrae are weakly opisthocoelous' was revised to 'anterior caudal vertebrae are amphicoelous' (the anterior articular surfaces of anterior caudal vertebrae are slightly concave). We disregarded some previous characters, such as: the cervicals are short and opisthocoelous (there is a lack of comparative taxa so we could not make a suitable comparison about the ratio of anteroposterior length of middle cervical centra divided by the height of the posterior articular surface of
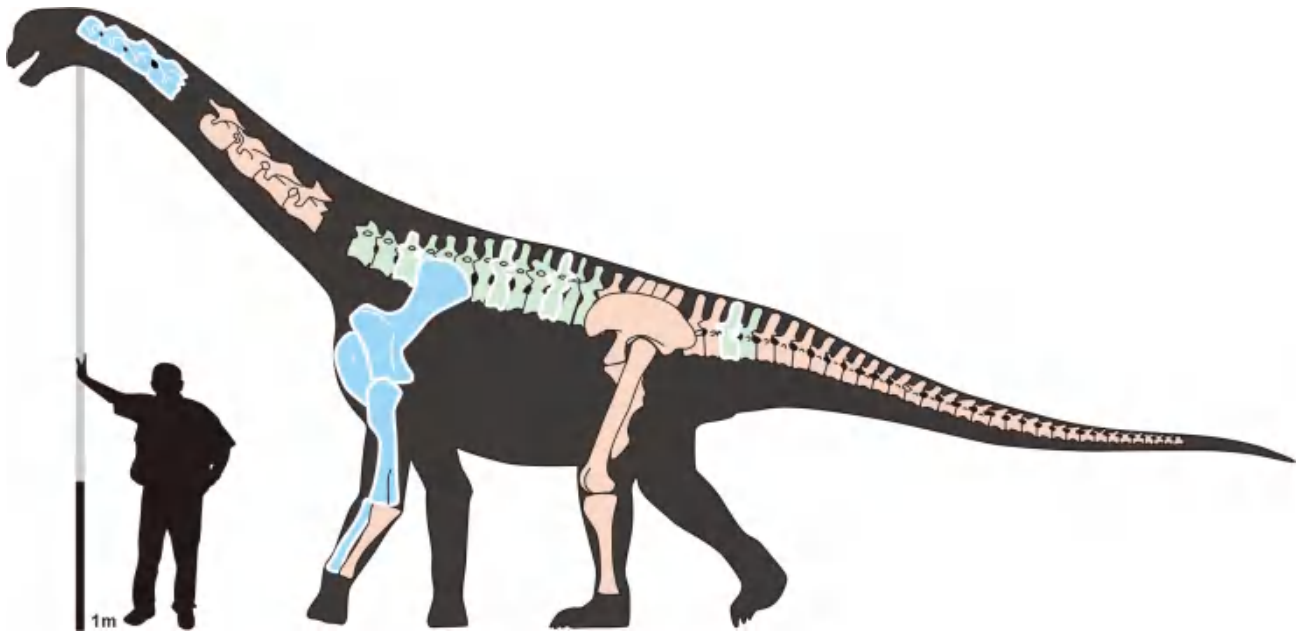
Figure 2. Reconstruction of Dashanpusaurus dongi. Reconstruction of the skeleton of Dashanpusaurus dongi in left lateral view. The elements in pink are from the holotype, those in blue are from the paratype and those in green are preserved in both holotype and paratype. Observed paratypic materials are outlined in white.

cervical centra, and cervicals of almost all sauropod taxa are opisthocoelous); the neural spines of the posterior dorsal vertebrae are broader transversely than anteroposteriorly (most sauropods share this character); the scapula is short and robust, and the posterior portion of the shaft extends prominently; the humerus is straight and robust with distinctly expanded proximal end; the ilium is anteroposteriorly extended with a pronounced anterior process; the femur is slender with a prominent femoral head; the fibula is a straight and robust element (all of the latter characters are indistinct, and many sauropod taxa share these states). Additionally, the four anterior cervical vertebrae were not mentioned in the previous paper (Peng et al. 2005). Therefore, we provide the first detailed description and comparison of them in this study.

Description and comparisons

Cervical vertebrae
Eight cervical vertebrae of the cervical series for the two specimens are present: four associated anterior cervical vertebrae from the paratype (maybe Cv3–6) and four loosely articulated middle posterior cervical vertebrae from the holotype (potentially Cv7–10). Cv4 is generally well preserved (Figs 3–5). By contrast, Cv3, Cv5–7 and Cv9 and 10 are only partly preserved and lacking neural arches. Cv8 is badly damaged and is mostly reconstructed with plaster. Some centra were

deformed during fossilization. The preserved anterior vertebrae (Cv3–6) are presumed to constitute the anterior series according to their morphology and measurements (e.g. the anterior condyles of these preserved anterior cervical vertebrae from the paratype are prominently anteroventrally projected, compared with the posterior articular surfaces; the ventral surfaces of the preserved anterior cervical vertebrae in the paratype are more dorsally curved than that in preserved cervical vertebrae in holotype) (these conditions are similar to those in many other sauropods such as Camarasaurus lewisi and Europasaurus holgeri: McIntosh et al. 1996a, figs 25–28; Carballido & Sander 2014, figs 4, 5), and according to a comparison of vEI ratio of each centrum with some eusauropod taxa (Camarasaurus sp., Camarasaurus lewisi, and some Eastern Asia sauropod taxa such as Shunosaurus lii, Omeisaurus tianfuensis and Mamenchisaurus youngi). The vEIs from the cervical vertebrae in the paratype and holotype are similar to the ratios of the anterior and posterior cervical vertebrae in Camarasaurus sp. The morphology of the lateral pneumatic fossae of Cv7–10 is distinctly different from that in Cv3–6, lacking the septa and small foramina situated in the lateral fossa of the latter. All centra are opisthocoelous (Figs 3, 4; see Tables 1 and 2 for measurements).

Anterior cervical vertebrae. The centra are opisthocoelous, with irregularly convex anterior articular surfaces and strongly concave posterior surfaces (Fig. 3; see Table 1 for measurements). The ventral surfaces are broad and gently concave transversely, rounding
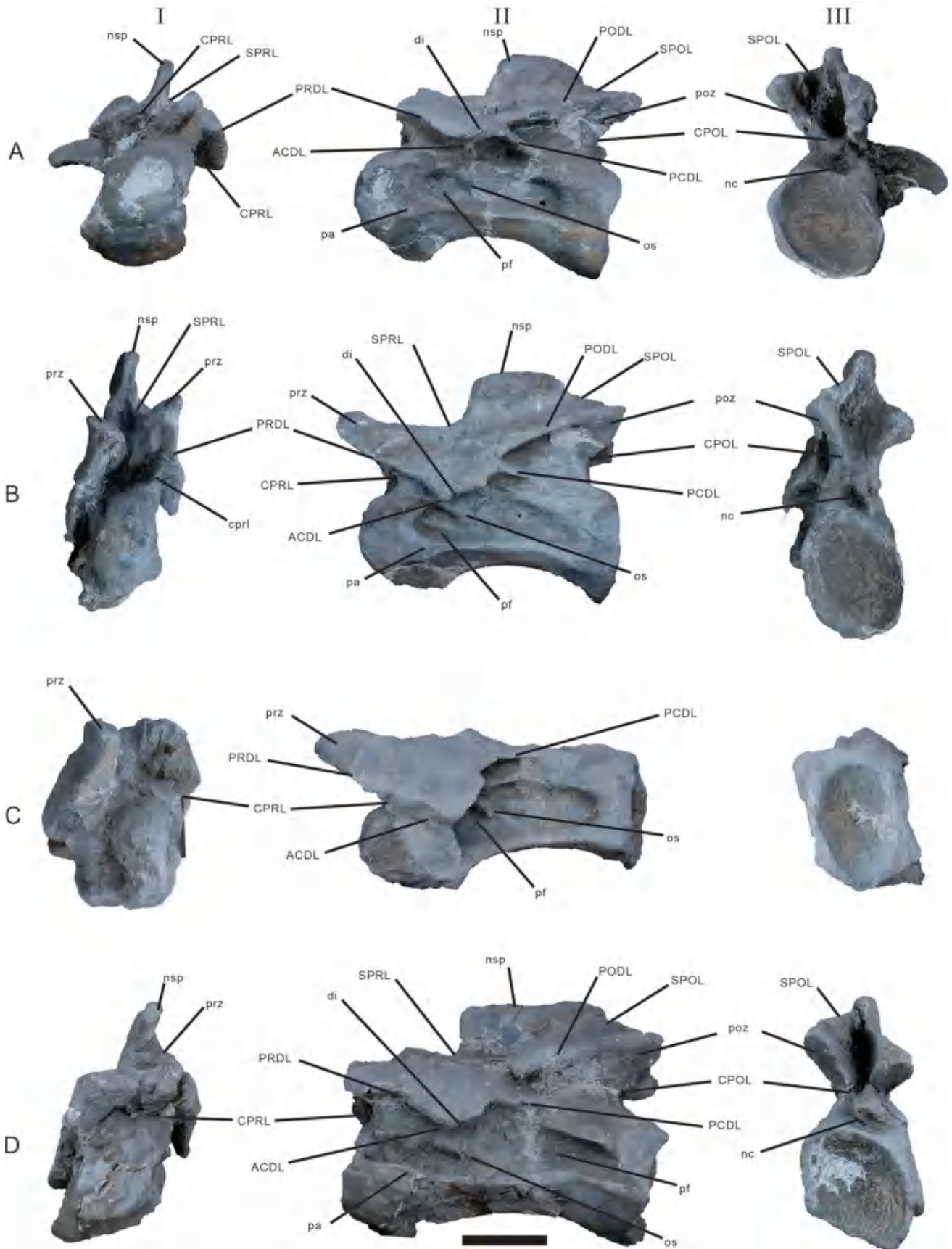
smoothly towards the lateral surfaces. The midline keels are low ridges and mildly convex on the anterior part of the ventral surfaces of Cv3 and 4. The midline keels are absent on subsequent anterior vertebrae. The posterior surface vEI ratio of the anterior cervical centra ranges from 1.42 to 1.23, with the highest ratio in Cv3. This value is lower than that in Bellusaurus sui (2.81) (Mo 2013, supplementary table). Based on the preserved morphology, the posterior articular surfaces are transversely compressed. Transversely compressed cervical vertebrae are found in most non-neosauropod eusauropods (e.g. Shunosaurus lii, Omeisaurus tianfuensis: He et al. 1988, table 6; Zhang 1988, table 5) and some neosauropod taxa such as Euhelopus zdanskyi and Galvesaurus herreroi (Barco et al. 2006, figs 2, 3; Wilson & Upchurch 2009). The articular facets of consecutive vertebrae in extant animals (e.g. birds, crocodilians, lizards and mammals) are of much the same shape, varying only gradually along the neck, and distortion of preserved sauropod cervical vertebrae is almost inevitable during taphonomy, fossilization and subsequent deformation (Taylor 2022). However, variation in the cervical articular condyles generally exists in many sauropod genera (e.g. Patagosaurus fariasi: Holwerda et al. 2021, table 2). If these articular surfaces were originally dorsoventrally compressed, this feature is a trait similar to most macronarian sauropods such as Camarasaurus lewisi (McIntosh et al. 1996a, figs 25–27; Upchurch 1998), and distinctly differs from Bellusaurus sui and the other sauropods from Dashanpu quarry that have transversely compressed posterior articular surfaces (e.g. Shunosaurus lii, Omeisaurus tianfuensis).

Pleurocoels occur on the lateral surfaces of the anterior centra, similarly to other sauropods such as Camarasaurus lewisi and Bellusaurus sui (McIntosh et al. 1996a, figs 25–27; Mo 2013, supplementary pl. 16). An excavation is situated at the anterior portion of the centrum of the anterior cervical vertebrae and there is a posterior smooth fossa on the posterior portion of the anterior cervical vertebrae. These are divided by an accessory septum (Fig. 3) that projects anterodorsally. The morphology of the pneumatic fossae resembles that in Bellusaurus sui and some other taxa such as Patagosaurus fariasi (Mo 2013, supplementary pl. 16; Holwerda et al. 2021, fig. 2), but differs from that in

Bashunosaurus kaijiangensis, which lacks a sub-dividing septum (Kuang 2004, fig. 1). These fossae gradually become larger and deeper on the middle to posterior cervical vertebrae. Some of the posterior fossae from the anterior cervical vertebrae are penetrated by small foramina on the central portion (Fig. 3A, B). The small notch on the dorsal margin of the posterior articular surface is absent, similar to the condition in Camarasaurus lewisi, Bellusaurus sui and early-diverging sauropod taxa such as Shunosaurus lii (Zhang 1988; McIntosh et al. 1996a; Mo 2013), whereas some taxa possess the notch, such as Europasaurus holgeri and Euhelopus zdanskyi (Wilson & Upchurch 2009; Carballido & Sander 2014, fig. 8).

The heights of the neural arches are about half the height of the centra. The neural arches are slightly taller than the neural spines, with a ratio reaching 1.1. The neural canal is dorsoventrally compressed with an elliptical outline. The prezygapophyses extend beyond the centra and are supported by the transversely thin CPRL, which seems to merge with the PRDL posteriorly. The CPRL is not divided, similar to that found in Bellusaurus sui, as is common in some early-diverging sauropods such as Shunosaurus lii (Zhang 1988; Mo 2013, supplementary pl. 17). An undivided CPRL is a plesiomorphic condition for non-diplodocids and this feature applies primarily to the middle to posterior cervical vertebrae (Upchurch 1998; Wilson 2002). The diapophyses are situated near the neurocentral junction along the anterior edge of the neural spine. The ventral surfaces of the diapophyses bear a slight concavity. A PCDL is present, as in most other sauropods such as Bellusaurus sui (Mo 2013, supplementary pl. 17). The PODL is prominent, resembling that in most sauropods, such as Camarasaurus lewisi and Bellusaurus sui (McIntosh et al. 1996a, figs 25–27; Mo 2013, supplementary pl. 17). The angle between the PODL and PCDL on the preserved anterior cervicals is between 39 and 46°. This condition is generally similar to that in Shunosaurus lii (Cv6: ∼39°) (Zhang 1988). By contrast, the range of this angle in the corresponding anterior cervical vertebrae of Camarasaurus lewisi and Camarasaurus sp. is much wider (Cv3–6: ∼50–80° and ∼25–40°, respectively) (McIntosh et al. 1996a, figs 25–28; Woodruff & Foster 2017, figs 14–17). This angle in Omeisaurus tianfuensis and

Figure 3. A–D, Dashanpusaurus dongi paratype anterior cervical vertebrae 3–6. I, anterior views; II, left lateral views; III, posterior views. Abbreviations: ACDL, anterior centrodiapophyseal lamina; CPOL, centropostzygapophyseal lamina; CPRL, centroprezygapophyseal lamina; di, diapophysis; nc, neural canal; nsp, neural spine; os, anterodorsally oblique strut; pa, parapophysis; PCDL, posterior centrodiapophyseal lamina; pf, pneumatic fossa or foramen; PODL, postzygodiapophyseal diapophyseal lamina; poz, postzygapophysis; PRDL, prezygodiapophyseal diapophyseal lamina; prz, prezygapophysis; SPOL, spinopostzygapophyseal lamina; SPRL, spinoprezygapophyseal lamina. Scale bar = 100 mm.

Figure 4. A–C, Dashanpusaurus dongi holotype middle to posterior cervical vertebrae 7, 9 and 10. I, anterior views; II, left lateral views; III, posterior views. Striped regions indicate reconstruction. Abbreviations: pa, parapophysis; pf, pneumatic fossa or foramen; vc, ventral concavity. Scale bar = 50 mm.

Mamenchisaurus youngi is slightly narrower than that in Dashanpusaurus dongi (Cv3–6: ∼29–42° and Cv3–5: ∼22–28°, respectively) (He et al. 1988; Ouyang & Ye 2002). Postzygapophyses extend slightly beyond the centra. The articular facets are concave and face ventrolaterally. The CPOL is not divided and extends ventromedially, resembling the condition of the CPRL.
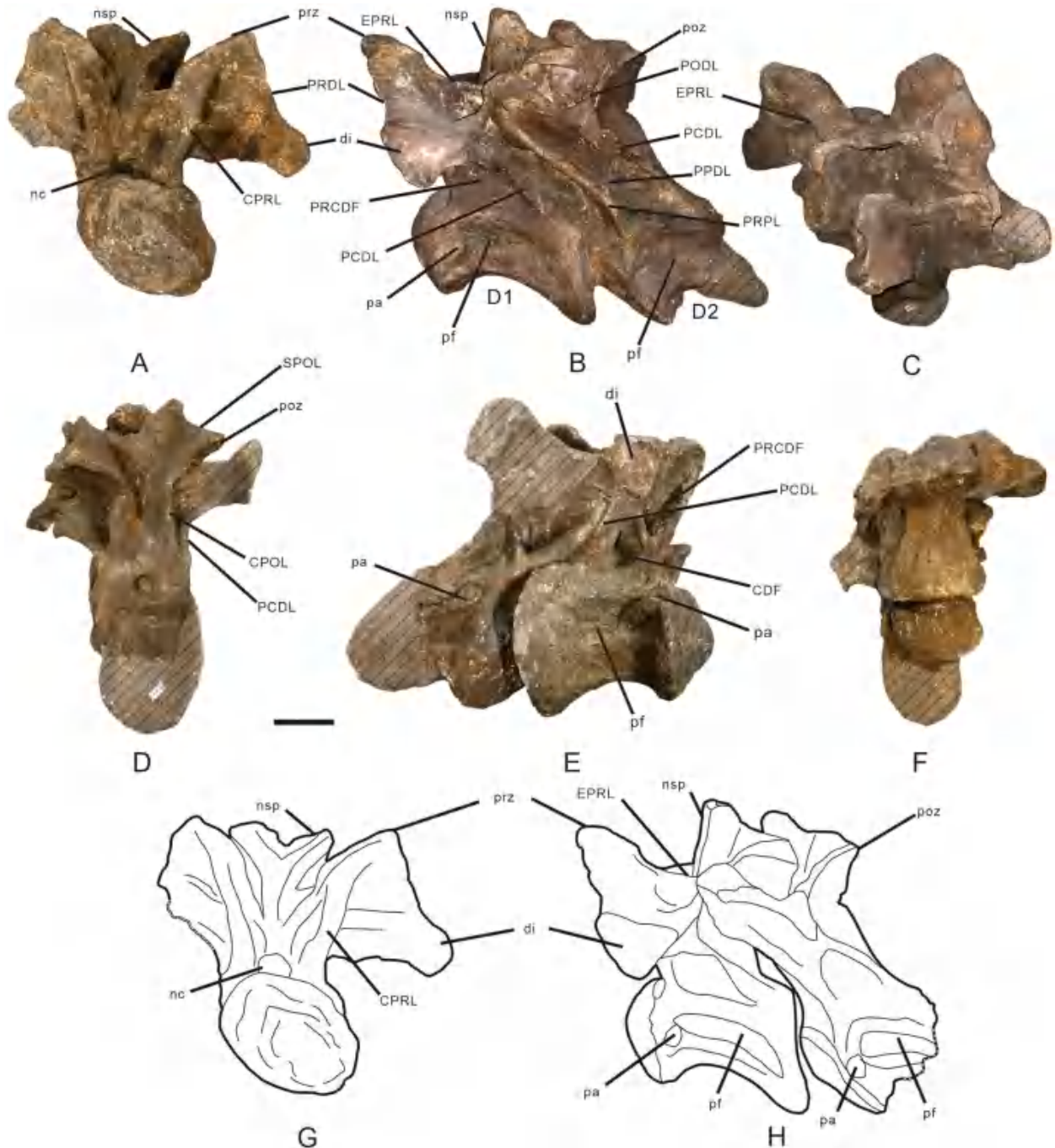
Figure 5. A–H, Dashanpusaurus dongi holotype anterior dorsal vertebrae 1 and 2. A and G, anterior view; B and H, left lateral view; C, dorsal view; D, posterior view; E, right lateral view; F, ventral view. Striped regions indicate reconstruction. Abbreviations: CDF, centrodiapophyseal fossa; CPOL, centropostzygapophyseal lamina; CPRL, centroprezygapophyseal lamina; D, dorsal vertebra; di, diapophysis; EPRL, accessory strut crossing the spinodiapophyseal fossa (SDF) of EPRL feature; nc, neural canal; nsp, neural spine; pa, parapophysis; PCDL, posterior centrodiapophyseal lamina; pf, pneumatic fossa or foramen; PODL, postzygodiapophyseal lamina; poz, postzygapophysis; PPDL, paradiapophyseal lamina; PRCDF, prezygapophyseal spinodiapophyseal fossa; PRDL, prezygodiapophyseal diapophyseal lamina; PRPL, prezygoparapophyseal lamina; prz, prezygapophysis; SPOL, spinopostzygapophyseal lamina. Scale bar = 50 mm.

The neural spines are essentially horizontal, measuring about half the length of the centra. These neural spines are dorsoventrally low and transversely narrow along their whole length. SPRLs and SPOLs start from the base of the neural spine, as in most sauropods such as Bellusaurus sui (Mo 2013). Prespinal laminae are
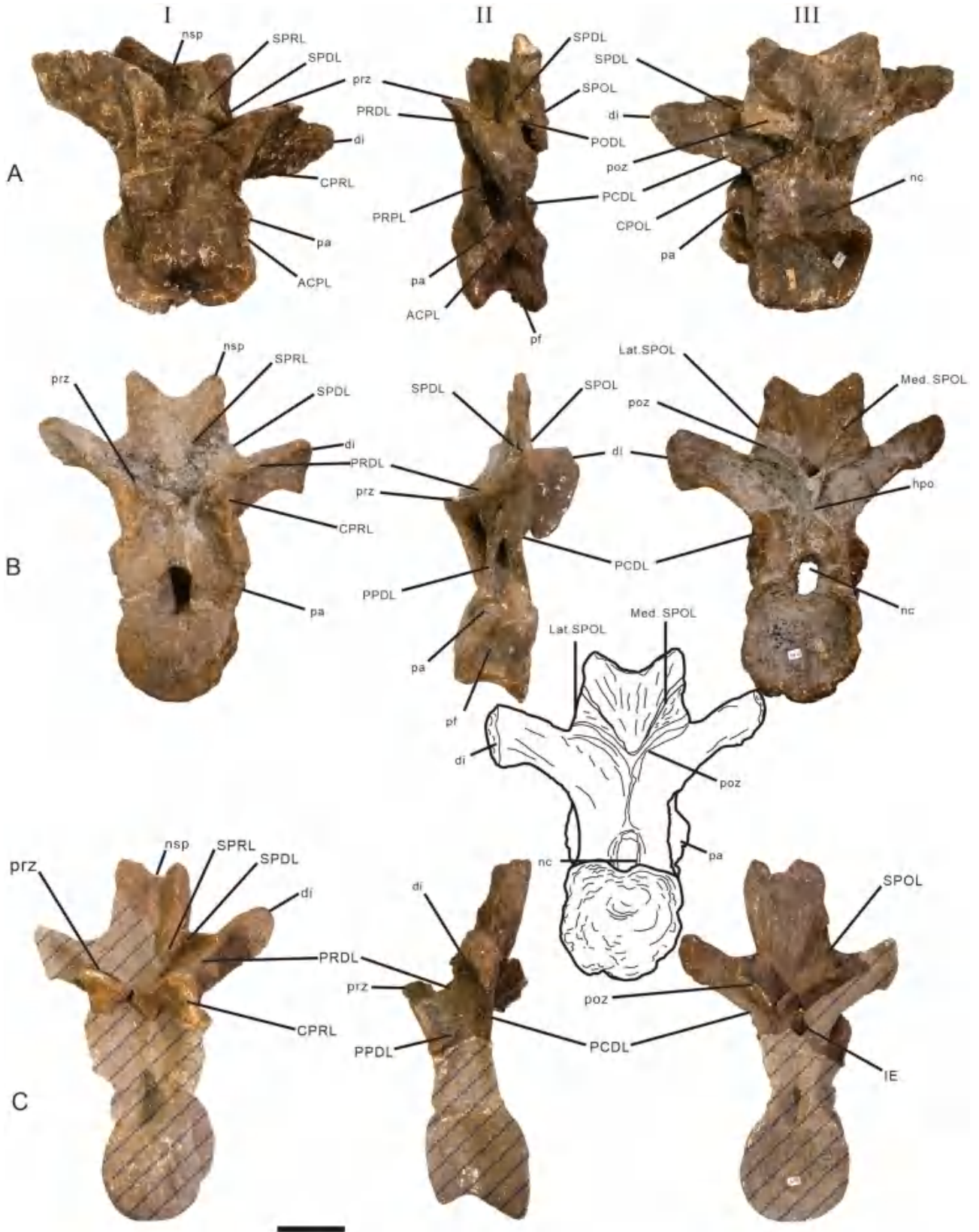
absent on the anterior cervical vertebrae, resembling the condition in Bellusaurus sui and in many other sauropods (e.g. Shunosaurus lii).

Middle to posterior cervical vertebrae. Only the centra from the holotype are well preserved, except for Cv8 which is nearly completely covered by plaster. The centra are opisthocoelous, with prominently hemispherical convex anterior articular surfaces and deeply concave posterior surfaces (Fig. 4; see Table 2 for measurements). It is worth noting that a dorsoventrally extended convexity is located on the lower portion of the anterior articular surface of Cv9. By contrast, the anterior margin of the anterior articular surface is flat in anterior view, and the prominently convex portion of the vertebra is situated at the centre of the centrum. Both the anterior and posterior articular surfaces are dorsoventrally compressed. The articular surfaces are transversely wider than dorsoventrally tall. This condition is similar to that in nearly all neosauropods, such as Camarasaurus lewisi (McIntosh et al. 1996a, figs 28–30), Bellusaurus sui (Mo 2013, supplementary pl. 18) and Lourinhasaurus alenquerensis (Mocho et al. 2014, fig. 3), and some eusauropods (e.g. Mamenchisaurus youngi: Ouyang & Ye 2002; Mannion et al. 2013). The ventral surfaces of the centra are prominently convex transversely, especially on the anterior portion of each centrum. The middle transverse convexity is keel-like and fades on the posterior portion of the centrum. Two deep, anteroposteriorly extended concavities are divided by the middle convexity on the anterior portion of the ventral surface (Fig. 4). The transverse widths are gradually reduced on the middle portion of the centrum. In contrast, the anterior and posterior portions are strongly expanded in ventral view. Ventrolateral ridges form the lateral margins of the two ventral concavities. The parapophyses, situated at the anterior portion of the centra near the anterior articular surfaces, are slightly laterally and ventrally extended. The articular surfaces of the parapophyses are elliptical in outline. The excavated parapophyses are commonly present in almost all neosauropods, such as Camarasaurus sp. (Woodruff & Foster 2017, fig. 17), excluding members of Somphospondyli (Upchurch 1998; Mannion et al. 2013). The articular surfaces are rough and oriented ventrolaterally. A pneumatic fossa is located on the lateral surface of the centrum and occupies almost its entire lateral surface. The anterior margin of the lateral fossa is rounded. This big excavation, with no dividing septum, extends from the anterior margin of the centrum to the posterior margin, as observed in Camarasaurus lewisi (McIntosh et al. 1996a, figs 28–30). It differs from the anterior cervical series and anterior-middle cervical vertebrae of Lourinhasaurus alenquerensis (Mocho et al. 2014, fig. 3) by containing a septum situated at the middle portion of the lateral surface that divides the lateral fossa. The deepest area is on the anterior portion of this excavation. There is no prominent boundary on the posterior margin of this excavation, whereas the anterior cervical vertebrae have a distinct posterior margin and multiple oblique struts dividing the lateral fossae. In the other sauropods recovered from Dashanpu quarry, the lateral fossae on the cervicals of Shunosaurus lii are deeply excavated with no prominent margin (Zhang 1988, fig. 25), whereas the posterior margin is present in Omeisaurus tianfuensis with multiple oblique struts dividing the lateral fossae (He et al. 1988, fig. 20).

Dorsal vertebrae

Thirteen dorsal vertebrae are preserved in the holotype and 12 in the paratype, although only six of the latter are well preserved (Figs 6–9; see Tables 1 and 2 for measurements). Most of the holotype dorsal vertebrae are well preserved, but some of them are only partly preserved (e.g. D10) and exhibit damage to the zygapophyses or centra. The well-preserved paratype dorsal vertebrae include one anterior vertebra, four middle vertebrae and one posterior vertebra. Rather than fully describing the anatomical features of these vertebrae, we divided the holotype and paratype dorsal series into three parts (anterior, middle and posterior), and documented changes along the vertebral sequence. D1–3 are presumed to be anterior dorsal vertebrae as the parapophysis is still touching the centrum. In addition, each centrum is opisthocoelous and the ventral margin is strongly arched dorsally in lateral view, unlike more posterior dorsals that have flat to concave articular surfaces (see Mannion et al. 2013; Tschopp et al. 2015, table 3). Additionally, a midline ventral keel is present on the centra of D1–3,

Figure 6. A–C, Dashanpusaurus dongi holotypic anterior and middle dorsal vertebrae. A, dorsal 3; B, dorsal 4; C, dorsal 5; I, anterior views; II, left lateral views; III, posterior views. Striped regions indicate reconstruction. Abbreviations: ACPL, anterior centroparapophyseal lamina; CPOL, centropostzygapophyseal lamina; CPRL, centroprezygapophyseal lamina; di, diapophysis; Lat. SPOL, lateral spinopostzygapophyseal lamina; Med. SPOL, medial spinopostzygapophyseal lamina; nc, neural canal; nsp, neural spine; pa, parapophysis; PCDL, posterior centrodiapophyseal lamina; pf, pneumatic fossa or foramen; PODL, postzygodiapophyseal lamina; poz, postzygapophysis; PPDL, paradiapophyseal lamina; PRDL, prezygodiapophyseal diapophyseal lamina; PRPL, prezygoparapophyseal lamina; prz, prezygapophysis; SPDL, spinodiapophyseal lamina; SPOL, spinopostzygapophyseal lamina; SPRL, spinoprezygapophyseal lamina. Scale bar = 50 mm.

Table 1. Measurements of paratypic vertebrae of Dashanpusaurus dongi. An asterisk (*) denotes a measurement based on an incomplete element. All measurements are in millimetres. Abbreviations: ACH, anterior centrum dorsoventral height; ACW, anterior centrum transverse width; Cd, caudal; CLB, centrum length with the condyle; Cv, cervical; D, dorsal; DFA, distance from anterior end of centrum to anterior margin of neural arch; DFP, distance from posterior end of centrum to posterior margin of neural arch; NAH, neural arch dorsoventral height (measured from dorsal margin of centrum up to the base of the postzygapophyses); NSH, neural spine dorsoventral height (measured from base of postzygapophyses up to neural spine summit); NSL, neural spine maximum anteroposterior length (measured above spinopostzygapophyseal laminae (SPOLs)); NSW, neural spine maximum transverse width; PCH, posterior centrum dorsoventral height; PCW, posterior centrum transverse width; Vn, vertebrae number (the number of dorsal and caudal vertebrae only presents the sequence of vertebrae).

Vn	CLB	ACH	ACW	PCH	PCW	DFA	DFP	NAH	NSH	NSL	NSW
Cv3	158	48	45	63	58	27	17	25	39	52	11
Cv4	157	63	47	78	59	23	18	36	30	55	13
Cv5	160	66	39	86	60	18	–	–	–	–	–
Cv6	189*	–	–	–	66	–	31	39	33	87	13
D1	93	–	–	–	180	16	–	130	90	27	140
D2	118	133	–	111*	150	13	26	150	130	35	100
D3	140	117	154	117*	160	14	–	140	150	39	97
Cd1	105	142	137	137	110	7	37	76	180	44	25

whereas this feature is absent in subsequent dorsals. We identify D4–8 as middle dorsal vertebrae and D9–13 as posterior dorsal vertebrae, and these preserve an internal excavation on the dorsal neural arch (IE), a thin accessory lamina contacting the prezygodiapophyseal and paraodiapophyseal laminae (AL) and excavation of the anterior articular surface of centra. The IE and AL are present in the middle dorsal series, and the anterior articular surface of the posterior dorsal centra is more excavated than the middle dorsal centra.

Anterior dorsal vertebrae. D1–3 are articulated and well preserved with the ventral portion of the posterior articular surface and right diapophysis of D2 being restored (Figs 5, 6A, 11A; see Tables 1 and 2 for measurements). The anterior dorsal vertebrae are opisthocoelous with prominently extended anterior dorsal centra. Both anterior and posterior articular surfaces are dorsoventrally compressed. The height-to-width ratio of the posterior articular surface of D3 is 0.80. It is worth noting that the anterior and posterior articular surfaces of D3 are taphonomically deformed to a quadrilateral outline rather than elliptical as is seen in other dorsal articular surfaces. The ventral surfaces of the centra are transversely convex and concave anteroposteriorly with a weakly developed midline keel. The ventrolateral ridge is absent from the ventral surfaces of the centra. The middle portion of the ventral surface is distinctly waisted in ventral view, and both anterior and posterior portions are laterally expanded. Two shallow concavities are situated on the anterior portion of the centrum near the anterior articular surface in ventral view. The two concavities are divided along the mid-sagittal plane. Laterally, the ventral margin is strongly arched dorsally in lateral view, especially in D2 and 3. The parapophyses are located at the anterior portion of the centra near the dorsal margin. They slightly extend anteroposteriorly

behind the articular ball and the articular surfaces are slightly ventrolaterally oriented. The articular facets are slightly concave and are laterally to mildly ventrally oriented with an elliptical outline. The lateral pneumatic fossa occupies the central portion of the lateral surface. This large excavation extends from the anterior articular surface to the posterior end with no divisions, and the deepest portion is situated dorsally. Also, the opening is posteriorly acute, as it is in the anterior dorsal vertebrae of nearly all macronarians (Upchurch 1998). The posterior margin of the lateral fossa on D3 is sub-triangular in outline, this differing from that in D2 of Camarasaurus sp., Bellusaurus sui and Lourinhasaurus alenquerensis, which all have elliptical fossae (Mo 2013, supplementary pl. 23; Mocho et al. 2014, fig. 5; Woodruff & Foster 2017, fig. 23). Additionally, the lateral fossa is much deeper, with some divided by septa in Camarasaurus sp., Bellusaurus sui and Lourinhasaurus alenquerensis (Mo 2013, supplementary pl. 23; Mocho et al. 2014, fig. 7; Woodruff & Foster 2017, fig. 23). There are no prominent boundaries on either the anterior or posterior margins of this excavation.

The neural arch is taller than the centrum, reaching approximately 1.1 times the height of the posterior articular surface of the centrum. These ratios are similar to those found in some early-diverging sauropod taxa such as Shunosaurus lii and Tongansaurus hei (Zhang 1988, fig. 31, D3: 1.47; Yang 2003, figs 3–5, anterior dorsal: 1.29) and differ from those in Camarasaurus sp. and Bashunosaurus kaijiangensis (Kuang 2004, fig. 1; Woodruff & Foster 2017, figs 23, 24). The prezygapophyses extend beyond the anterior articular surface of each centrum. The articular surface of the prezygapophysis is irregularly elliptical in outline. Both prezygapophyses are rugose and slightly concave centrally. The articular surfaces of the prezygapophyses are transversely extended and dorsomedially oriented. The

Table 2. Measurements of holotypic vertebrae of Dashanpusaurus dongi. An asterisk (*) denotes a measurement based on an incomplete element. All measurements are in millimetres. Abbreviations: ACH, anterior centrum dorsoventral height; ACW, anterior centrum transverse width; Cd, caudal vertebra; CLB, centrum length with condyle; Cv, cervical vertebra; D, dorsal vertebra; DFA, distance from anterior end of centrum to anterior margin of neural arch; DFP, distance from posterior end of centrum to posterior margin of neural arch; NAH, neural arch dorsoventral height (measured from dorsal margin of centrum up to the base of the postzygapophyses); NSH, neural spine dorsoventral height (measured from base of postzygapophyses up to neural spine summit); NSL, neural spine maximum anteroposterior length (measured above spinopostzygapophyseal laminae (SPOLs)); NSW, neural spine maximum transverse width; PCH, posterior centrum dorsoventral height; PCW, posterior centrum transverse width; S, sacral vertebra; Vn, vertebrae number.

Vn	CLB	ACH	ACW	PCH	PCW	DFA	DFP	NAH	NSH	NSL	NSW
Cv7	209	127	140	136	145	56	69	–	–	–	–
Cv9	238	149	153	142	171*	77	–	–	–	–	–
Cv10	244	99	122	141	148	57	–	–	–	–	–
D1	229	102	151	136	167	53	52	138	78	11	129
D2	212*	137*	148	144*	136	–	27	172	111	10	134
D3	116	121	153	122	148	31	27	128	151	17	172
D4	101	102	146	144	151	14	11	169	152	17	138
D5	–	–	–	–	–	–	–	–	153	26	101
D6	–	–	–	–	–	–	–	–	156	31	102
D7	–	–	–	–	–	–	–	–	174	37	98
D8	93	152	173*	177*	188*	12	14	–	–	–	–
D9	124	164	139	182*	158*	9	12	–	–	–	–
D11	–	–	–	–	–	–	–	–	198	52	112
D12	–	–	–	–	–	–	–	–	222	73	124
D13	121	169	204	189	205	22	22	216	222	73	106
S1	132	184	209	172	214	37	58	188	234	93	119
S2	122*	246*	203*	197*	151*	8	–	165*	133*	101	106*
S3	147	207	156	197	163	–	–	192	169	94	117
S4	156	199	162	184	154	–	–	178	193	97	119
S5	157	187	158	181	162	–	68	157	214	105	109
Cd1	114	206	182	213	194	4	8	134	225	90	69
Cd2	106	221	196	212	195	9	41	116	213	85	58
Cd3	139	–	198	–	225	–	–	–	–	–	–
Cd4	133	182*	171*	204	226	–	–	–	–	–	–
Cd5	117	212	181	196	170	11	23	117	183*	87	56
Cd6	118	195	167	184	162	11	9	112	186	72	57
Cd7	101	177	175	179	178	6	13	98	169	59	54
Cd8	108	187	148	146	131	3	6	89	183*	74	52
Cd9	118	174	121	162	109	–	–	–	–	–	–
Cd10	119	128	131	128	127	–	–	–	–	–	–
Cd11	143	96*	154*	109*	170*	–	–	–	–	–	–
Cd12	118	129	127	136	130	–	–	–	–	–	–
Cd13	109	132	141	131	146*	–	–	–	–	–	–
Cd14	117	128	126	134	123	18	41	–	–	–	–
Cd15	117	119	112	125	116	26	49	–	–	–	–
Cd16	115	120	118*	112*	108*	–	–	–	–	–	–
Cd17	105	101	90*	100	95	–	36	–	–	–	–
Cd18	98	95	99	95	99*	–	–	–	–	–	–
Cd19	105	95	102	100	96	–	–	–	–	–	–
Cd20	110	93	80+	99	86	23	39	–	–	–	–
Cd21	110	89	91	89	98	34	–	–	–	–	–
Cd22	103	91	87	100	86	19	37	–	–	–	–
Cd25	129	87	103	86	97	29*	35*	–	–	–	–
Cd26	130	88	97*	88	101	30	–	–	–	–	–
Cd27	127	92	90	91	91	36	–	–	–	–	–
Cd28	122	81	80	79	82	31	26	–	–	–	–
Cd29	105	70	72	72	77	–	–	–	–	–	–
Cd30	115	68	60*	62	20	–	–	–	–	–	–
Cd31	110	71	72	70	72	19	29	23	40	–	–
Cd32	107	62	65	55	56	–	–	–	–	–	–
Cd33	106	61	59	55	61	–	–	–	–	–	–
Cd34	95	60	61	60	60	–	–	–	–	–	–

articular surfaces are oriented at ∼30° to the horizontal. The prezygapophyses are supported ventrally by a transversely broadened CPRL. This lamina on D1 is not divided and extends dorsally and slightly laterally, contacting the middle portion of the prezygapophysis, as occurs in Camarasaurus supremus (Osborn & Mook 1921, pl. LXXI), Apatosaurus ajax (Upchurch et al. 2004a, pl. IIIM) and many other sauropod taxa (e.g. Patagosaurus fariasi: Holwerda et al. 2021, fig. 9). By contrast, in some eusauropod taxa such as Camarasaurus sp. (Woodruff & Foster 2017, fig. 22), Klamelisaurus gobiensis (Moore et al. 2020, fig. 8E) and Europasaurus holgeri (Carballido & Sander 2014, fig. 16), the CPRLs extend to the medial end of the prezygapophyses, and in other taxa (e.g. Rapetosaurus krausei: Curry Rogers 2009, fig. 14) they reach the lateral portion of the prezygapophyses. Moreover, the distal end of the CPRL of D1 does not prominently extend transversely to the point it contacts the TPRL and/or PRDL, whereas in some taxa the distal end of the CPRL is distinctly transversely extended and intersects the TPRL and/or PRDL rather than directly contacting the prezygapophysis. For example, this feature in Camarasaurus supremus (Osborn & Mook 1921, pl. LXXI) is transversely extended, contacting the TPRL; in Rapetosaurus krausei (Curry Rogers 2009, fig. 14) the CPRL prominently intersects the PRDL; and the CPRLs on D1 of Mamenchisaurus youngi are prominently extended, connecting the PRDL and TPRL (Ouyang & Ye 2002, fig. 29). The two TPRLs meet each other at the mid-sagittal plane and the junction forms the dorsal margin of the neural canal. Anteriorly, the neural canals are dorsoventrally compressed with an irregular quadrilateral shape. By contrast, these canals in the posterior cervicals are transversely compressed with an elliptical outline in posterior view. The diapophyses are robust, situated on the dorsal margin of the neural arches, and project laterally. The articular surfaces of the diapophyses are sub-triangular in outline, and slightly concave. The postzygapophyses are dorsolaterally inclined as in other sauropods. The epipophyses are situated at the posterior portion of the postzygapophyses near the posterior margin of the vertebrae. This feature is present in the cervical vertebrae of most sauropods, whereas a prominent epipophysis is uncommon in the dorsal vertebrae (Mannion et al. 2019). However, Dashanpusaurus dongi shares this prominent condition with some turiasaurs (Tendaguria tanzaniensis, Moabosaurus utahensis), Mamenchisaurus youngi and some other sauropod taxa (Ouyang & Ye 2002, fig. 20; Britt et al. 2017, fig. 19; Mannion et al. 2019, figs 19, 20). These rugose tubercles are sub-elliptical in outline and do not extend beyond the posterior margin of postzygapophysis. The

hyposphene-hypantrum system is not prominent but is rather a short, robust convexity that is situated on the dorsal margin of the neural canal beginning in D3. It should be noted that the orientation of the hyposphene-hypantrum system could be due to deformation during preservation. The ACDL is a thin element that exists on the anteroventral surface of the diapophysis. It contacts the ventral apex of the articular surface of the diapophysis. The PCDL expands anteroposteriorly and it is much more robust than the ACDL. It connects the posterior portion of the centrum to the posteroventral portion of the diapophysis. The PRDL and PODL are stout and extend from the base of the prezygapophysis and postzygapophysis, respectively, to the distal portion of the diapophysis. Both EPRLs are strongly extended from the anterior extension of the epipophyses to the posterior margin of the prezygapophyses. This condition is similar to that in Euhelopus zdanskyi, Camarasaurus and some other eusauropod taxa (e.g. Klamelisaurus gobiensis, Xinjiangtitan shanshanesis, Hudiesaurus sinojapanorum) where a prominent lamina is located on the posterior cervical vertebrae (see the detailed comparison in the Discussion, below; McIntosh et al. 1996a; Wilson & Upchurch 2009; Moore et al. 2020; Zhang et al. 2020; Upchurch et al. 2021). The CPOL is not divided, extends ventromedially and supports the postzygapophyses ventrally.

The neural spines are dorsally and slightly posteriorly oriented; their height is about 0.57 the length of the posterior surface of the centrum in D1. This ratio is similar to that of Camarasaurus sp. (D1, 0.56: Woodruff & Foster 2017, fig. 23). The height of the neural spine in D3 is slightly greater than the height of the posterior surface of the centrum. This condition differs from that in Camarasaurus sp. where the height of the centrum is greater than that of the neural spine (Woodruff & Foster 2017, figs 23, 24). The neural spines are bifurcated, as occurs in some macronarians such as Camarasaurus, Lourinhasaurus alenquerensis and Opisthocoelicaudia skarzynskii (Borsuk-Bialynicka 1977, fig. 2; Mocho et al. 2014, fig. 7; Woodruff & Foster 2017, figs 23, 24), some non-neosauropod eusauropods (e.g. Mamenchisaurus youngi: Ouyang & Ye 2002, figs 19–21), and diplodocoids such as Apatosaurus ajax and Amargasaurus cazaui (Salgado & Bonaparte 1991, fig 7; Upchurch et al. 2004a, pl. 3). The neural spines are shallowly bifurcated, differing from the deep bifurcation that begins in the basal portion of the neural spine of anterior dorsal vertebrae in Camarasaurus sp. and Apatosaurus ajax (Upchurch et al. 2004a, pl. 3; Woodruff & Foster 2017, figs 23, 24). The shallowly bifurcated condition of Dashanpusaurus dongi is more similar to that in Bashunosaurus kaijiangensis,

Mamenchisaurus youngi and Klamelisaurus gobiensis (Ouyang & Ye 2002, figs 19–21; Kuang 2004, fig. 3). In addition, the dorsal and lateral margins of the metapophyses of Dashanpusaurus dongi have acute angles in orientation (Figs 5, 6), but in Bashunosaurus kaijiangensis these margins are continuous with a sub-rounded outline in anterior view (Kuang 2004, fig. 3). In general, neural spine bifurcation is an unusual feature present in some sauropod clades such as Mamenchisauridae and Neosauropoda (e.g. Ouyang & Ye 2002, figs 19–21). This morphology is typically seen in the cervical and dorsal vertebrae, and it appears to have evolved at least five times, in mamenchisaurids, flagellicaudatans and early-diverging macronarians (e.g. Camarasaurus, Dashanpusaurus), Euhelopodidae sensu D′Emic (2012) and titanosaurs (e.g. Opisthocoelicaudia skarzynskii: Borsuk-Bialynicka 1977), with no apparent reversals (Taylor & Wedel 2013). Bifurcated neural spines are widespread in Jurassic East Asian eusauropod lineages, especially in Late Jurassic Mamenchisaurus-like genera (e.g. Mamenchisaurus youngi, M. hochuanensis, Tienshanosaurus chitaiensis, Xinjiangtitan shanshanesis, Qijianglong guokr, the ′Thailand mamenchisaurid′, Klamelisaurus gobiensis, and Hudiesaurus sinojaponorum) and macronarians (e.g. Bellusaurus sui) (Young 1937; Young & Zhao 1972; Ouyang & Ye 2002; Mo 2013; Suteethorn et al. 2013; Wu et al. 2013; Zhao 1993; Xing et al. 2015b; Moore et al. 2020; Zhang et al. 2020; Upchurch et al. 2021). Most of the bifurcated neural spines are on posterior cervical and anterior dorsal vertebrae of these taxa. The Middle Jurassic Lingwulong shenqi exhibits two dorsally directed metapophyses of the neural spine in its middle cervicals to anterior dorsals that create a deep and transversely narrow ′V′-shaped notch (with the two metapophyses separated narrowly or nearly sub-parallel as they extend from base to apex; the two metapophyses are narrow ′V′-shaped in anterior or posterior view; Xu et al. 2018; Fig. 7A). Another Middle Jurassic bifurcated sauropod, Bashunosaurus kaijiangensis from the lower Shaximiao Formation, has two slightly dorsolaterally projecting metapophyses with an open ′V′-shaped outline in anterior view (Kuang 2004, fig. 3). The Late Jurassic Mamenchisaurus youngi, M. hochuanensis and Qijianglong guokr have limited bifurcation on their first dorsal neural spine and the two metapophyses are anteroposteriorly extended (transversely compressed). They are distinct from the sub-parallel (narrow ′V′-shaped) metapophyses of M. hochuanensis (Fig. 7B), and the metapophyses are more dorsolaterally extended (wide ′V′-shaped) in M. youngi and Qijianglong guokr (Fig. 7D; Xing et al. 2015b, fig. 13). The neural spines of the anterior dorsals in Klamelisaurus gobiensis are bifurcated at the distal portion with the two metapophyses projecting sub-parallel to each other in anterior view (wide ′U′-shaped, with two metapophyses nearly subparallel and dorsally extending from base to apex) (Fig. 7J; Moore et al. 2020, fig. 8). Additionally, the preserved posterior cervical neural spine of Tienshanosaurus chitaiensis shares a wide ′V′-shaped notch with the upper portion invaded (Fig. 7E; Young 1937, fig. 1). By contrast, the aforementioned ′bifurcated neural spine′ taxa lack the medial process between the two rod-like metapophyses (wide ′V′-shaped) that existed in the posterior cervical vertebrae of Hudiesaurus sinojaponorum (Fig. 7H; Upchurch et al. 2021, figs 2, 3). In Camarasaurus sp. (Osborn & Mook 1921, pls LXVII–LXX; Woodruff & Foster 2017, figs 15–24), the bifurcation is situated at the upper portion of the neural spine with transversely wide/narrow ′U′-shaped (cervicals) and narrow ′V′-shaped (anterior dorsals) metapophyses in anterior or posterior view (Fig. 7C), and broad and deep notches (wide ′V′-shaped) in Camarasaurus supremus. It seems that macronarians usually share these wide ′V′-shaped notches that shallowly or deeply invade the dorsal vertebrae (e.g. Borsuk-Bialynicka 1977, fig. 2; McIntosh et al. 1996a, figs 34, 35). Woodruff & Fowler (2012) suggest that at the onset of larger body size, neural spine bifurcation performs a biomechanical function and could become significantly related to horizontal positioning of the neck. As the earliest and more ′weakly′ developed bifurcated taxon, Dashanpusaurus dongi possibly indicates the small body size in this era. In anterior view, the dorsal end of the neural spine on D3 is ′V′-shaped in outline without a deep notch as occurs in the other anterior dorsal neural spines. Notably, the two metapophyses of the anterior dorsal neural spines of Dashanpusaurus dongi are transversely extended. This condition differs from those in other ′bifurcated′ sauropods that have anteroposteriorly extended or ′rod-shaped′ metapophyses (e.g. Camarasaurus sp., Hudiesaurus sinojaponorum; Woodruff & Foster 2017, fig. 22; Upchurch et al. 2021, figs 2, 3). The anterior two dorsal vertebrae lack SPDLs, so no lamina divide the SDF. The SPDL of D3 extends from the base of the diapophysis to the base of the neural spine and is approximately vertical in orientation. The SPRL is a prominent ridge that extends from the base of the prezygapophysis to the summit of the neural spine. This element is much more robust on D3 and makes a distinctly central concavity in dorsal view. The SPOLs are well-developed and more robust than the SPRLs and extend from the summit of the neural spine to the posterior portion (at the base of the epipophysis). In dorsal
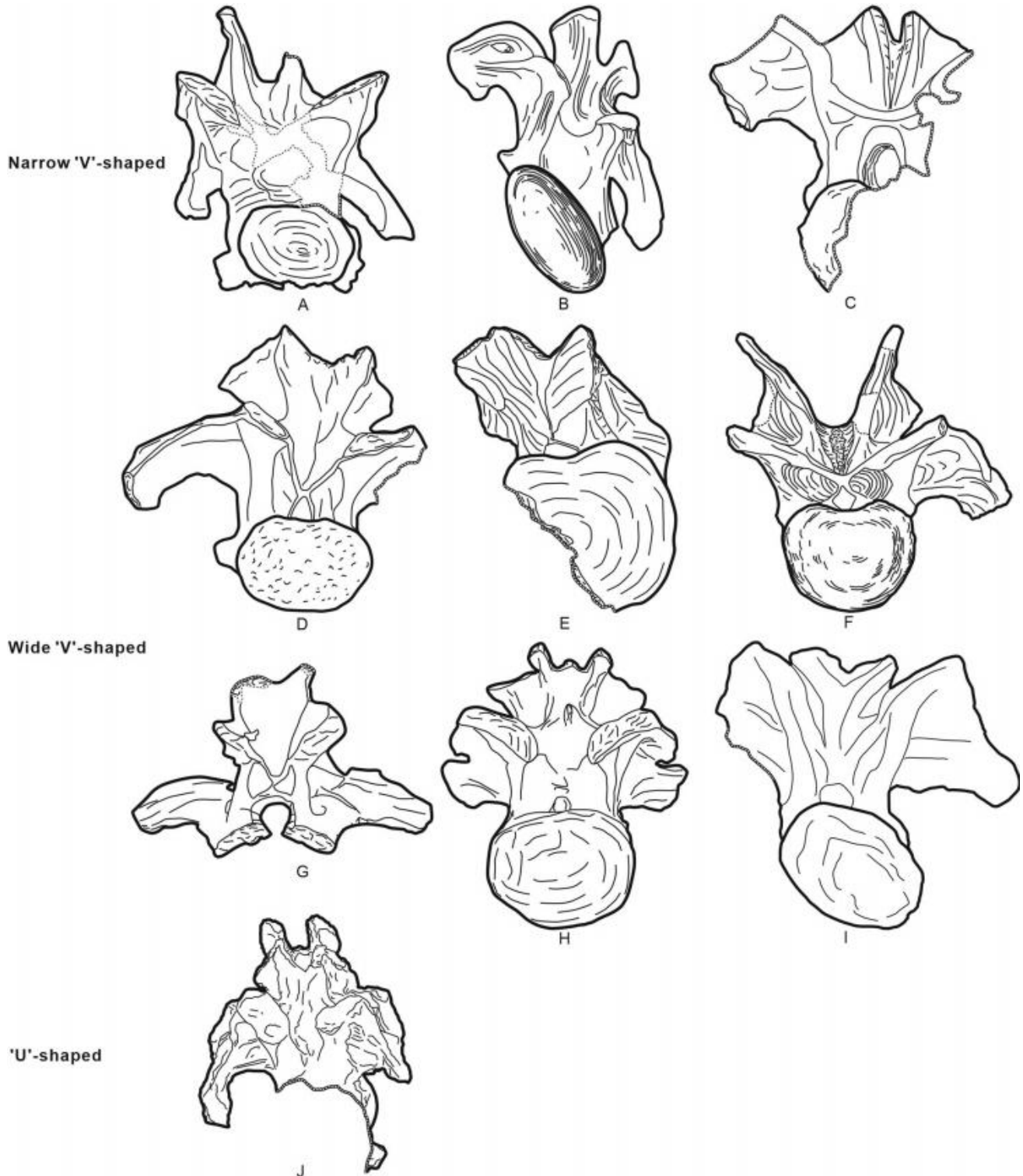
Figure 7. Bifurcated vertebrae of some Middle–Late Jurassic sauropod taxa. A–C, narrow 'V'-shaped metapophyses of bifurcated neural spines; D–I, wide 'V'-shaped metapophyses of bifurcated neural spines; J, 'U'-shaped metapophyses of bifurcated neural spines. A, bifurcated posterior cervical vertebra of Lingwulong shenqi (Xu et al. 2018, supplementary fig. 4b); B, D2 of Mamenchisaurus hochuanensis (Young & Zhao 1972, fig. 6[2]); C, D1 of Camarasaurus sp. (Woodruff & Foster 2017, fig. 23II); D, D2 of Mamenchisaurus youngi (Ouyang & Ye 2002, fig. 20A); E, bifurcated cervical neural spine of Tienshanosaurus chitaiensis (Young 1937, fig. 1B); F, D1 of Apatosaurus ajax (Upchurch et al. 2004a, pl. 3M); G, anterior bifurcated dorsal vertebrae of Bellusaurus sui (Mo 2013, pl. 25B); H, posterior bifurcated cervical neural spine of Hudiesaurus sinojapanorum (Upchurch et al. 2021, fig. 2C); I, D1 of Dashanpusaurus dongi (this paper); J, D1–2 of Klamelisaurus gobiensis (Moore et al. 2020, fig. 8E).

view, the combination of SPOLs and two metapophyses forms a 'W'-shaped outline.

Middle dorsal vertebrae. The middle dorsal vertebrae of the holotype and paratype are partly preserved except for D4 and two dorsals of the paratype (Figs 6B, C, 8, 9, 11B, C; see Tables 1 and 2 for measurements). The centrum and the distal end of the right diapophysis of D5 are not preserved. The centra are not preserved in D6–8. Additionally, part of the posterior portion of the neural arch and distal end of the right diapophysis of D6, the lower portion of the neural arch, and the distal end of the diapophysis of D7 are missing in the holotype. Most of the centrum and part of the lower portion of the neural arch are preserved on D8. The anterior articular surface of the centrum is flat to slightly concave. This contrasts with the posterior articular surface which is more concave than the anterior one. This condition is similar to that found in some early-diverging sauropod taxa such as Shunosaurus lii and Patagosaurus fariasi which have flat anterior articular surfaces and concave posterior articular surfaces in the middle dorsal series (Zhang 1988; Holwerda et al. 2021). This differs from Omeisaurus tianfuensis, Mamenchisaurus youngi, Camarasaurus lewisi, Lourinhasaurus alenquerensis, Bellusaurus sui and most other eusauropod taxa that have opisthocoelous centra (He et al. 1988, fig. 30; McIntosh et al. 1996b, pl. 5; Ouyang & Ye 2002, figs 23–25; Mo 2013, pl. 26; Mocho et al. 2014, fig. 5). The height-to-width ratio of the posterior articular surface of D4 is 0.99. Based on the preserved portions of the articular surfaces of centra, the articular surfaces are sub-circular and slightly dorsoventrally compressed. The articular surfaces of the centra are prominently dorsoventrally compressed in most macronarians, such as Camarasaurus lewisi and Lourinhasaurus alenquerensis (McIntosh et al. 1996b, pl. 5, table 3; Mocho et al. 2014, fig. 5). The ventral surfaces of the centra are slightly convex and the central portion is slightly concave transversely and flat anteroposteriorly. No midline keel is observable on the preserved centrum. A central concavity is present on the ventral surface of D9, but this is most likely due to poor preservation. The ventral surface of the centrum is convex transversely and the ventrolateral ridge is absent. A large, but shallow, pneumatic fossa is situated at the lateral surface of the centrum. The pneumatic fossa is elliptical in outline and occupies most of the lateral surface. Each margin of this fossa is rounded, whereas that in Euhelopus zdanskyi has an acute posterior margin (Wilson & Upchurch 2009, fig. 16). The deepest part of this opening is on the anterior portion. No internal septum divides the lateral pneumatic fossa, as in Euhelopus zdanskyi (Wilson & Upchurch 2009, fig. 16). It differs

from that of some taxa, such as Omeisaurus puxiani and Analong chuanjieensis, with an internal ridge on the lateral pneumatic excavation (Sekiya 2011, figs 16–18; Ren et al. 2021, fig. 2; Tan et al. 2021, fig. 4).

The neural canals are transversely compressed and elliptical in outline. The vertebral foramen is transversely compressed and widens vertically. The heights of the neural arches are slightly more than that of the centra, reaching about 1.2 of the heights of the posterior articular surfaces on D4. The inner concavity of the neural canals is greater than the anterior and posterior openings. This condition is also observed in some early-diverging taxa such as Barapasaurus tagorei (Wedel 2005, fig. 7.1; Bandyopadhyay et al. 2010). The parapophyses are situated on the anterodorsal portion of the lateral surface of the neural arch below the prezygapophyses and are triangular in lateral view. The articular surface of the parapophysis projects laterally and slightly dorsally. The articular surfaces of the parapophyses are rugose and slightly concave. The ACPL is a robust element and extends anteroventrally from the anterodorsal portion of the centrum to the anteroventral margin of the parapophysis in lateral view. The ACPL is approximately parallel to the PPDL on D4. The prezygapophyses anterolaterally extend beyond the anterior articular surface of each centrum. The articular surfaces of the prezygapophyses are elliptical with their long axes extending anterolaterally. They project dorsomedially with the central portion being slightly concave. The articular surfaces of the prezygapophyses are oriented dorsally and slightly medially, and slope ventrally towards the anterior vertebral margin. The prezygapophyses are supported ventrally by the anterolaterally extended CPRLs. The CPRLs are transversely widened along their anterior edge compared with the posterior portion (Fig 8C). In anterior view, the medial portion of the prezygapophyses is curved medially to contact the TPRLs. The TPRLs connect at the mid-sagittal plane with the midline lamina. The diapophyses are anteroposteriorly broadened and dorsoventrally flattened plates. The two transverse processes extend dorsolaterally, and the lateral part is slightly ventrolaterally bevelled. The dorsolaterally oriented diapophysis is similar to that in many early-diverging sauropods, such as Shunosaurus lii and Cetiosaurus oxoniensis (Zhang 1988, figs 31, 32; Upchurch & Martin 2003, fig. 5), and is similar to that found in Camarasaurus lewisi (McIntosh et al. 1996a, figs 31–34). This condition differs from that in many sauropod taxa (e.g. Apatosaurus ajax, Mamenchisaurus youngi, Bashunosaurus kaijiangensis) where laterally oriented diapophyses are common (Ouyang & Ye 2002, figs 22–24; Kuang 2004, fig. 4; Upchurch et al. 2004a, pl. 5). The articular surface of the postzygapophysis is
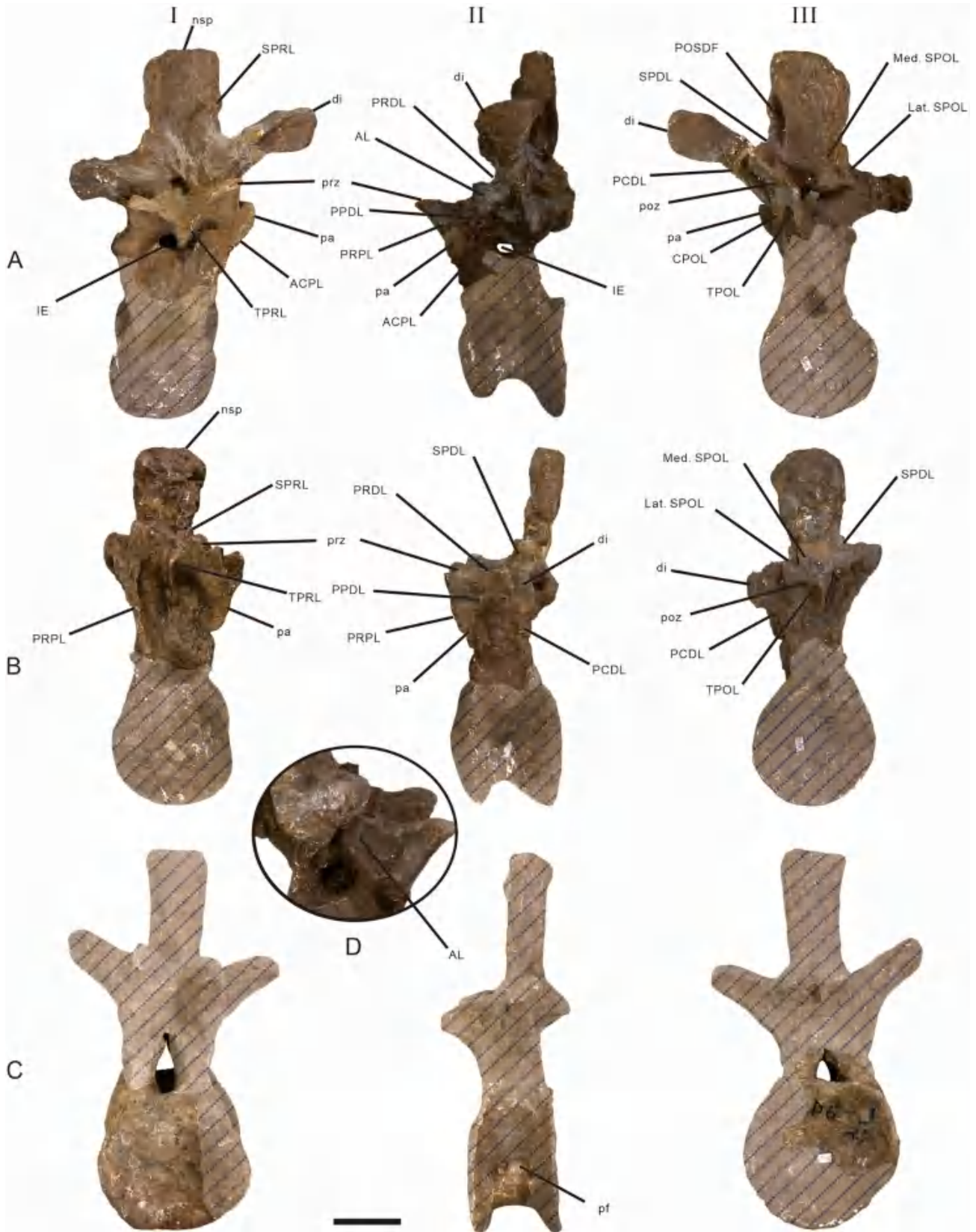
ventrolaterally oriented and the medial portion extends medially to contact the CPOLs. The CPOLs are not divided, as occurred in the CPRLs. The CPOLs extend ventromedially and the TPOLs fuse at the midline above the neural canal. In posterior view, the hyposphene-hypantrum system projects above the neural canal and is laminar in shape. The PRDL extends from the base of the prezygapophysis to the base of diapophysis and gradually becomes narrower. The PPDL extends from the posterodorsal base of the parapophysis to the anteroventral portion of the diapophysis. It is orientated at ∼45° to the horizontal in lateral view. The PODL is robust but short and contacts the bases of the postzygapophysis and diapophysis. The PCDL is approximately perpendicular to the horizontal and projects from the dorsoposterior margin of the centrum to the posteroventral base of the diapophysis. There is a robust AL in contact with the PRDL and PPDL that is oriented at ∼80° to the horizontal. It is worth noting that an IE is situated below the diapophysis and separated from the neural canal on D5 and D6 (Figs 6C, 8A, 9). This pneumatic chamber is absent in Camarasaurus lewisi, Bellusaurus sui and most other sauropod taxa (e.g. Omeisaurus spp.: He et al. 1988; McIntosh et al. 1996b, pl. 5; Mo 2013; Tan et al. 2021). Notably, the internal pneumatic chamber was reported in the middle to posterior dorsal neural arches of Patagosaurus fariasi and is possibly shared with Cetiosaurus and Barapasaurus (Holwerda et al. 2021, figs 13–16), whereas this feature is only present in the middle dorsal neural arches of Dashanpusaurus dongi. The internal pneumatic excavation (IE) is situated below the postzygapophyses on D5 (Fig. 6C). By contrast, the opening from this chamber is elliptical in outline, widens vertically and is oriented ventrally to the postzygapophysis. In D6, at least five sets of foramina (two lateral ones in the CDF, two anteriorly situated in the CPRF and SPRF, and the last one situated posteriorly in the CPOF) provide entry to this internal pneumatic chamber. The two lateral foramina are situated in the CDF, and are irregularly quadrangular (left lateral one) and oval (right lateral one) in shape with the long axis anterior-posterior projected. The anterodorsal opening is located at the bottom of the SPRF and has an irregular elliptical outline with its long

axis dorsolaterally oriented, and the dorsal margin of this foramen contacts the SPRLs. The anteroventral opening is situated in the upper portion of the CPRF below the two prezygapophyses with the TPRL overhanging the anterodorsal surface of this foramen. This opening is sub-triangular in outline, with the ventral margin connecting with the midline lamina. The posterior opening occupies some ventral areas of the SPOF and the upper portions of the CPOF and is sub-rounded to oval in shape. Due to breakage on the right postzygapophysis and TPOL, the missing right TPOL may connect to the left one and divide the posterior foramen into dorsal and ventral sections. Generally, both foraminal openings of the dorsal neural arches of Dashanpusaurus dongi and Patagosaurus fariasi are situated at the junctions of the neural arches and neural spines. However, the openings in Dashanpusaurus dongi suggest it is a thin sheet of bone and is easily broken. Due to the lower portion not being preserved, the exact internal spaces of these pneumatic chambers and whether these chambers are separated from the neural canal are uncertain. However, openings that connect the internal chamber and a thin sheet of bone around the foramina indicate the internal spaces of the chamber are relatively expanded.

The neural spines are anteroposteriorly compressed throughout the middle dorsal series and have a thick, plate-like appearance. They project dorsally and slightly posteriorly, much like the anterior dorsals. The neural spines of D4 and 5 are bifurcated, whereas those of subsequent dorsal vertebrae are unbifurcated. In the distal part of D4 and 5, a steep-sided 'V'-shaped trough is present. By contrast, the neural spine troughs in the anterior dorsal vertebrae of Mamenchisaurus youngi and Klamelisaurus gobiensis are prominently 'U'-shaped (Ouyang & Ye 2002, fig. 20; Moore et al. 2020, fig. 9). Anteriorly, the two metapophyses are triangular in outline and project dorsolaterally. In dorsal view, the bifurcated neural spine is laterally extended and the two metapophyses and the middle portion are situated along the same plane. This condition is similar to the metapophyses on the posterior cervical vertebrae. The degree of bifurcation and width of the neural spines are prominently reduced from D3 to D5. Additionally, the dorsal

Figure 8. Dashanpusaurus dongi holotypic middle dorsal vertebrae. A, dorsal 6; B, dorsal 7; C, dorsal 8; D, close-up of accessory lamina of dorsal 4 in right lateral view. I, anterior views; II, left lateral views; III, posterior views. Striped regions indicate reconstruction. Abbreviations: ACPL, anterior centroparapophyseal lamina; AL, accessory lamina between PRDL and PPDL; CPOL, centropostzygapophyseal lamina; di, diapophysis; IE, internal excavation; Lat. SPOL, lateral spinopostzygapophyseal lamina; Med. SPOL, medial spinopostzygapophyseal lamina; nsp, neural spine; pa, parapophysis; PCDL, posterior centrodiapophyseal lamina; pf, pneumatic fossa or foramen; PODL, postzygodiapophyseal lamina; POSDF, postzygapophyseal spinodiapophyseal fossa; PPDL, paradiapophyseal lamina; PRDL, prezygodiapophyseal diapophyseal lamina; PRPL, prezygoparapophyseal lamina; prz, prezygapophysis; SPDL, spinodiapophyseal lamina; SPRL, spinoprezygapophyseal lamina; TPOL, intrapostzygapophyseal lamina; TPRL, intraprezygapophyseal lamina. Scale bar = 50 mm.
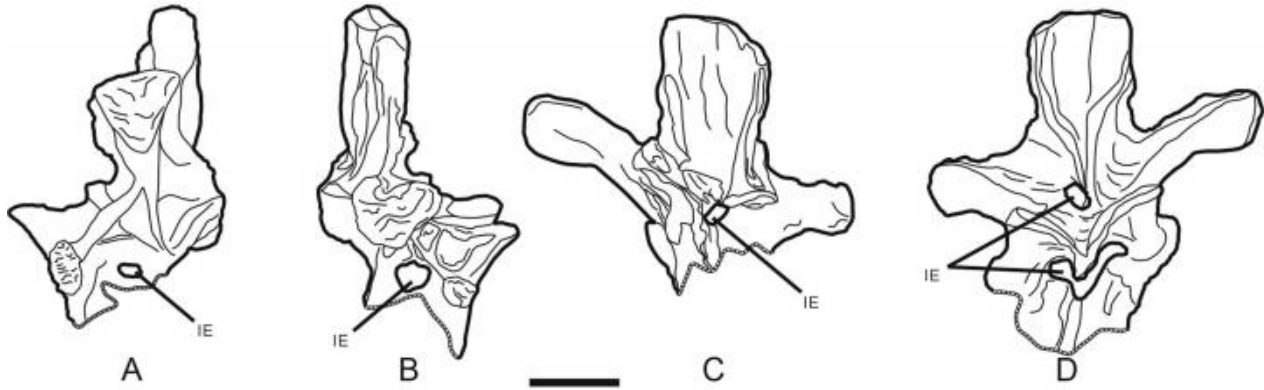
Figure 9. Internal excavation in Dashanpusaurus dongi holotypic middle dorsal vertebrae 6. A, left; B, right; C, lateral, posterior; and D, anterior views. Abbreviation: IE, internal excavation. Scale bar = 50 mm.

concavity only occupies the central portion of the distal end of the neural spine on D5 as opposed to the fully concave distal end of another two anterior neural spines. This generally makes the distal end of the two metapophyses transversely flat in anterior or posterior view. In anterior view, the neural spines of the remaining preserved middle dorsal vertebrae are slightly laterally expanded at their base. The distal end of each neural spine is mildly convex with a flattened central portion. The lateral margins of the distal ends are laterally extended when compared with the basal portion of the neural spines. In dorsal view, the anterior margin of the distal neural spines is prominently concave. By contrast, the posterior margins of the distal end are generally flat. The SPRL is stout and is oriented from the base of the prezygapophysis to the summit of the neural spine. By contrast, the SPOLs are slender and extend from the base of the postzygapophysis to the upper portion of the neural spine. The Med. SPOLs extend from the summit of the neural spine to the medial base of the postzygapophyses. The basal portion of the Med. SPOL is robust. This lamina is also observable in Camarasaurus lewisi and Apatosaurus louisae (Gilmore 1936, pl. 25, D3; McIntosh et al. 1996a, fig. 32), whereas the basal portion of the lamina is slenderer when compared with that in Dashanpusaurus dongi. This lamina is absent in Mamenchisaurus youngi, Klamelisaurus gobiensis and many other sauropods such as Opisthocoelicaudia skarzynskii (Borsuk-Bialynicka 1977, fig. 2; McIntosh et al. 1996a, fig. 31; Ouyang & Ye 2002, figs 20, 21; Moore et al. 2020, fig. 9). The SPDL curves smoothly from the base of the diapophysis to the base of the neural spine. It is worth noting that the POSDF is a large and deep dorsoventrally located fossa that widens from the base of the neural spine to the upper portion on D4, whereas it is extremely weak on D5. The deepest portion of this excavation is situated on the upper part of the neural spine.

Posterior dorsal vertebrae. The posterior dorsal vertebrae are partly preserved (Figs 10, 12A; see Tables 1 and 2 for measurements). The anterior portion of the centrum and lower portion of the neural arch of D9 are preserved. D10 is almost completely reconstructed with plaster. The upper portion of the neural arch, right diapophysis (only preserved in D12), zygapophyses, and neural spine are preserved in D11 and 12. The right diapophysis and the lower portion of the centrum of D13 are missing in the holotype. The posterior dorsal centra are amphicoelous. This condition is similar to that in some early-diverging sauropod taxa (e.g. Shunosaurus lii) and some diplodocoids, whereas most later-diverging sauropod taxa, such as Camarasaurus lewisi, Lourinhasaurus alenquerensis and Bellusaurus sui, have opisthocoelous centra (McIntosh et al. 1996b, pl. 5; Mo 2013, pl. 30; Mocho et al. 2014, fig. 5). The amphicoelous centrum of the posterior dorsal vertebrae of basal sauropods such as Tazoudasaurus naimi, Shunosaurus lii, Barapasaurus tagorei, Cetiosaurus oxoniensis and Patagosaurus fariasi became opisthocoelous in Omeisaurus spp. and Mamenchisaurus spp. (this is thought to be a synapomorphy, although the taxonomic contents of Mamenchisauridae remain controversial). By contrast, the centrum are amphicoelous in some diplodocoids and basal macronarians (e.g. Lingwulong shenqi (Tschopp et al. 2015; Xu et al. 2018), and opisthocoelous in Europasaurus holgeri (Carballido & Sander 2014, figs 21, 22). The anterior and posterior articular surfaces are dorsoventrally compressed, as occurs in the anterior and middle dorsal series. This condition is similar to that in Camarasaurus lewisi and Lourinhasaurus alenquerensis (McIntosh et al. 1996b, pl. 5, table 3; Mocho et al. 2014, fig. 5). The ventral surface of each centrum is transversely convex and anteroposteriorly concave, with no midline keel. The lateral and ventral surfaces of the centrum merge smoothly into each other near the ventral end in ventral view. The lateral
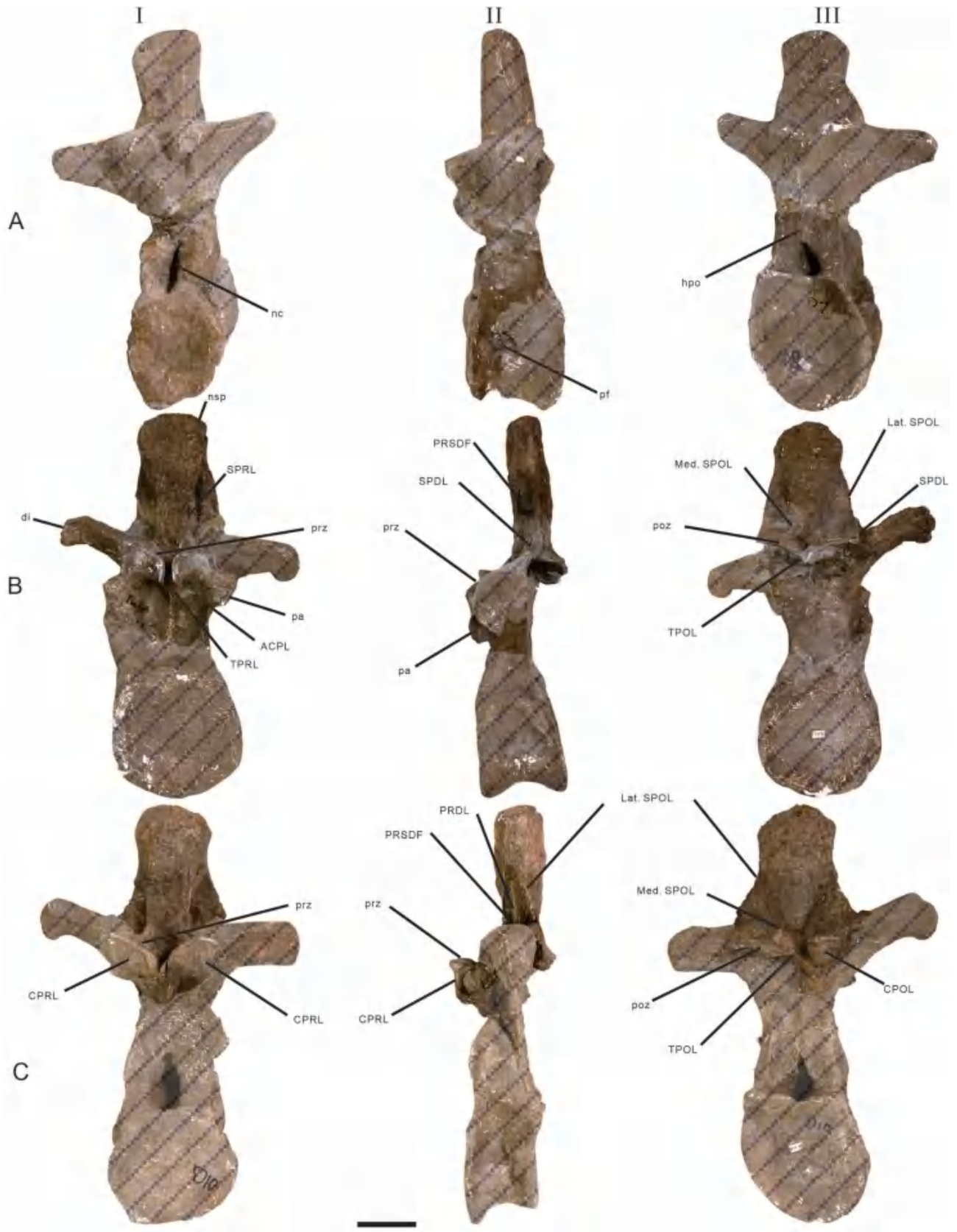
pneumatic fossa is located at the upper portion of the lateral surface of the centrum. This fossa is a large but shallow excavation with an elliptical outline. It occupies almost the whole upper portion of the centrum and some lower portions of the neural arch. The posterior margin of the lateral pneumatic fossa is rounded and there is no dividing septum. By contrast, a dorsoventrally extending internal septum divides the lateral pneumatic excavations of some posterior dorsal centra in *Bellusaurus sui* (Mo 2013, pl. 30).

The height of the neural arch is slightly greater than the posterior surfaces of the centra (D13: 1.2). This condition differs from that in *Camarasaurus lewisi* and *Tastavinsaurus sanzi* where the neural arch is shorter than the centrum in posterior dorsal vertebrae (McIntosh et al. 1996b, pl. 5; Canudo et al. 2008, fig. 3). The neural canals are teardrop-shaped in outline. These neural canals are transversely compressed with the apex of the teardrop projecting dorsally. The inner concavities of the neural canals are bigger than the anterior and posterior openings, as occurs in the middle dorsal vertebral series. The parapophyses are located on the anterodorsal portion of the lateral surface of the neural arch between the prezygapophysis and diapophysis. These are oriented laterally and the articular surface of the parapophysis is irregularly concave with an elliptical outline. The PRPL extends from the anterodorsal base of the parapophysis to the distal end of the prezygapophysis below the articular surface. It is oriented at ~45° to the horizontal. The PPDL and ACPL project from the dorsal and ventral base of the parapophysis, respectively. Moreover, these two laminae are almost in the same plane and are extended approximately vertically. It is worth noting that these two laminae are prominently extended laterally on the last two dorsal vertebrae and especially so on D12. The ACPL is more robust and distinctly laterally extended on D11 when compared with the ACPL on the more anterior posterior dorsal vertebrae. It extends from the base of the parapophysis to the lower portion of the neural arch. By contrast, the PPDL and ACPL are stouter on the last dorsal vertebra. These two laminae are generally parallel and are oriented from the middle portion of the ventral surface of diapophysis to the parapophysis and then to the anterodorsal margin of the centrum. This condition is absent on the posterior-

most dorsal vertebrae of *Camarasaurus lewisi* (McIntosh et al. 1996b, pl. 5). Based on the last, mostly complete, dorsal vertebra, the prezygapophysis extends at approximately the same level or slightly beyond the anterior articular surface of the centrum. The prezygapophyses are supported ventrally by the CPRLs. The CPRLs are parallel to each other. The articular surface of the prezygapophysis is oval in outline. The articular surface of the prezygapophysis is slightly concave in its central portion with a long axis that projects anterolaterally. It is oriented dorsomedially and slopes ventrally towards the anterior edge. The TPRLs contact the medially curved medial portion of the prezygapophysis and connect at the midline. The diapophysis is an anteroposteriorly broadened and dorsoventrally flattened plate. It projects laterally and slightly dorsally with the distal end slightly ventrally extended. The diapophyses of D12 are laterally and slightly ventrally curved. The articular surface of the diapophysis projects laterally and slightly ventrally. The postzygapophysis projects beyond the posterior articular surface of the centrum. The articular surface of the postzygapophysis is ventrolaterally facing and the medial portion is curved medially to contact the CPOLs. The CPOLs are single elements, similar to the CPRLs. The hyposphene-hypantrum system is not well preserved, but it seems robust based on the partly preserved basal portion on D12. The PRDL and PODL extend from the base of the prezygapophysis and postzygapophysis to the anterior and posterior base, respectively, of the diapophysis. Both the PRDL and the PODL of the posterior dorsal vertebrae are parallel to the horizontal, whereas the PODL of D12 is dorsoposteriorly extended.

The height of the neural spine is generally equal to the height of the posterior surfaces of the centra. The neural spines are anteroposteriorly compressed and they maintain this depth, and a thick, plate-like shape, through the entire series. They are slightly laterally extended at the summit. The distal end of the neural spine is transversely convex and anteroposteriorly flat. This condition is similar to that in the middle dorsal vertebral series. A flattened area on the central portion of the dorsal surface of the neural spines and the lateral margin of the distal end merges smoothly with the lateral surface of the neural spine. In dorsal view, the

Figure 10. *Dashanpusaurus dongi* holotype posterior dorsal vertebrae. A, dorsal 9; B, dorsal 11; C, dorsal 12. I, anterior views; II, left lateral views; III, posterior views. Striped regions indicate reconstruction. Abbreviations: ACPL, anterior centroparapophyseal lamina; CPOL, centropostzygapophyseal lamina; CPRL, centroprezygapophyseal lamina; hpo, hyposphene-hypantrum system; di, diapophysis; nc, neural canal; nsp, neural spine; pa, parapophysis; pf, pneumatic fossa or foramen; poz, postzygapophysis; PRDL, prezygodiapophyseal diapophyseal lamina; PRSDF, prezygapophyseal spinodiapophyseal fossa; prz, prezygapophysis; SPDL, spinodiapophyseal lamina; SPOL, spinopostzygapophyseal lamina; SPRL, spinoprezygapophyseal lamina; TPOL, intrapostzygapophyseal lamina; TPRL, intraprezygapophyseal lamina. Scale bar = 50 mm.
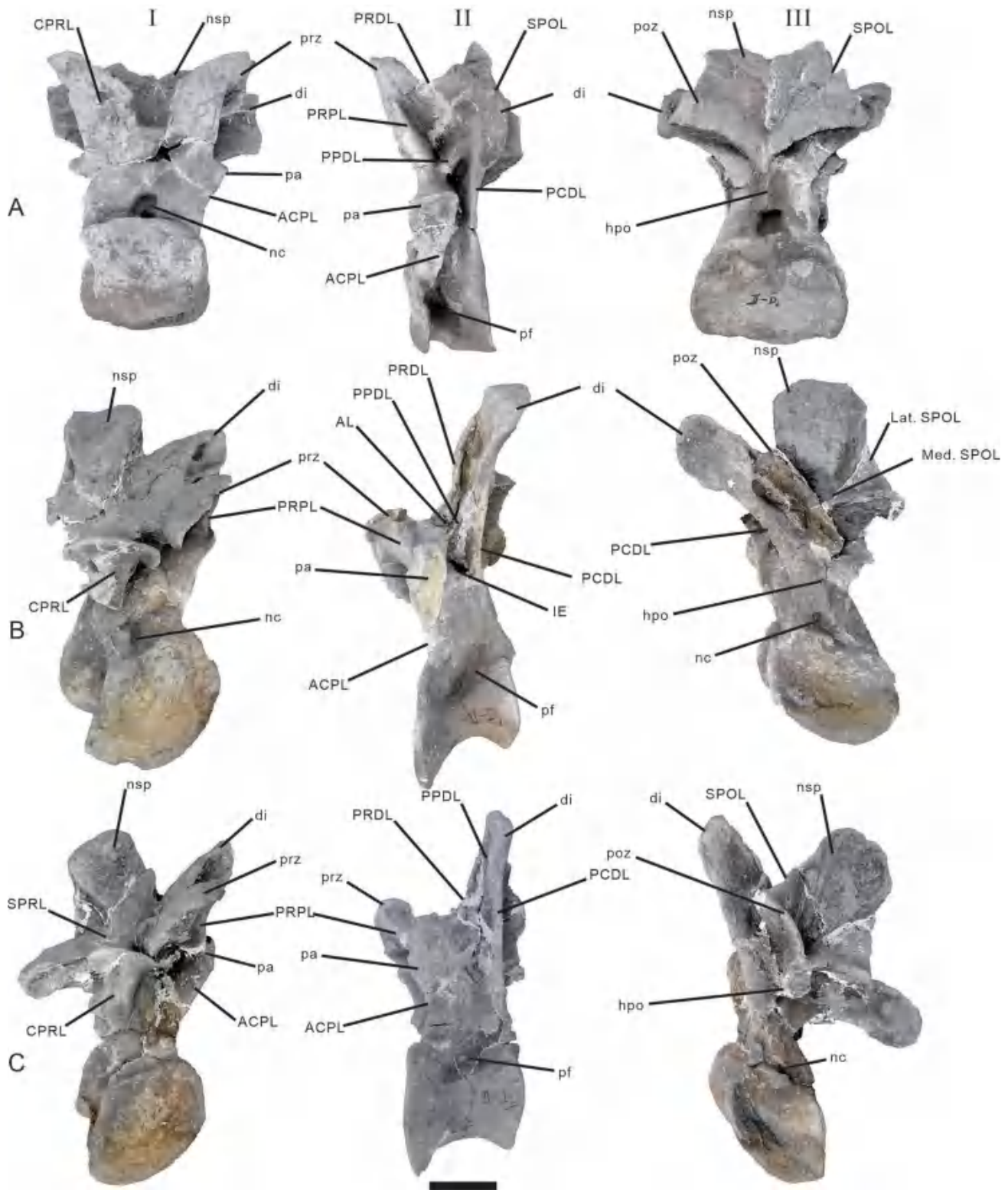
Figure 11. A, Dashanpusaurus dongi paratype anterior; B, C, middle dorsal vertebrae. I, anterior views; II, left lateral views; III, posterior views. Abbreviations: ACPL, anterior centroparapophyseal lamina; AL, accessory lamina; CPRL, centroperzygapophyseal lamina; di, diapophysis; hpo, hyposphene; nc, neural canal; nsp, neural spine; pa, parapophysis; pf, pneumatic fossa or foramen; poz, postzygapophysis; PCDL, posterior centrodiapophyseal lamina; PPDL, parapophyseal diapophyseal lamina; PRDL, perzygodiapophyseal diapophyseal lamina; PRPL, prezygoparapophyseal lamina; prz, prezygapophysis; SPOL, spinopostzygapophyseal lamina. Scale bar = 100 mm.

distal end of the neural spine is sub-rectangular in out-
line. The neural spines, except for D13, are dorsally ori-
ented. The neural spine of D13 projects slightly
anteriorly. The PRSL anteriorly extends on the base of
the neural spine (Fig. 12). The SPRL is a thin, promin-
ent lamina that extends from the base of the prezyga-
pophysis to the middle portion of the neural spine. By
contrast, the SPOL extends from the distal end of the
postzygapophysis to the middle portion of the neural
spine. It is worth noting that the SPOLs are distinctly
laterally expanded. They differ from those in the middle
and anterior dorsal vertebrae in that they extend along
the lateral margin of the neural spine to the
postzygapophysis.

Sacral vertebrae

Five sacral vertebrae are well preserved as part of the
holotype (Figs 12B, 13; see Table 2 for measurements).
S2, the centrum of S3 and S5 are partly covered in
plaster (including the anterior articular surface, the pre-
zygapophyses and the anterior portion of the neural
spine of S2; and the ventral surfaces of S3 and S5).
S2–5 are fused. Since all of the sacral vertebrae are
loosely preserved and were not in articulation with the
ilium, we initially identified S1 as the last dorsal based
on some features such as the anterior and posterior
articular surfaces of the centrum being dorsoventrally
compressed, a condition that is similar to the rest of
the dorsal series, whereas the sacral vertebrae are trans-
versely compressed. Then, we re-identified S1 as the
first sacral, for the following reasons: the triangular ali-
form processes preserved on the middle to posterior
dorsal vertebrae (including D13) are present and project
mildly laterally, whereas this process is absent on S1;
the diapophyses of S1 are laterally oriented and the
distal end is slightly ventrally oriented, as occurs in the
sacral vertebrae, whereas that in D13 is more similar
to the other middle to posterior dorsal vertebrae with
the transverse process oriented laterally and slightly
dorsally; the diapophyses of S1 are more robust and
dorsoventrally extended than D13 with the SPDL
strongly laterally extended nearly to the articular sur-
face of the diapophysis; and the diapophysis and para-
pophysis seem fused like the transverse process and
they are supported by a robust lamina that extends
from the dorsal portion of the centrum. This lamina is
stouter than that on D13 (the lamina on D11 is the
PPDL and does not extend to the dorsal margin of the
centrum). Additionally, although some vertebrae are
partially preserved, the whole dorsal vertebrae series is
preserved as a loosely articulated series, meaning that
the total number of dorsal and sacral vertebrae is cer-
tain and the dorsal + sacral series are either 13 + 5 or

14 + 4. In sauropods, most eusauropods share 13 or
fewer dorsal vertebrae + 4 or more sacral vertebrae,
except Haplocanthosaurus (probably 14 + 5) (Hatcher
1903; Xu et al. 2018), and the dorsal and sacral verte-
brae trend towards a reduction or increase, respectively,
in number (e.g. Xu et al. 2018). In addition, some
non-titanosauriform macronarians, such as Euhelopus
zdanskyi, have 13 dorsal vertebrae (Wilson &
Upchurch 2009). The ribs of S2, the right rib of S3
and the left rib of S5 are not preserved. All of the
sacral centra are probably amphicoelous based on S1
and the anterior articular surface of S2 and posterior
articular surface of S5. The articular surfaces of S3
and S5 are elliptical in outline. The number of sacral
vertebrae is similar to that of many later-diverging sau-
ropods (e.g. Camarasaurus). Four sacral vertebrae are
seen in earliest-diverging sauropods, such as
Shunosaurus lii and Barapasaurus tagorei (He et al.
1988; Bandyopadhyay et al. 2010), while Patagosaurus
fariasi, some later-diverging non-neosauropod eusauro-
pods and many neosauropods share five or more sacral
vertebrae (e.g. Mamenchisaurus youngi; Camarasaurus
lewisi, Euhelopus zdanskyi, Opisthocoelicaudia skarzyn-
skii: Borsuk-Bialynicka 1977; McIntosh et al. 1996a;
Ouyang & Ye 2002; Wilson & Upchurch 2009;
Holwerda et al. 2021). Among East Asian Jurassic
sauropod lineages, Shunosaurus lii, most Omeisaurus
spp. (except O. jiaoi) and other early-diverging
eusauropods share four sacral vertebrae. Many later-
diverging non-neosauropod eusauropods (e.g.
Mamenchisaurus spp., Xijiangtitan shanshanensis) and
the diplodocoid Lingwulong shenqi have five sacral
vertebrae (Ouyang & Ye 2002; Wu et al. 2013; Xu
et al. 2018). Moreover, six sacral vertebrae were
reported in Klamelisaurus gobiensis (Moore et al.
2020). The anterior and posterior articular surfaces of
the centrum are transversely compressed. The trans-
versely compressed nature of the centra differs from
that in Camarasaurus lewisi which has dorsoventrally
compressed sacral centra (McIntosh et al. 1996b, pls 9,
10). The sacrum angle is ∼16.5° (see Vidal et al.
2020) and resembles that in Camarasaurus grandis and
Diplodocus carnegii (Vidal et al. 2020, table 1:
Camarasaurus grandis, 17.5°; Diplodocus carnegii,
16.0°). Non-neosauropods, such as Mamenchisaurus
youngi (ZDM0083: Vidal et al. 2020, table 1) and
Jobaria (Vidal et al. 2020, table 1), preserve sacral
angles of 15.8° and 15.0°, respectively. The ventral
surfaces of the sacral vertebrae are anteroposteriorly
concave and transversely convex. Ventrally, the lateral
portion of the ventral surface smoothly merges with
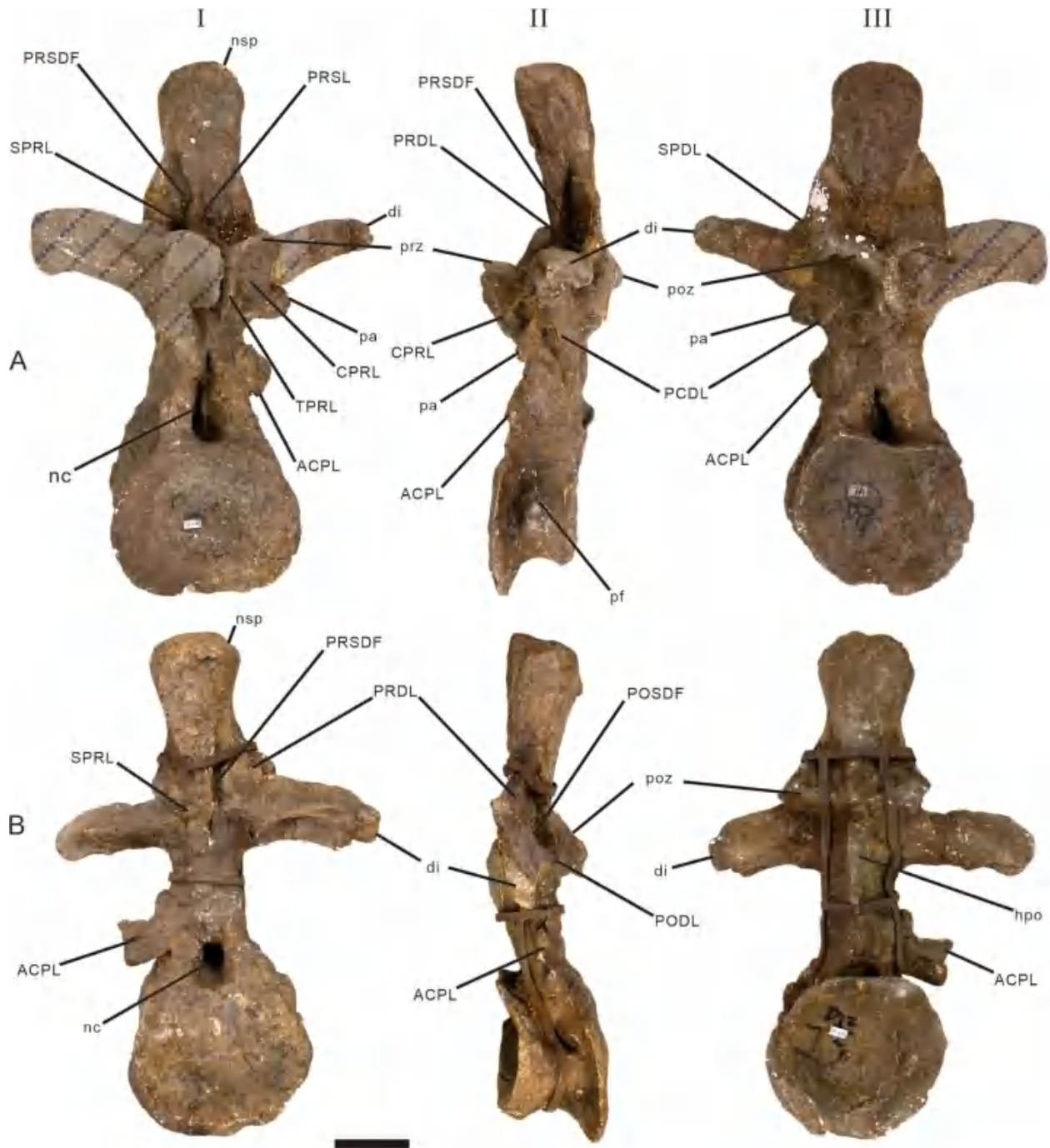the lateral surface and the transition of the two surfaces
is continuous.

Figure 12. Dashanpusaurus dongi holotype posterior dorsal vertebra and the first sacral vertebra. A, dorsal 13; B, sacral 1. I, anterior views; II, left lateral views; III, posterior views. Striped regions indicate reconstruction. Abbreviations: ACPL, anterior centroparapophyseal lamina; CPRL, centroprezygapophyseal lamina; di, diapophysis; hpo, hyposphene; nc, neural canal; nsp, neural spine; pa, parapophysis; pf, pneumatic fossa or foramen; PODL, postzygodiapophyseal lamina; poz, postzygapophysis; PRDL, prezygodiapophyseal diapophyseal lamina; PRSDF, prezygapophyseal spinodiapophyseal fossa; prz, prezygapophysis; SPDL, spinodiapophyseal lamina; SPRL, spinoprezygapophyseal lamina; TPRL, intraprezygapophyseal lamina. Scale bar = 50 mm.

No prominent pneumatic fossa exists on the lateral surface. A small concavity can be found on the lower portion of S4 behind the sacral rib in lateral view. A similar concavity is situated at the upper portion of the centrum near the posterior surface. In Bellusaurus sui a distinct lateral depression occupies the centra (Mo 2013). The lower part of the sacral rib occupies the whole anterior portion of the centrum on S2–4. It is a

robust element that extends laterally and dorsally from the ventral portion of the centrum.

The height of the neural arch is lower than that of each centrum and resembles those found in Camarasaurus lewisi and Bellusaurus sui (McIntosh et al. 1996b, pls 9, 10; Mo 2013, pl. 33). The anterior neural canal of S2 is invisible due to being covered by plaster. The posterior neural canal of S5 is sub-rectangular in outline with the long axis of this opening being transversely extended. The articular surfaces of the prezygapophyses are slightly projected dorsally in lateral view. Each prezygapophysis is covered by the previous postzygapophysis. The articular surface of the postzygapophysis projects ventrolaterally. The medial portion of the postzygapophysis extends medially to contact the CPOL. For the partly preserved posterior portion of the neural arch on S5, the hyposphene-hypantrum system is absent. The sacral rib is the most prominent element of the neural arch as it occupies the vast majority of parts of the neural arch and is near-vertically projected. The sacral rib is roughly 'C'-shaped with acetabular and alar 'arms' in anterior view. The ICF is situated at the middle portion of the sacral rib. The iliac articular surface of the sacral rib is irregularly concave. The articular surface of the upper arm on S3 for the ilium is sub-elliptical in outline with the long axis dorsoventrally extended, and the articular surface of S4 is sub-triangular in outline. The dorsal margin of the iliac articular surface is flat and it extends anteroposteriorly to contact with the prezygapophysis and postzygapophysis, respectively. The articular portion for the vertebra of sacral ribs is anteroposteriorly widened at the lateral ridge to the articular surface of the vertebrae. The portion below the iliac articular surface of the sacral rib weakly develops an inner curve to form the middle portion of the 'C'-shape. The lower articular surface of the sacral rib is not preserved. It is most likely that the articular surface of the sacral rib was as stout as the upper articular surface, based on the lower preserved portion of S3. The sacricostal yoke can be observed between S2 and S4 in left lateral view (Fig. 12).

The neural spines project dorsally and slightly anteriorly in lateral view, as occurred in most eusauropods such as Camarasaurus lewisi (McIntosh et al. 1996b, pl. 10). They differ from those in Bellusaurus sui in that the last neural spine of the sacral vertebrae of the latter taxon is oriented dorsoposteriorly (Mo 2013, pl. 33). All the sacral neural spines are fused. These are transversely compressed with a plate-like outline. The neural spines maintain this depth along the sacral vertebral series. The posterior surface of the sacral neural spines is generally parallel to the posterior articular surface of S4. The upper portion of the neural spine is mildly laterally expanded compared with the base of the neural spine. This distal ends of the fused neural spines do not consist of a dorsal 'plate', as occurs in Camarasaurus lewisi (McIntosh et al. 1996a, fig. 42), whereas this plate exists in Tastavinsaurus sanzi and many other sauropod taxa such as Mamenchisaurus youngi and most somphospondylans (Ouyang & Ye 2002, fig. 29; Canudo et al. 2008, fig. 5; Poropat et al. 2016). The distal ends of the neural spines are transversely convex and anteroposteriorly flat. The SPOLs are robust and extend from the base of postzygapophysis to the middle portion of the neural spines. The SPDL is absent on the sacral vertebrae. The lateral surfaces of the neural spines are irregularly flat.

Caudal vertebrae

Thirty-six total caudal vertebrae are preserved: 34 from the holotype and two anterior vertebrae from the paratype (Figs 14–21; see Tables 1 and 2 for measurements). The caudal vertebrae of the holotype are preserved in sequence, and immediately adjacent to the sacrum. The two paratype anterior caudals were isolated. Cd23 and 24 are mostly reconstructed and vertebrae after Cd34 are not preserved. Most of the partially preserved caudal vertebrae lack their neural arches. Rather than fully describing the anatomical features of each vertebra, we divided the preserved caudal series into three parts, and document changes along the sequence. We divided the preserved caudal vertebrae by referring to Tschopp et al. (2015, table 3) and Mannion et al. (2013). Cd1–8 are suggested as the anterior-most series with transverse processes extending onto the neural arch. The caudal vertebrae preserve normal transverse processes in Cd9–15 compared to the anterior-most ones – these are also suggested as part of the anterior series. We regarded Cd16–30 as middle caudal vertebrae as they lack transverse processes but retain well-developed neural spines and postzygapophyses. Due to reduction of the postzygapophyses we regard Cd31–4 as posterior caudal vertebrae. Based on the morphology of the posterior surface of the centrum, the diameters of the anterior and posterior articular surfaces, and the prominence of the neural arches on the preserved posterior vertebrae, we assume that there were originally other posterior caudals that were not preserved. Cd1 is defined as the first caudal vertebra following the first report of this taxon. In addition, although the transverse processes of Cd1 and 2 are missing, the robust PRDL and the laterally extended base of the neural spine indicates that these two caudal vertebrae were situated near the sacrum. Thus, we define the preserved Cd1 as the first caudal vertebra.
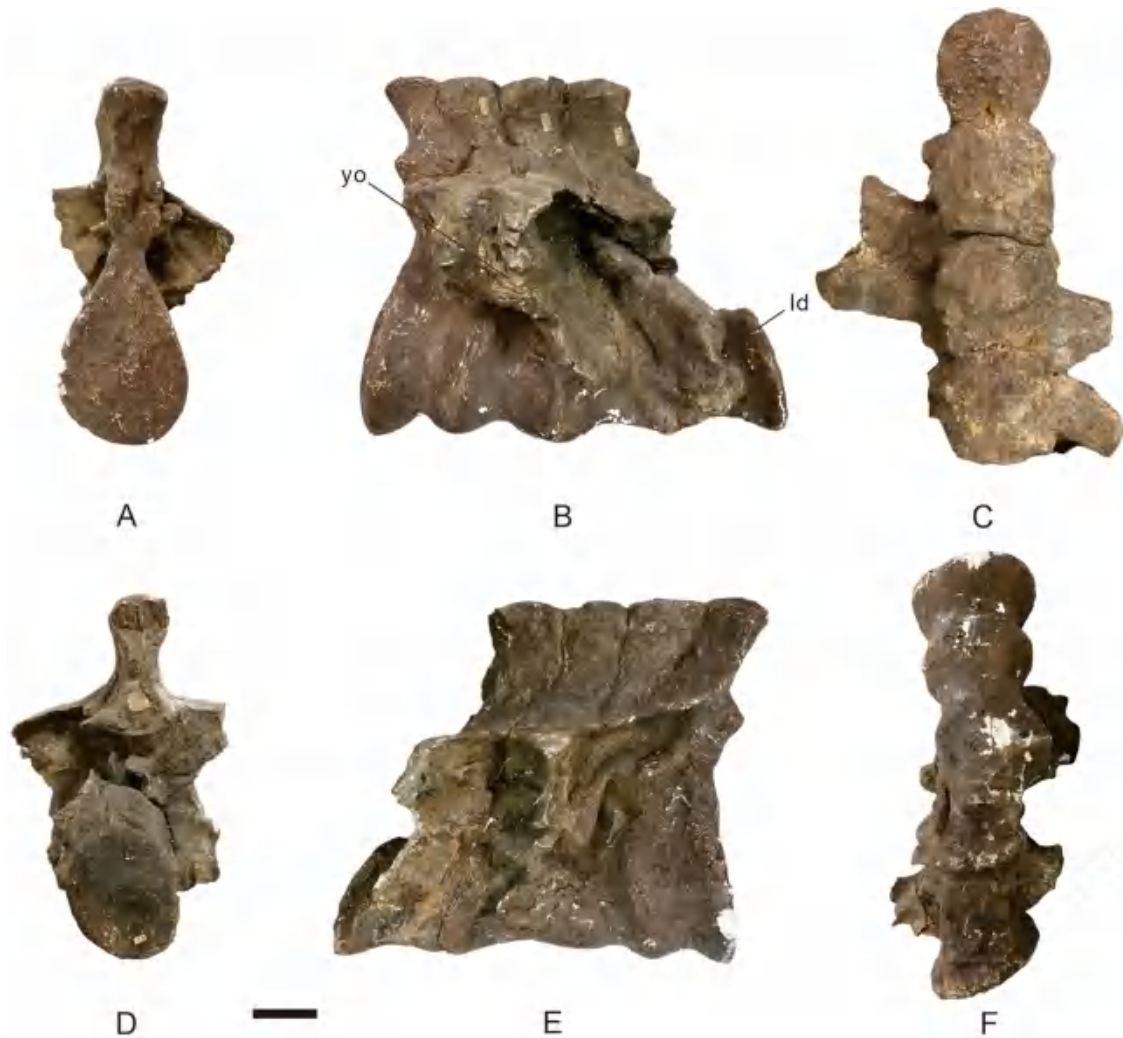
Figure 13. Dashanpusaurus dongi holotype sacral vertebrae 2–5. A, anterior view; B, left lateral view; C, dorsal view; D, posterior view; E, right lateral view; and F, ventral view. Abbreviations: ld, lateral depression; yo, sacricostal yoke. Scale bar = 50 mm.

Anterior caudal vertebrae. Centra of the anterior caudal vertebrae are generally amphiplatyan to amphicoelous (Figs 14–18; see Table 2 for measurements). The anterior-most caudal centra have concave anterior articular surfaces and a flat posterior articular surface, resembling those in Cd1 and 2 of Shunosaurus lii (Zhang 1988). The centra of subsequent caudal vertebrae are amphicoelous. Amphicoelous caudal centra are also known in Camarasaurus lewisi and most other early-diverging sauropod taxa such as Shunosaurus lii and Omeisaurus tianfuensis (Zhang 1988; McIntosh et al. 1996b, pls 12–14). In addition, some of the anterior caudal centra are more similar to those of sauropod taxa such as Lourinhasaurus alenquerensis with concave anterior and flat posterior articular surfaces, respectively (Mocho et al. 2014, fig. 12). The centra differ from those of Bellusaurus sui, which have procoelous anterior

centra (Mo 2013, pls 35, 36). The anteroposterior lengths of the anterior centra are uniform in morphology, a condition similar to that of most sauropods except for a few taxa (e.g. Tornieria africana: Remes 2006). The ratio of the anteroposterior length of each centrum to the mean average diameter of the anterior articular surface is about 0.60 on the anterior-most caudals, with subsequent anterior caudals having ratios of 0.8–1.0. The same ratio in Camarasaurus lewisi is ∼0.59 on the anterior-most caudals and around 0.77 on subsequent ones (McIntosh et al. 1996b, table 7). Most of the anterior centra are transversely compressed, with a few being dorsoventrally compressed. The condition of this change is similar to that in Omeisaurus tianfuensis and Camarasaurus lewisi (He et al. 1988, table 10; McIntosh et al. 1996b, table 7). Some early-diverging sauropods, such as Vulcanodon karibaensis and
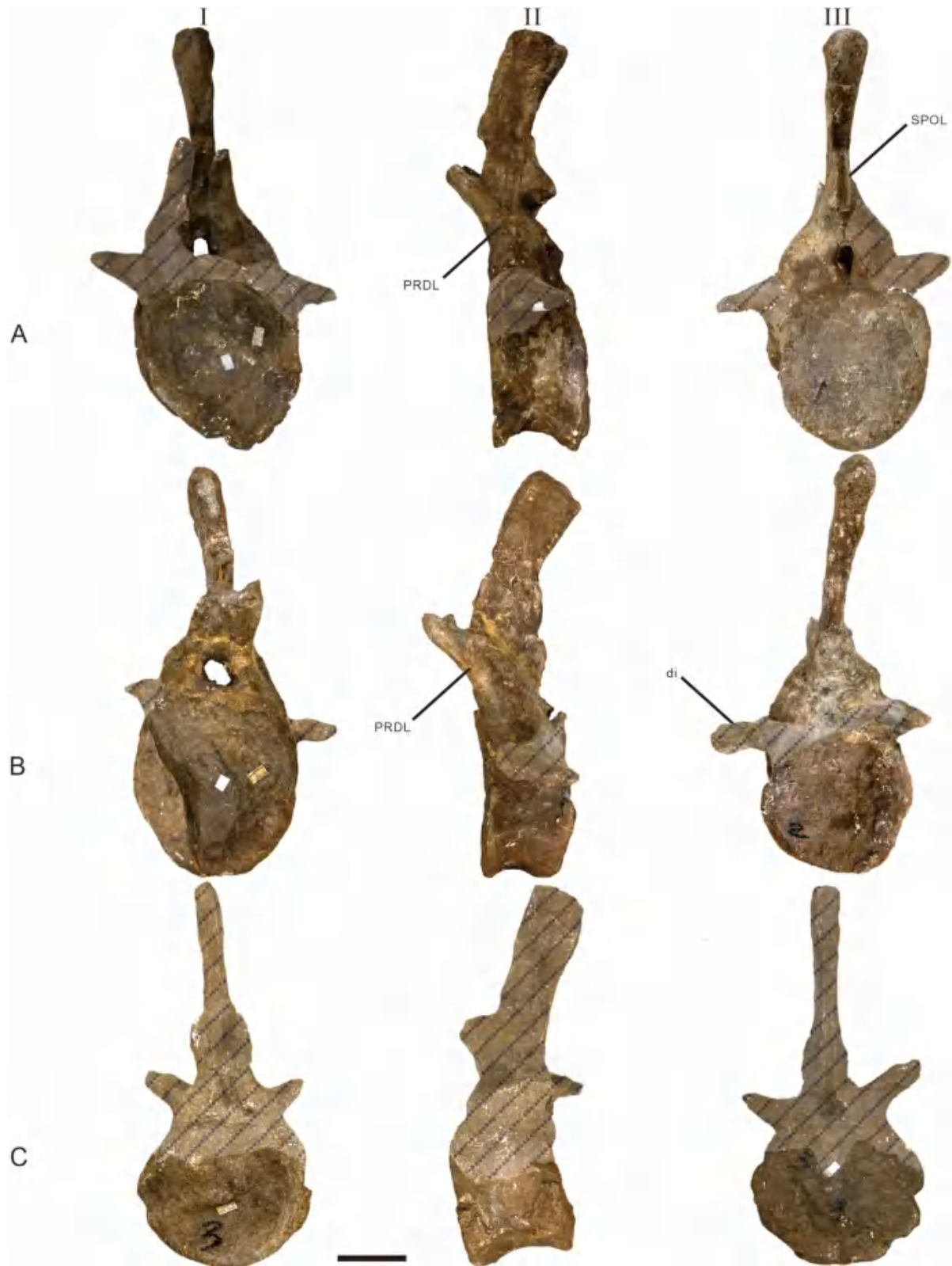
Figure 14. A–C, Dashanpusaurus dongi holotype caudal vertebrae 1–3. I, anterior views; II, left lateral views; III, posterior views. Striped regions indicate reconstruction. Abbreviations: di, diapophysis; PRDL, perzygodiapophyseal diapophyseal lamina; SPOL, spinopostzygapophyseal lamina. Scale bar = 50 mm.

Shunosaurus lii, bear transversely compressed anterior centra (Cooper 1984, fig. 13; Zhang 1988, table 7), whereas many sauropods, such as Cetiosaurus oxoniensis and Mamenchisaurus youngi, share dorsoventrally compressed anterior caudal centra (Ouyang & Ye, 2002, table 7; Upchurch & Martin 2003, fig. 6). The ventral surfaces of the anterior-most centra are transversely convex with no excavations or ridges. The ventrolateral ridge is absent on the anterior-most centra, whereas it is present on Cd9. The ventral surfaces of the anterior caudal vertebrae from the paratype are transversely concave. Furthermore, no shallow ventrolateral ridges are located on the anterior caudal vertebra, similar to that in Bellusaurus sui (Mo 2013, pl. 35). A ventral concavity exists on Cd8–12 and it is anteroposteriorly and transversely concave. This concavity is prominent on Cd9 and gradually becomes shallower to Cd12, and it is absent on subsequent anterior caudal vertebrae. The lateral pneumatic fossa is absent from the anterior caudal series.

Neural arches of the anterior caudal vertebrae are anteriorly situated on the anterior caudal centra, as in Camarasaurus lewisi (McIntosh et al. 1996a, figs 43–47). The neural canals are elliptical in outline and widen dorsally. The prezygapophyses are narrow. The prezygapophyses are steeply inclined anterodorsally on the anterior caudal vertebrae when viewed laterally. They extend beyond the anterior articular surfaces of the centra. The articular surfaces of the prezygapophyses are dorsomedially oriented. They are oriented at ∼75° to the horizontal. The postzygapophyses do not extend beyond the posterior articular surface just above the middle portion of each centrum. They project mediolaterally and then are medially curved to the dorsal surface of the neural canal. Laminae are poorly developed, as in other early-diverging sauropod taxa. The PRDL, SPRL and SPOL are present on the anterior caudal vertebrae. As with most sauropods, the PRDL is robust. The transverse process disappears after Cd15, a condition common in most sauropod taxa, exceptions to this being Camarasaurus lewisi and Analong chuanjieensis in which the transverse processes disappear after Cd10 (McIntosh et al. 1996b, pl. 14; Ren et al. 2021). By contrast, the lamination on the paratype caudal vertebrae is poorly developed. Only the PRDL and SPRL are observable in the two vertebrae (Cd1 and 2; Fig. 14A, B). Furthermore, the SPRLs of the paratype are small, short ridges that rapidly fade out onto the anterolateral margins of the neural spines. The transverse process is situated on the dorsal margin of a centrum. The cross-section of each transverse process is elliptical in outline. No tubercle or concavity exists on the dorsal or ventral surface of the transverse processes. The transverse process is triangular and tapers distally, similar to that in

Camarasaurus lewisi (McIntosh et al. 1996b, pl. 12). The transverse processes are ventrolaterally projected, again similar to that in Camarasaurus lewisi. This condition is common in most sauropods, such as Tazoudasaurus naimi and Omeisaurus tianfuensis (He et al. 1988, fig. 34; Allain & Aquesbi 2008, fig. 15).

The height of the anterior neural spine is greater than the height of the posterior articular surface of each centrum. The neural spines are laterally expanded distally. The distal ends of neural spines are transversely convex and anteroposteriorly flat, with an irregularly flat central portion. The transitions between the distal surface and lateral surfaces are continuous. Laterally, the neural spines project dorsoposteriorly and are slightly curved in the holotype, whereas the neural spines of the paratype are straight. These are plate-like in outline and roughly quadrilateral in cross section. The neural spines are transversely compressed. This condition is similar to that in Camarasaurus lewisi (McIntosh et al. 1996b, pl. 11). The SPRL extends from the base of the prezygapophysis to the middle portion of the neural spine. By contrast, the SPOLs extend from the distal end of the postzygapophysis to the middle portion of the neural spine.

Middle caudal vertebrae. Most of the middle caudal vertebrae are only partially preserved, with reconstructed neural arches and neural spines (Figs 19–21A; see Table 2 for measurements). All the centra of the middle caudal vertebrae are amphicoelous. The anteroposterior lengths of the centra are slightly shorter than the anterior caudal vertebral series. All of the anterior and posterior articular surfaces are sub-circular in outline. The ventral surface is transversely and anteroposteriorly concave. The narrow concavity of the ventral surface anteroposteriorly extends to both the anterior and posterior margins of the articular surfaces. A ventrolateral ridge is absent on the ventral surface. The lateral margin of the ventral surface merges with the lateral surface smoothly. In ventral view, the lateral surfaces are prominently concave, and the narrowest part of the ventral surface is situated in the middle portion. Some lateral surfaces of the centra are irregularly concave with low ridges anteroposteriorly extended from the centrum (e.g. Fig.19B, C). The lateral pneumatic fossa is absent from the lateral surface, as with most sauropod taxa.

The heights of the neural arches of the middle caudal vertebrae are much shorter than those of the centra. These are about one-half to one-third the height of the posterior articular surfaces. The neural arches are located over the midpoint and occupy the anterior portion of the dorsal margin of each centrum. The neural canals are elliptical in outline, with a dorsal margin narrower than the ventral margin. The prezygapophyses are narrowly extended. These projections are anterodorsally
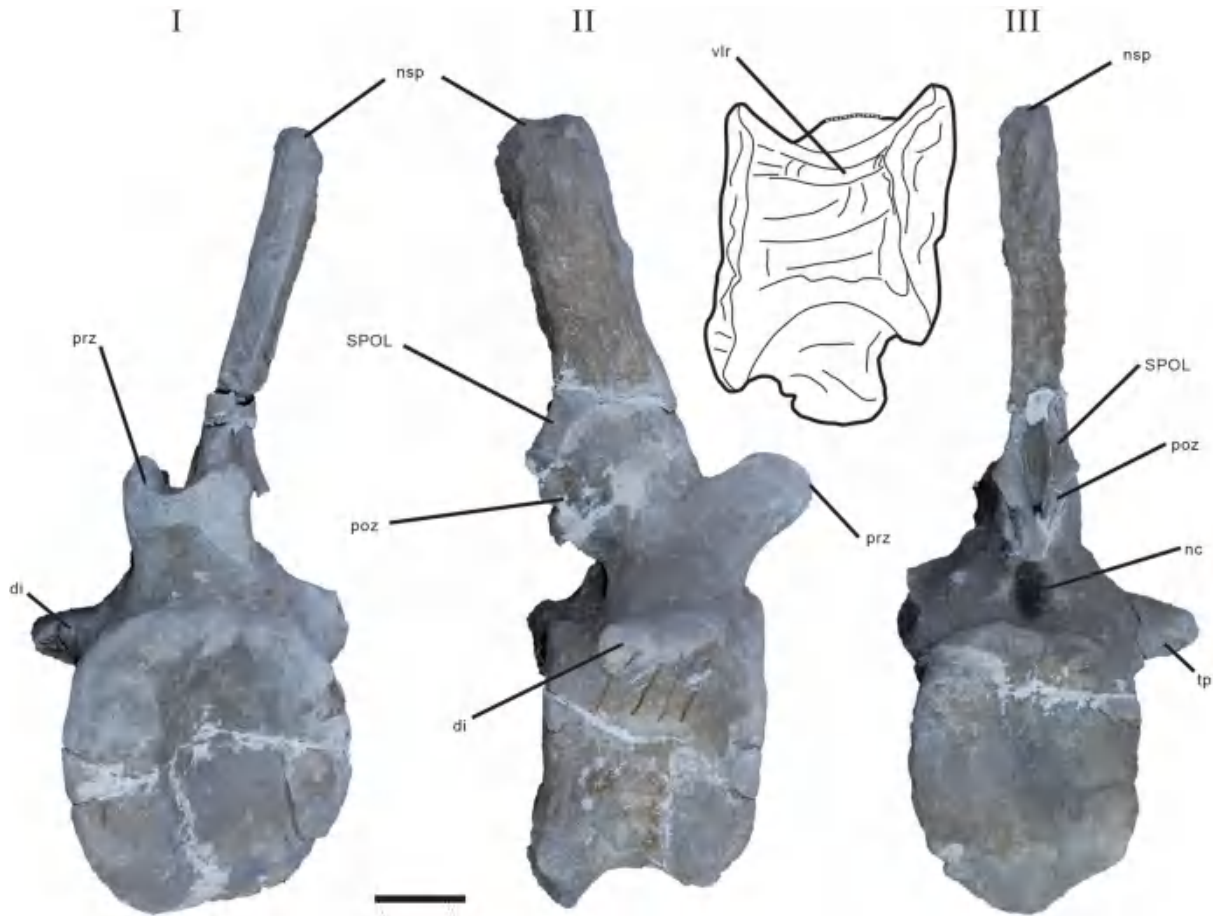
Figure 15. Dashanpusaurus dongi paratype anterior caudal vertebra in (I) anterior, (II) right lateral and (III) posterior views. Abbreviations: di, diapophysis; nc, neural canal; nsp, neural spine; prz, prezygapophysis; poz, postzygapophysis; SPOL, spinopostzygapophyseal lamina; vlr, ventrolateral ridge. Scale bar = 50 mm.

beyond the anterior articular surface of the centrum. The articular surfaces of the prezygapophyses are dorsolaterally oriented. These are oriented at ~80° to the horizontal. The postzygapophyses do not extend beyond the posterior articular surface of each centrum.

Posterior caudal vertebrae. Four posterior caudal vertebrae are present (Cd31–34) and are partly preserved, with incomplete neural arches and spines (Fig. 21B–E; see Table 2 for measurements). The centrum of the posterior caudal vertebra is amphicoelous. The ventral surface is transversely convex and anteroposteriorly concave with a small anteroposteriorly extended, low ventral ridge situated in the mid-centrum. Two concavities are located on the central portion of the anterior and posterior margins of the ventral surface, respectively. In ventral view, the lateral margins are concave with the concavity located on the middle portion. The transition between the ventral and lateral surfaces is continuous. Low ridges extend anteroposteriorly on the lateral surface. The lateral pneumatic fossa is absent from the lateral surface. The preserved distal end of the neural spine extends beyond the posterior articular surface.

Scapula

Only the left scapula from the paratype is partially preserved. The posterior end of the scapular blade and the acromion are incomplete (Fig. 22A, B; see Table 3 for measurements). We describe the scapula and coracoid with its long axis orientated horizontally. The scapular blade is dorsoposteriorly expanded and becomes increasingly robust ventrally and dorsally towards the stout distal end, resembling the condition found in Rebbachisaurus garasbae and Shunosaurus lii (Zhang 1988, fig. 43; Wilson & Allain 2015, fig. 13). By contrast, the distal end does not extend ventrally in sauropod taxa such as Bellusaurus sui, Yuanmousaurus jiangyiensis and Omeisaurus tianfuensis (He et al. 1988,
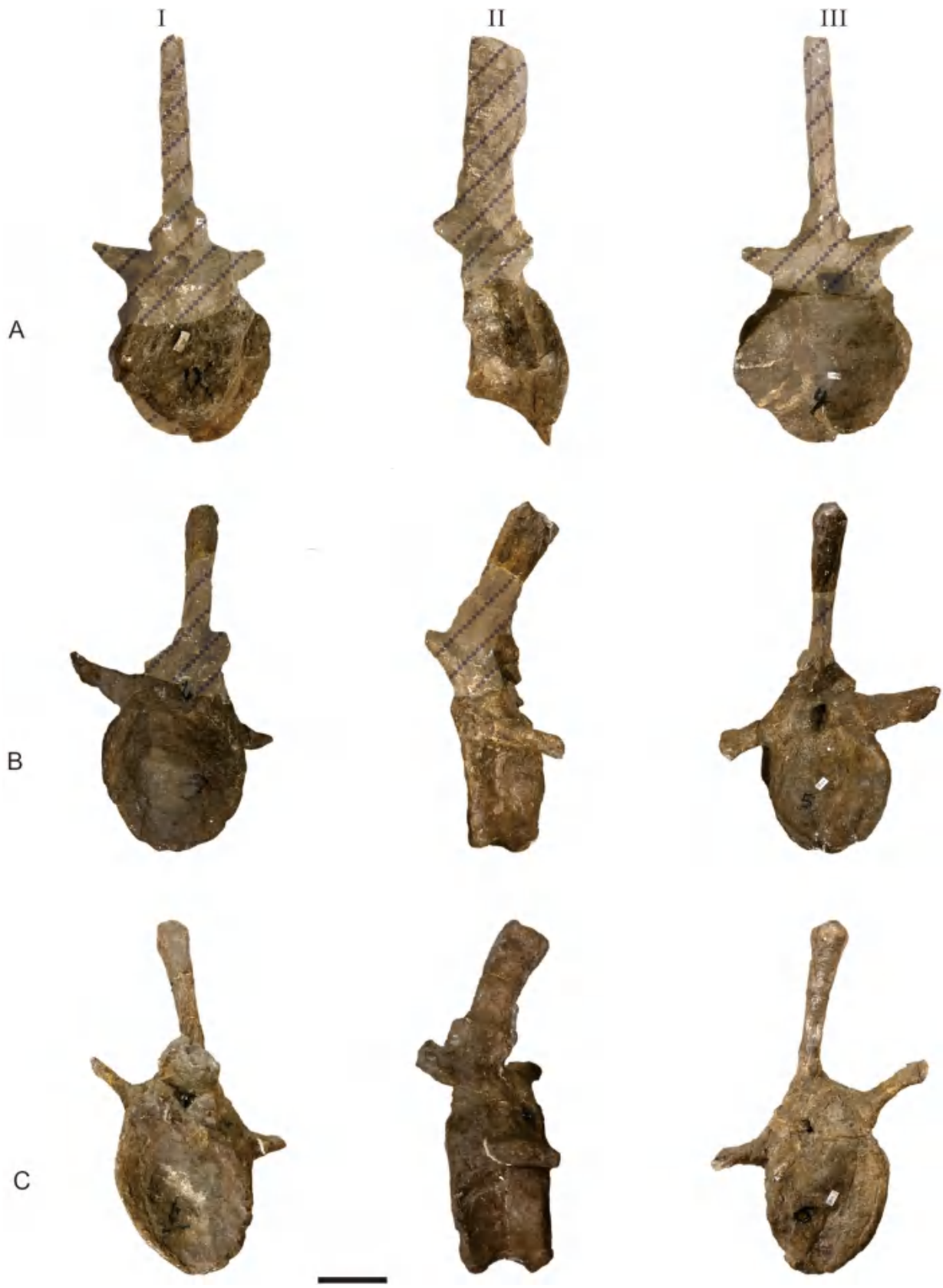
Figure 16. A–C, Dashanpusaurus dongi holotype caudal vertebrae 4–6. I, anterior views; II, left lateral views; III, posterior views. Striped regions indicate reconstruction. Scale bar = 50 mm.

fig. 41; Lü et al. 2006, fig. 7; Mo 2013, pl. 46). In anterodorsal view, the scapular blade is moderately medially curved with the proximal end being more deflected. The ratio of the maximum dorsoventral height of the scapular blade vs the minimum dorsoventral height of the scapular blade is >2.0, similar to the condition present in Omeisaurus tianfuensis, Apatosaurus ajax and Chubutisaurus insignis (He et al. 1988; Upchurch et al. 2004a; Carballido et al. 2011a). In cross-section the scapular blade is 'D'-shaped, as in many sauropod taxa such as Camarasaurus lewisi, Apatosaurus ajax, Haplocanthosaurus priscus and Amargasaurus cazaui (Hatcher 1903; Salgado & Bonaparte 1991; McIntosh et al. 1996a; Upchurch et al. 2004a).

The lateral surface of the expanded proximal plate bears a wide shallow concavity that occupies the anterior and dorsal portions, defined by an acromial ridge caudally (Fig. 22). According to the preserved portion, the acromial ridge is well developed, as in most neosauropods (Upchurch et al. 2004b). The posterior margin of the shallow concavity is defined by the acromial ridge in the upper part of the proximal plate and is much more prominent in Apatosaurus ajax, Bellusaurus sui and some other taxa such as Mamenchisaurus youngi (Ouyang & Ye 2002, fig. 33; Upchurch et al. 2004a, fig. 4; Mo 2013, pl. 46). The bounds of this concavity are a low, broad ridge that extends anterodorsally forming an angle of ∼60° with the long axis of the scapular blade (Fig. 22), similar to that in Bellusaurus sui (basal portion: 75°) and Apatosaurus ajax (70°) (Upchurch et al. 2004a, fig. 4; Mo 2013, pl. 46). Laterally, the coracoid articulation is perpendicular to the long axis of the scapular blade, similar to Omeisaurus tianfuensis (He et al. 1988, fig. 41). This differs from what is found in some taxa where the same concavity and long axis of the scapula form an acute angle (e.g. Shunosaurus lii: Zhang 1988, fig. 43; Bellusaurus sui: Mo 2013, pl. 46). The scapular blade becomes increasingly expanded ventrally towards the glenoid. The scapular glenoid is subtriangular in shape. The articular surface of the glenoid is slightly concave and slightly laterally oriented.

Coracoid

The left coracoid from the paratype is well preserved (Fig. 22C–E; see Table 3 for measurements). This element is most robust at the glenoid. Towards its dorsal margin, the coracoid narrows transversely. The anterior margin is intermediate in thickness between the glenoid area and the dorsal margin. The lateral surface is convex, especially the central area around the coracoid foramen, whereas the medial surface is deeply concave. The articular surface of the glenoid is sub-triangular and dorsoventrally expanded in outline with a convex medial

margin and straight posteromedial and posterior margin where it articulates with the scapula. The ratio of the anteroposterior length of the coracoid to the maximum length of scapula-coracoid articulation is <1.5. The morphology of the anterodorsal margin of the coracoid is rounded, resembling that in many taxa such as Camarasaurus lewisi (McIntosh et al. 1996a, fig. 61). The coracoid foramen is elliptical and situated at midheight of the coracoid dorsoventrally, close to the junction with the scapula. The coracoid foramen can be observed on both lateral and medial surfaces and perforates the bone posteromedially. In lateral view, the dorsal and anterior margins of the coracoid merge smoothly into each other. The infraglenoid lip of the coracoid is absent, similar to that in most sauropods such as Camarasaurus lewisi (McIntosh et al. 1996a, fig. 61).

Humerus

The left humerus of the paratype is well preserved (Fig. 23A–F; see Table 3 for measurements). The HRI (the average of the greatest widths of the proximal end, midshaft, and distal end of humerus/length of the humerus) value is 0.32. In anterior view, the proximal and distal portions of the humerus expand gradually towards the lateral and medial margins, giving the proximal end a 'fan'-like shape. The proximal width is 45% of the total length of the humerus. Generally, a value of 0.4 or greater is plesiomorphic for eusauropods and is present in nearly all non-turiasaurian and non-neosauropod sauropods (e.g. Shunosaurus lii [0.48], Cetiosaurus oxoniensis [0.40], Mamenchisaurus youngi [0.42]; Bellusaurus sui [0.41]; Tehuelchesaurus benitezii [44%]) and greater than that in Camarasaurus lewisi (0.36), Lourinhasaurus alenquerensis (0.39) and Galveosaurus herreroi (0.32) (He et al. 1988, table 9; McIntosh et al. 1996b, table 9; Ouyang & Ye 2002, table 8; Upchurch & Martin 2003, table 3; Sánchez-Hernández 2005; Carballido et al. 2011b, fig. 15; Mo 2013, pl. 48; Mocho et al. 2014; Xu et al. 2018). In lateral view, the anterior margin of the articular surface is anteriorly extended (Fig. 23) in Dashanpusaurus dongi, similar to Camarasaurus lewisi (McIntosh et al. 1996a, fig. 62F). In contrast, it is weak in Bellusaurus sui and some early-diverging taxa such as Omeisaurus (He et al. 1988, fig. 44; Tang et al. 2001; Mo 2013, pl. 48). The humeral head extends posteriorly in dorsal view, similar to Euhelopus zdanskyi, whereas a distinctive humeral head is absent in most non-neosauropod sauropods (Poropat et al. 2016). In proximal view, the proximal surface of the humerus is sigmoidally curved from the medial margin of the humerus to the lateral margin, as in Camarasaurus lewisi and Bellusaurus sui. The supracoracoideus tuberculum is absent on the proximolateral
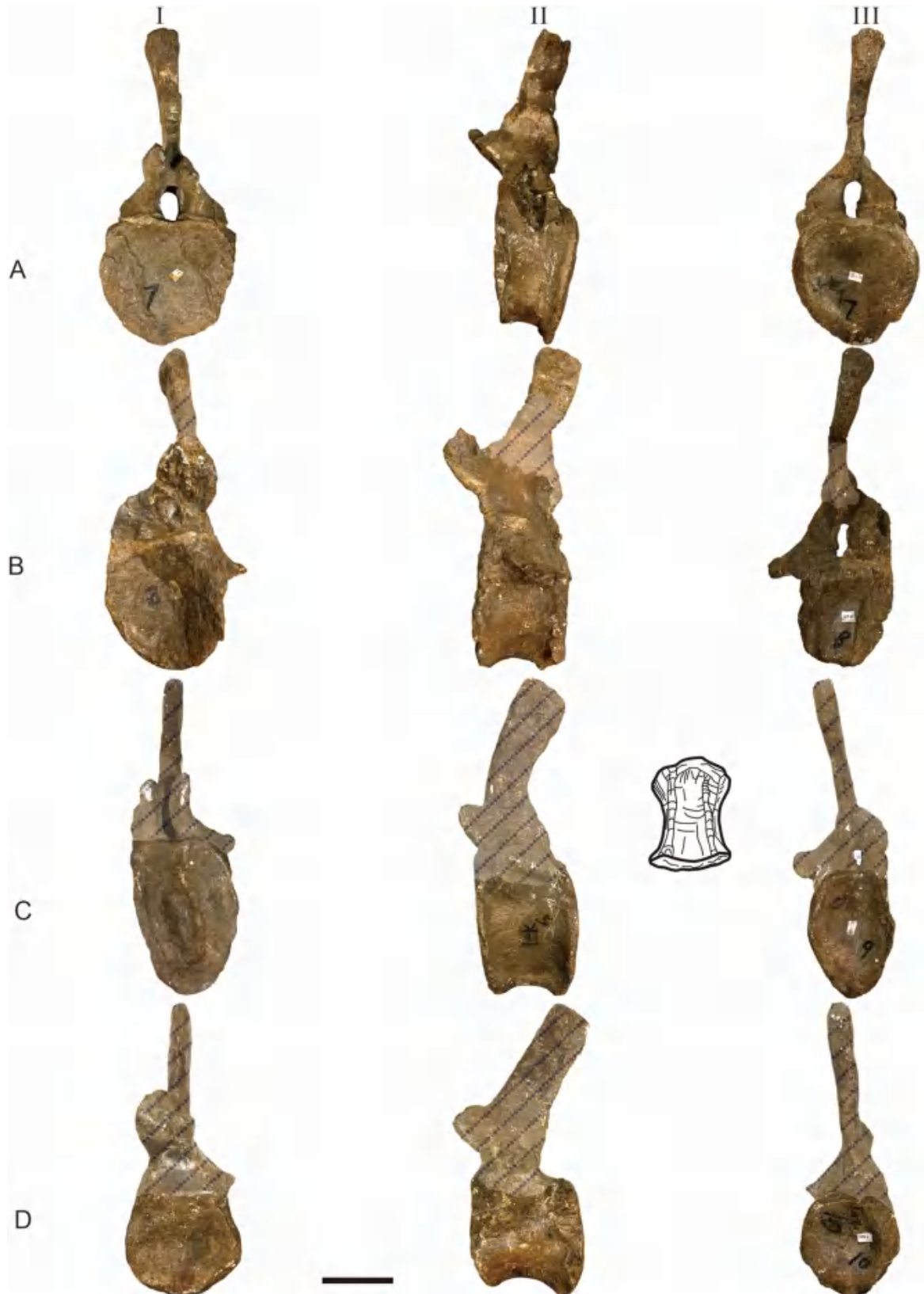
Figure 17. A–C, Dashanpusaurus dongi holotype caudal vertebrae 7–10. I, anterior views; II, left lateral views; III, posterior views. Striped regions indicate reconstruction. Scale bar = 50 mm.
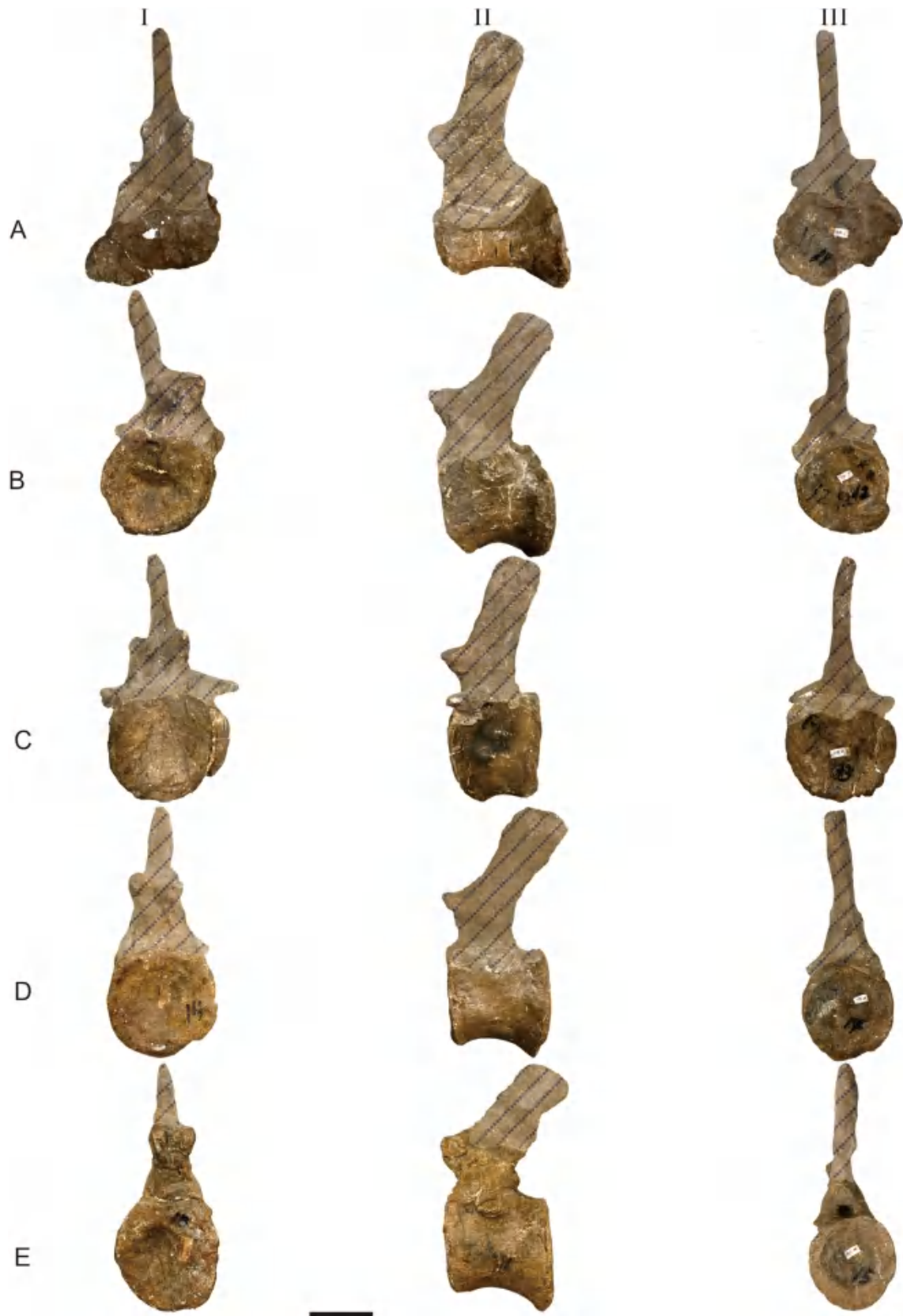
Figure 18. A–C, Dashanpusaurus dongi holotype caudal vertebrae 11–15. I, anterior views; II, left lateral views; III, posterior views. Striped regions indicate reconstruction. Scale bar = 50 mm.
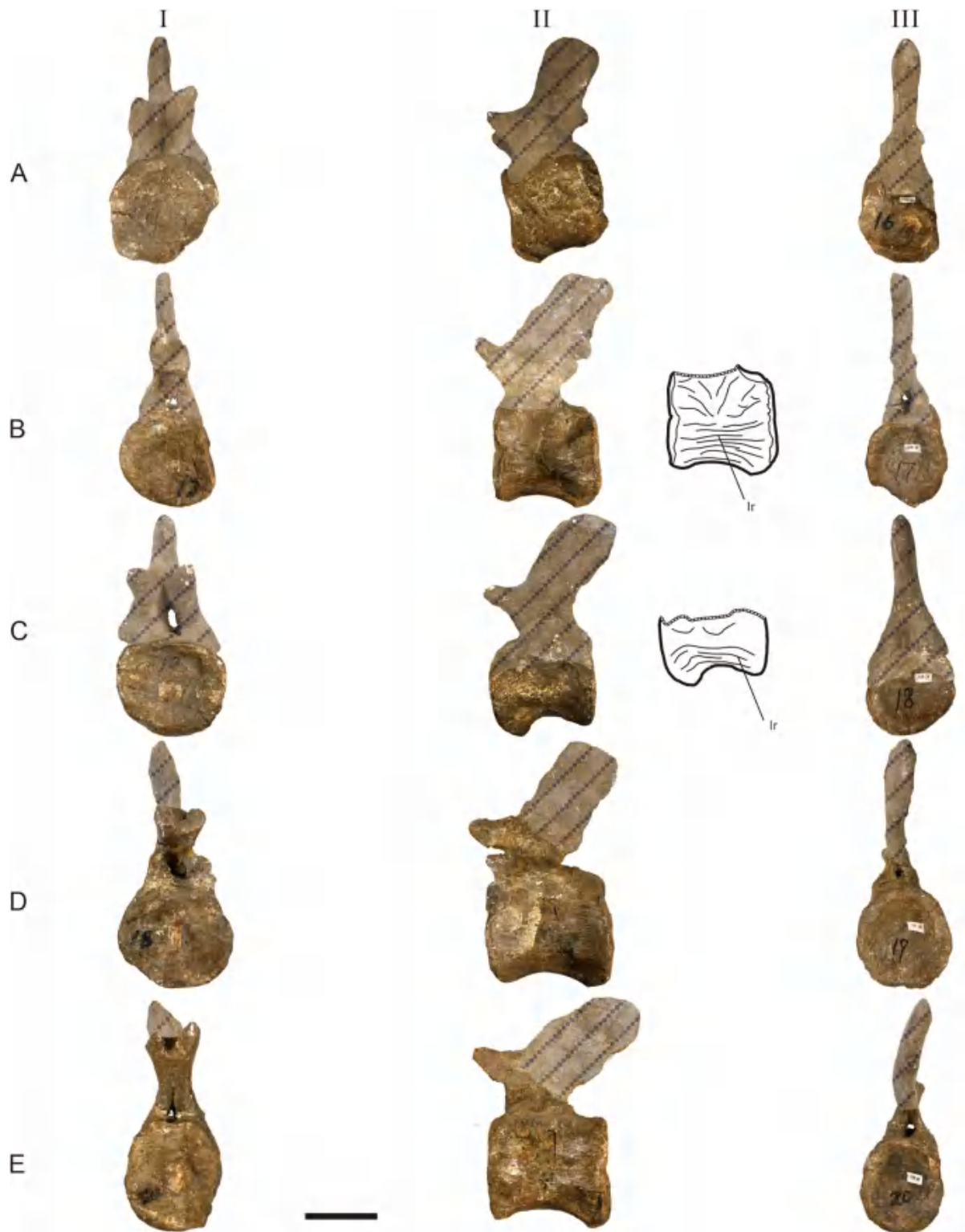
Figure 19. A–C, Dashanpusaurus dongi holotype caudal vertebrae 16–20. I, anterior views; II, left lateral views; III, posterior views. Striped regions indicate reconstruction. Abbreviation: lr, lateral ridge. Scale bar = 50 mm.

Figure 20. A–G, Dashanpusaurus dongi holotype caudal vertebrae 21–29 (excluding 23 and 24). I, anterior views; II, left lateral views; III, posterior views. Striped regions indicate reconstruction. Scale bar = 50 mm.

Figure 21. A–G, Dashanpusaurus dongi holotype caudal vertebrae 30–34. I, anterior views; II, left lateral views; III, posterior views. Striped regions indicate reconstruction. Scale bar = 50 mm.

portion of the humerus, differing from some other neo-sauropods with a prominent supracoracoideus tuberculum, such as Suuwassea emilieae, Opisthocoelicaudia skarzynskii and Saltasaurus loricatus (Borsuk-Bialynicka 1977, fig. 7; Powell 1992, fig. 31; Harris 2006, fig. 3).

The length of the deltopectoral crest is ∼0.45 the total length of the humerus (in Camarasaurus lewisi it is 0.43). It is orientated slightly anterolaterally, which is similar to the condition found in Camarasaurus lewisi and Bellusaurus sui. By contrast, some sauropod taxa (e.g. Opisthocoelicaudia skarzynskii) share an anteromedially orientated deltopectoral crest (Borsuk-Bialynicka 1977, fig. 7). The deltopectoral crest is restricted to the lateral margin of the humerus, this condition resembling most sauropods such as Camarasaurus lewisi. The cross-section of the midshaft is elliptical, similar to that in Camarasaurus lewisi and Bellusaurus sui. This feature is plesiomorphic for gravisaurians. The width of the cross section is 0.18 of the total length of the humerus, which is a little greater than Camarasaurus lewisi (0.15) and Bellusaurus sui (0.15) (McIntosh et al. 1996b, table 9; Mo 2013, pl. 48), and 0.15 or more is plesiomorphic for sauropods (Moore et al. 2020).

The distal end of the humerus is quadrilateral in shape, and the two condyles are slightly convex with coarse surfaces. The distal width is 0.33 of the total length of the humerus. The anteroposterior length of the radial condyle is similar to the ulnar condyle, as occurs in Bellusaurus sui and some mamenchisaurids (e.g. Omeisaurus tianfuensis) (He et al. 1988, fig. 44; Mo 2013, pl. 48). Four minute ridges are situated on the
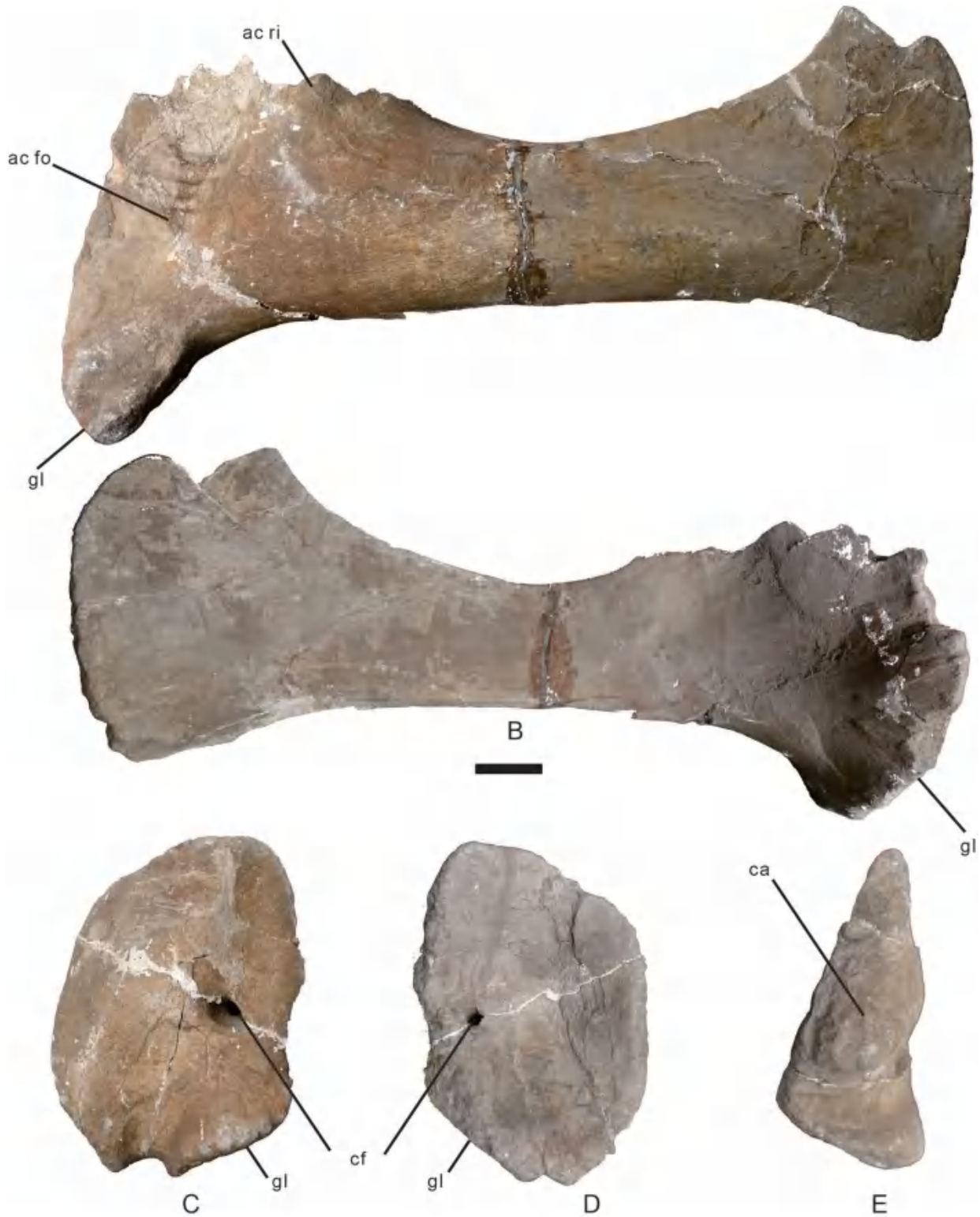
Figure 22. A, B, Dashanpusaurus dongi paratype left scapula; and C–E, coracoid. A and C, lateral views; B and D, medial views; E, posterior view. Abbreviations: ac fo, acromial fossa; ac ri, acromial ridge; ca, coracoid articular surface; cf, coracoid foramen; gl, glenoid. Scale bar = 100 mm.

Table 3. Measurements of pectoral girdle and forelimb of paratype. An asterisk (*) denotes a measurement based on an incomplete element. All measurements are in millimetres. Abbreviation: HRI, the average of the greatest widths of the proximal end, mid-shaft and distal end of humerus/length of humerus (after Wilson & Upchurch 2003).

Element	Dimension	Measurement
Scapular (left)	Total straight-line length (from junction with coracoid to the distal tip of the scapular blade)	1060
	Width of distal part of scapular blade	390*
	Width of narrowest part of scapular blade	171
	Maximum transverse thickness of the distal end of scapular blade	54
	Maximum width of the proximal expansion of the scapula (between the anterodorsal and posteroventral corners)	390*
	Length of glenoid surface along its long axis	192*
	Transverse width of the glenoid (measured at the junction with the coracoid)	143
Coracoid (left)	Anteroposterior length on lateral surface	325
	Dorsoventral length on lateral surface	518
	Transverse width of scapular articular surface	148
	Dorsoventral length of scapular articular surface	290*
	Transverse width of the glenoid (measured at the junction with the scapula)	119
	Dorsoventral length of the glenoid	215
Humerus (left)	Length	935
	Proximal end maximum mediolateral width	414
	Proximal end maximum anteroposterior width	161
	Distance from proximal end to distal tip of deltopectoral crest	363
	Mediolateral width at midshaft	167
	Anteroposterior width at midshaft	83
	Distal end maximum mediolateral width	313
	Distal end maximum anteroposterior width	142
	HRI	0.32
Left radius (left)	Length	614
	Proximal end maximum mediolateral width (long axis)	191
	Proximal end maximum anteroposterior width	68
	Mediolateral width at midshaft	85
	Anteroposterior width at midshaft	55
	Distal end maximum mediolateral width	143
	Distal end maximum anteroposterior width	95

anterodistal edge of the humerus. Some taxa share two accessory processes on the anterodistal edge of the humerus (e.g. mamenchisaurids, Patagosaurus fariasi, Apatosaurus ajax, Bellusaurus sui). All of the ridges are slightly convex, extending along the lower portion of the shaft. Moreover, several ridges extend along the long axis to the upper portion of the humeral anterior surface.

Radius
The paratype left radius is well preserved (Fig. 23G–M; see Table 3 for measurements). The length of the radius is 0.66 the length of the humerus; similar to that in Camarasaurus lewisi (0.71), Bellusaurus sui (0.60), Lourinhasaurus alenquerensis (0.73) and Tehuelchesaurus benitezii (0.66) (McIntosh et al. 1996b, table 9: Rich et al. 1999; Mo 2013, pls 48, 50; Mocho

et al. 2014). Proximally, the maximum width of the radius is 23% of the total length (Camarasaurus lewisi is 24%; Bellusaurus sui is 33%; Lourinhasaurus alenquerensis is 25%; Tehuelchesaurus benitezii is 35%). The proximal end is nearly oval in outline with a mildly concave medial surface that meets the anteromedial process of the ulna. This shape of the proximal end is similar to that of Camarasaurus lewisi, Bellusaurus sui and early-diverging sauropods (e.g. Vulcanodon karibaensis, Shunosaurus lii, Barapasaurus tagorei) (Dong et al. 1983; Cooper 1984; McIntosh et al. 1996a; Tang et al. 2001; Bandyopadhyay et al. 2010; Mo 2013). The surface of the proximal end is nearly flat with a slightly concave area along the central portion, and there is a bump oriented anteromedially (which is also present in some mamenchisaurids, Patagosaurus fariasi, Camarasaurus lewisi and Saltasaurus loricatus:

Figure 23. A–F, Dashanpusaurus dongi paratype left humerus; and G–M, radius. A and G, anterior views; B and H, posterior views; C and J, medial views; D and I, lateral views; E and K, proximal views; F and M, distal views; L, cross section of radius. Abbreviations: acf, anconeal fossa; AP, accessory process; bde, bevelled distal end; dpc, deltopectoral crest; lc, lateral condyle; mc, medial condyle; M. cor, tuberosity for attachment of M. coracobrachialis; mp, medial process; pmcr, posteromedial convex of lower part of radius; pp, posterior process. Scale bar = 100 mm.

Bonaparte 1986b, fig. 60; He et al. 1988, fig. 45; Powell 1992, fig. 33; McIntosh et al. 1996b, pl. 18F; Sekiya 2011, fig. 43A). The dorsal surface of the proximal end is nearly perpendicular to the long axis of the shaft, resembling that in Camarasaurus lewisi and Bellusaurus sui (McIntosh et al. 1996b, pl. 18; Mo 2013, pl. 50). By contrast, the posterior portion of the radial proximal end is posterodorsally projected, and the middle portion of the radial proximal end is prominently concave in Lourinhasaurus alenquerensis and Tehuelchesaurus benitezii (Rich et al. 1999, fig. 12; Mocho et al. 2014, fig. 16). The cross-section of the radial midshaft is elliptical.

The distal surface of the radius is flat, with an elliptical outline. A prominent elongated convex area exists on the posteromedial surface of the distal portion (Fig. 23H), as occurs in Camarasaurus lewisi, and other taxa such as mamenchisaurids (McIntosh et al. 1996b, pl. 18G; Ren et al. 2020, fig. 4). The radial distal condyle is nearly perpendicular relative to the long axis of the shaft with a rugose articular surface. This condition resembles that found in other sauropods (e.g. Shunosaurus lii, Camarasaurus lewisi, Apatosaurus ajax, Bellusaurus sui, Alamosaurus: Gilmore 1946, fig. 7; He et al. 1988, fig. 47; McIntosh et al. 1996b, pl. 18; Upchurch et al. 2004a, fig. 6; Mo 2013, pl. 50).
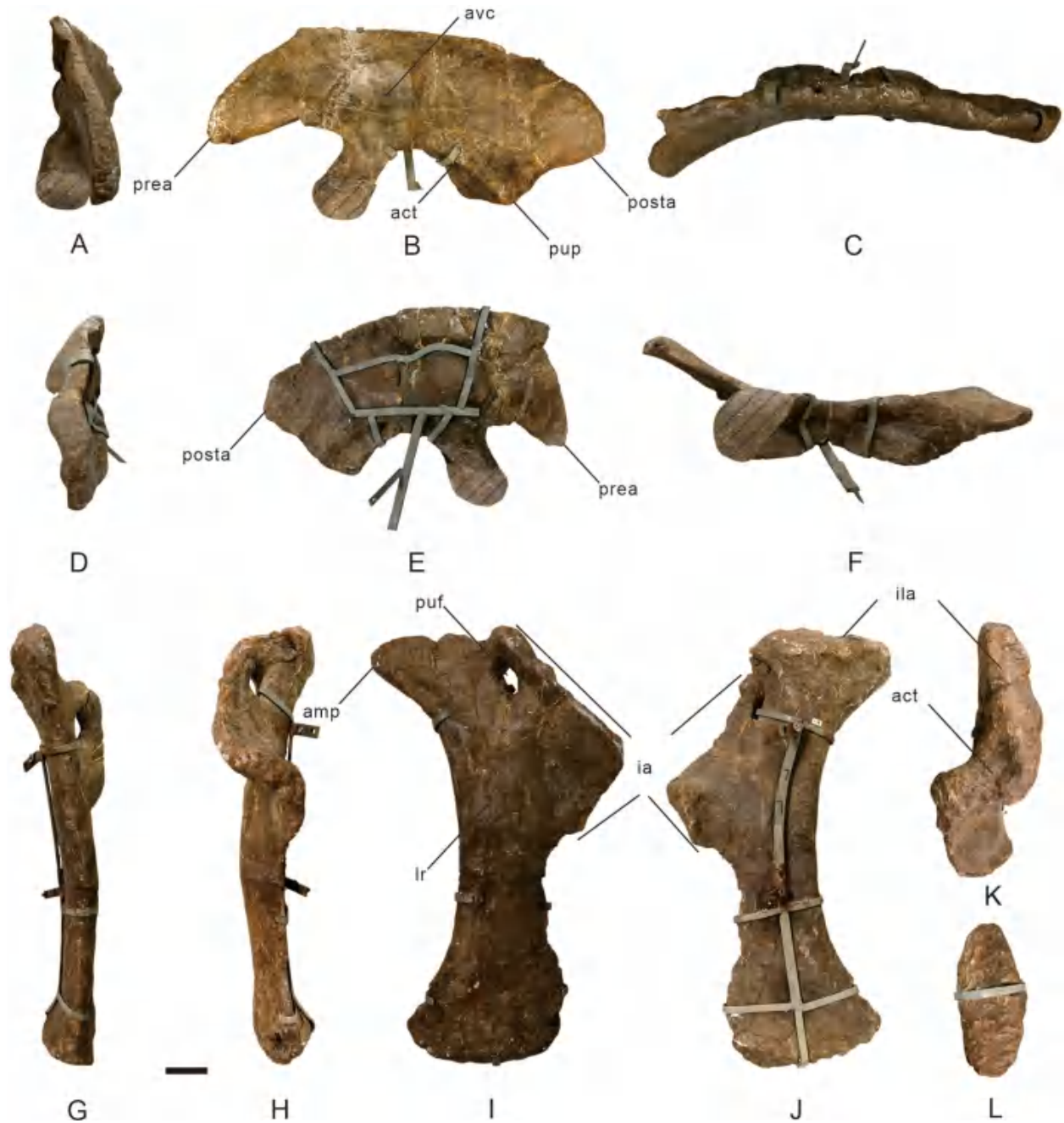
Figure 24. A–F, Dashanpusaurus dongi holotype left ilium; and G–L, pubis. A and G, anterior views; D and H, posterior views; E and J, medial views; B and I, lateral views; C and K, proximal views; F and L, distal views. Striped regions indicate reconstruction. Abbreviations: act, acetabulum; amp, ambiens process; avc, anteroventral concavity of ilium; ila, iliac articulation; posta, postacetabular process; prea, postacetabular process; puf, pubic foramen; pup, pubic peduncle. Scale bar = 50 mm.

Ilium

The holotype left ilium is partially preserved with an incomplete distal end of the pubic peduncle (reconstructed in plaster). In lateral view, the dorsal margin of the ilium is semicircular (Fig. 24A–F; see Table 4 for measurements). This condition is regarded as a synapomorphy of Eusauropoda and is seen in many taxa such as Camarasaurus lewisi, Bellusaurus sui and

Lourinhasaurus alenquerensis (McIntosh et al. 1996b, pl. 10; Mo 2013, pl. 56; Mocho et al. 2014, fig. 18; Xu et al. 2018). We suggest that the preacetabular process projects beyond the anterior end of the pubic peduncle in a lateral view (e.g. Camarasaurus lewisi, Bellusaurus sui and some early-diverging sauropods such as Shunosaurus lii, Barapasaurus tagorei and Omeisaurus tianfuensis (He et al. 1988, fig. 49; Zhang 1988, fig. 51;

McIntosh et al. 1996b, pl. 10; Bandyopadhyay et al. 2010, fig. 11; Mo 2013, pl. 56), whereas the two elements extend to the same level in Lourinhasaurus alenquerensis (Mocho et al. 2014, fig. 18). In lateral view, the preacetabular process is angular, similar to that in Bellusaurus sui (Mo 2013, pl. 56), and the ventral surface of the preacetabular process is curved dorsally. By contrast, the preacetabular process is sub-rounded laterally in many macronarians such as Camarasaurus lewisi (McIntosh et al. 1996a, fig. 67). The orientation of the preacetabular process is anterolateral to the body axis of the ilium, as occurred in most later-diverging sauropod taxa such as Camarasaurus lewisi and Bellusaurus sui (McIntosh et al. 1996b, pl. 10; Mo 2013, pl. 56). The transverse width of the distal end is prominently broader than the basal portion of the preacetabular process. The highest point of the iliac dorsal margin is situated posterior to the base of the pubic peduncle, similar to Camarasaurus lewisi, Bellusaurus sui, Lourinhasaurus alenquerensis, and Apatosaurus ajax (McIntosh et al. 1996a, fig. 67; Upchurch et al. 2004a, fig. 9; Mo 2013, pl. 56; Mocho et al. 2014, fig. 18). The same point is located anterior to the base of the pubic peduncle in other sauropods, such as Tastavinsaurus sanzi (Canudo et al. 2008, fig. 10). The preacetabular process suffered a slight distortion that makes the anterior-most margin of the process mildly ventrally projected. The angle between the ventral surface of the preacetabular process and the anterior face of the pubic peduncle is ∼90°, as in Bellusaurus sui, Tastavinsaurus sanzi, Omeisaurus tianfuensis, Cetiosaurus oxoniensis and Apatosaurus ajax, which also have an approximately right angle between the two elements (He et al. 1988, fig. 49; Upchurch & Martin 2003, fig. 11; Upchurch et al. 2004a; Canudo et al. 2008, fig. 10; Mo 2013, pl. 56). Along the parasagittal section, the iliac lobe is approximately at the same plane as the two peduncles, and the anteroventral portion of the iliac lobe is slightly inwardly concave. The distal end of the postacetabular process is rounded, which makes the dorsal and ventral surfaces of this process merge smoothly. Medially, the dorsal portion of the ilium is coarsely textured along the articular surfaces of the sacral ribs. The acetabulum is concave. Both the anterior and posterior portions of the acetabulum are broader than the middle portion. The ventrolateral surface of the postacetabular process lacks a prominent brevis fossa, a condition that occurs in all sauropods (Gauthier 1986).

The pubic peduncle curves anteroventrally. The transverse width is similar to the iliac lobe. The anterior surface of the pubic peduncle is mildly convex. The lateral and medial surfaces gradually and smoothly merge with the anterior surface of the pubic peduncle. Two ridges are formed by the meeting of the lateral and medial surfaces, respectively, with the posterior surface. The ischial peduncle is distinctly reduced anteroposteriorly when compared with the pubic peduncle and resembles that found in Camarasaurus lewisi, Bellusaurus sui, Lourinhasaurus alenquerensis, Tastavinsaurus sanzi, and most other gravisaurians (McIntosh et al. 1996a, fig. 67; Canudo et al. 2008, fig. 10; Mo 2013, pl. 56; Mocho et al. 2014, fig. 18; Xu et al. 2018). The distal end of the ischial peduncle is transversely compressed. The articular surface of the peduncle is sub-triangular in outline, with one apex contacting the medial margin of the acetabulum and one apex contacting the lateral margin of the postacetabular process, respectively.

Pubis

The left pubis from the holotype is well preserved (Fig. 24G–L; see Table 4 for measurements). The ischial articulation is medially oriented, with an 'S'-shaped outline. The length of the ischial articulation is about 0.41 the proximodistal length of the shaft. The articular surface of the ischial articulation is irregularly rough. The acetabular articular surface extends transversely to the shaft and is slightly transversely and anteroposteriorly concave. The length of the iliac articular surface is 0.37 the proximodistal length of the shaft. The iliac articulation is transversely compressed with a slightly concave articular surface. The pubic foramen is situated on the upper portion of the shaft, located between the ischial and iliac articulations, and below the acetabular articular surface. This foramen is elliptical in outline and projects medioposteriorly.

The pubic shaft has a comma-shaped outline in horizontal cross section. This condition is similar to that in Camarasaurus lewisi, Bellusaurus sui, Apatosaurus ajax and other sauropod taxa (McIntosh et al. 1996a, fig. 69; Upchurch et al. 2004a, fig. 10; Mo 2013, pl. 57). It is formed by a shallowly concave medial surface and a strongly convex lateral surface. The lateral surface includes an acute flange-shaped anterior portion and a flat posterior portion. There is a ridge situated near the anterolateral margin that extends dorsoventrally (Fig. 24). The lateral convexity curves away from the posterior margin and is buttressed at the posterior part of the distal expansion. The distal end is anteroposteriorly extended. The anteroposterior length of the pubis is about 0.37 the total length of the shaft. The anterior portion of the distal end distinctly extends anteriorly with a sub-triangular outline, similar to that in Camarasaurus lewisi (McIntosh et al. 1996b, pl. 30). In anterior view, the lateral surface curves laterally to merge with the distal surface and form an acute angle. By contrast, the

Table 4. Measurements of pelvic girdle and hindlimb of holotype. An asterisk (*) denotes a measurement based on an incomplete element. All measurements are in millimetres.

Element	Dimension	Measurement
Ilium (left)	Length (between the tips of the anterior and posterior lobes)	813
	Length of anterior lobe (from the tip of this lobe to the base of the pubic peduncle)	265
	Length of posterior lobe (from the tip of this lobe to the base of the ischial peduncle)	184
	Length of pubic peduncle	165*
	Width of preacetabular	57
	Width of mid-portion of iliac blade	29
	Width of postacetabular	48
	Transverse width of the distal end of the pubic peduncle	125*
	Transverse width of the dorsal margin of the acetabulum	89
	Length of ischial peduncle	66
	Transverse width of ischial peduncle	130
	Height of the iliac blade above the pubic peduncle	303
	Diameter of acetabulum between the pubic and ischial peduncles	272*
Pubis (left)	Length (from distal end to the point where the iliac articulation meets the acetabular margin)	722
	Length of iliac articulation along its lateral edge	268
	Maximum transverse width of the acetabular surface	83
	Dorsoventral length of ischial articulation	293
	Maximum transverse width of the ischial articulation	54
	Maximum diameter of obturator foramen	61
	Anteroposterior diameter of distal end	264
	Maximum transverse width of distal end	101
	Maximum width of pubic shaft immediately below the pelvic basin	66
Femur (left)	Length	1100
	Maximum anteroposterior width of the proximal head	56
	Maximum anteroposterior width of greater trochanter	150
	Transverse width of proximal end	350
	Distance from the proximal end of the femur to the top of the 4th trochanter	535
	Anteroposterior length of midshaft	92
	Transverse width of midshaft	165
	Minimum midshaft perimeter	455
	Anteroposterior length of distal end	184
	Transverse width of distal end	278
	Anteroposterior width of the tibial condyle	146*
	Anteroposterior width of fibular condyle	184
Tibia (left)	Length	660
	Maximum anteroposterior diameter of the proximal end	137
	Maximum transverse diameter of the proximal end (including cnemial crest)	310
	Anteroposterior length of midshaft	58
	Transverse width of midshaft	120
	Perimeter of midshaft	310
	Transverse width of distal end	185
	Anteroposterior width of distal end	184

medial surface near the distal end is flat and forms a right angle in anterior view. This condition resembles that in Bellusaurus sui (Mo 2013, pl. 57). However, the distal end of the pubis is prominently medially expanded in Camarasaurus lewisi (McIntosh et al. 1996b, pl. 30). The distal end is elliptical in outline with an irregular concavity on the distal surface.

Femur
The holotype left femur is partially preserved with the middle portion of the posterior surface and fibular condyle reconstructed with plaster (Fig. 25A–F; see Table 4 for measurements). The femoral head projects medially and a little dorsally. This condition is similar to that in Camarasaurus lewisi, Bellusaurus sui, Lourinhasaurus alenquerensis, Shunosaurus lii, Barapasaurus tagorei, Chuanjiesaurus anaensis and Chubutisaurus insignis (Zhang 1988, fig. 53; McIntosh et al. 1996a, fig. 70; Bandyopadhyay et al. 2010, fig. 13; Carballido et al. 2011a, fig. 14; Sekiya 2011, fig. 52; Mo 2013, pl. 57; Mocho et al. 2014, fig. 21). It differs from that in Aragosaurus ischiaticus, Tastavinsaurus sanzi and Omeisaurus tianfuensis, which have a dorsolaterally oriented femoral head (He et al. 1988, fig. 52; Canudo et al. 2008, fig. 13; Royo-Torres et al. 2014, fig. 15).

Figure 25. A–F, Dashanpusaurus dongi holotype left femur; and G–L, tibia. A and G, anterior views; B and H, posterior views; C and I, medial views; D and J, lateral views; E and K, proximal views; F and L, distal views. Striped regions indicate reconstruction. Abbreviations: 4th, fourth trochanter of femur; cc, cnemial crest; dac, distal anterior concavity; fc, fibular condyle; fmr, median ridges on femoral anterior surface; lb, lateral bulge; lm, lateral malleolus; md, medial deflection; mm, medial malleolus; tc, tibial condyle; tfi, tuberculum fibularis. Scale bar = 50 mm.

The dorsal surface of the proximal end is irregularly concave. Laterally, the femoral head projects slightly beyond both the anterior and posterior surfaces of the shaft. The posterior surface is more expanded than the anterior surface. There is no constriction between the femoral head and the greater trochanter. The lesser trochanter is not observable, resembling the condition in Camarasaurus lewisi and other eusauropod taxa such as Bellusaurus sui (McIntosh et al. 1996a, fig. 70; Mo 2013, pl. 57). A lateral bulge (defined as the lateral expansion and a dorsomedial orientation of the dorsolateral margin of the femur: see Salgado et al. 1997) is

present and the proximolateral margin above the lateral bulge is medial to the lateral margin of the distal half of the shaft (see Mannion et al. 2013; Moore et al. 2020). Both are found on the lateral surface of the upper femur, similar to Aragosaurus ischiaticus, Tastavinsaurus sanzi, Europasaurus holgeri and many non-neosauropods such as Omeisaurus tianfuensis and Chuanjiesaurus anaensis (He et al. 1988, fig. 52; Canudo et al. 2008, fig. 13; Sekiya 2011, fig. 52; Royo-Torres et al. 2014, fig. 15; Carballido et al. 2020, fig. 11L). This condition differs from that in Camarasaurus lewisi, Bellusaurus sui and many other sauropod taxa (e.g. Apatosaurus louisae,
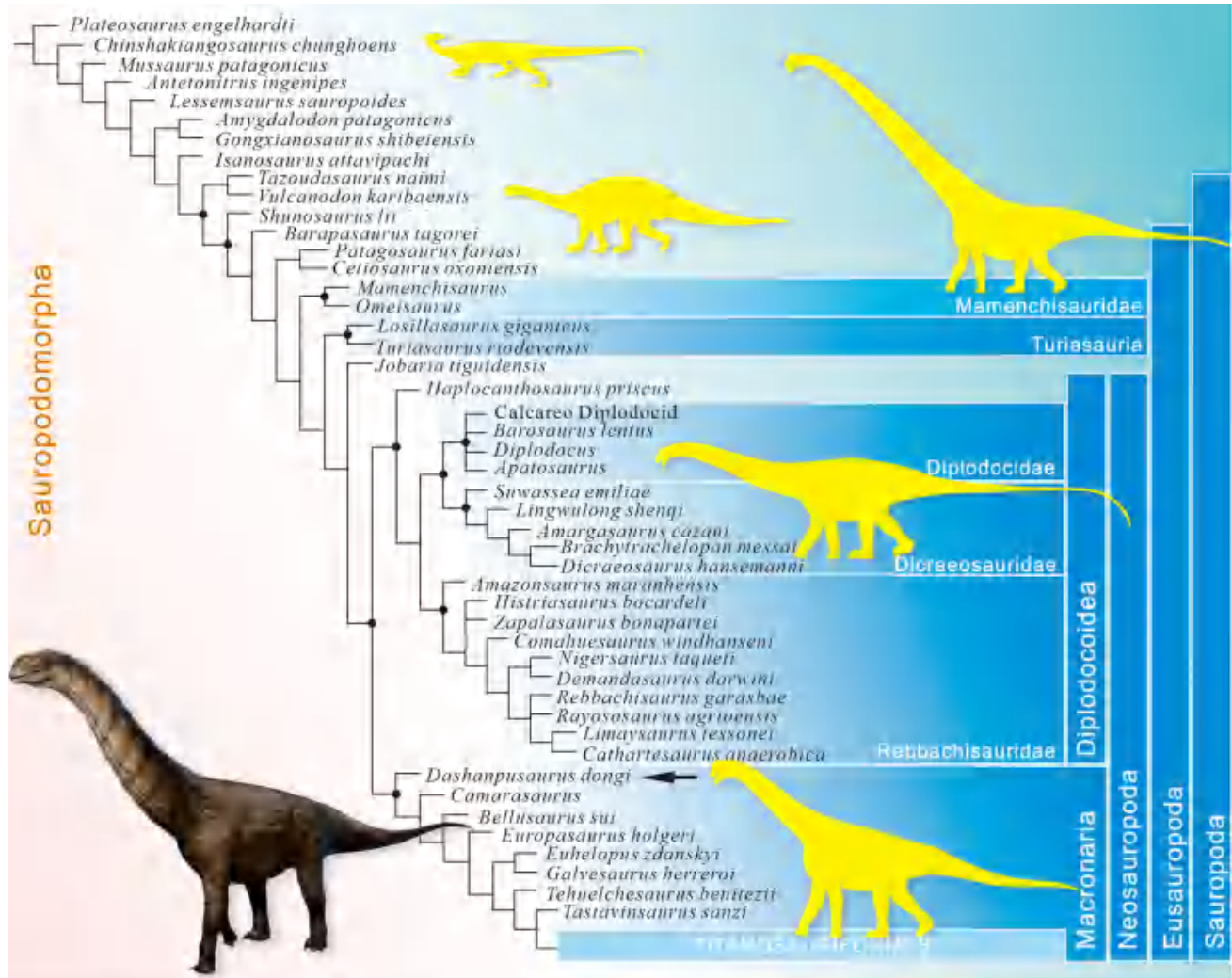
Figure 26. Strict consensus tree of the equal weights parsimony (EWP) analysis from the main data set depicting the phylogenetic position of Dashanpusaurus dongi. Life reconstruction of Camarasaurus by crytivo.com.

Saltasaurus loricatus) without a lateral bulge (Gilmore 1946; Powell 1992, fig. 37; McIntosh et al. 1996a, fig. 70; Mo 2013, pl. 57).

The femoral shaft is straight with the distal third being prominently expanded when compared with the midshaft. This trait is also observed in Camarasaurus lewisi (McIntosh et al. 1996a, fig. 70) and Mamenchisaurus youngi (Ouyang & Ye 2002, fig. 40). It is worth noting that two dorsoventrally extended ridges are situated on the medial and lateral margins of the anterior surface. The two ridges occupy the upper portion of the anterior surface from the base of the femoral head to the middle portion of the femoral shaft (Fig. 25). A shallow concavity is formed by the two ridges. This concavity of the anterior surface also exists on the femoral anterior surface in Bellusaurus sui but is not formed by two prominent ridges (Mo 2013, pl. 59).

The shaft is a transversely expanded ellipse in cross-section throughout most of its length, except the proximal and distal ends. The fourth trochanter is situated near the mid-sagittal plane of the femur and is slightly medially located. This condition resembles that of Bellusaurus sui, Shunosaurus lii, Omeisaurus tianfuensis and many other sauropod taxa such as Spinophorosaurus nigerensis (Zhang 1988, fig. 53; He et al. 1988, fig. 52; Remes et al. 2009, fig. 4; Mo 2013, pl. 59; Moore et al. 2020). That in Camarasaurus lewisi is located on the posteromedial margin of the shaft (McIntosh et al. 1996a, fig. 70). Medially, the distal end of the fourth trochanter is flat.

The transverse width-to-femoral midshaft ratio of the distal femur is 1.68. In anterior or posterior views, the medial and lateral surfaces of the distal end are expanded at the same level. By contrast, the medial
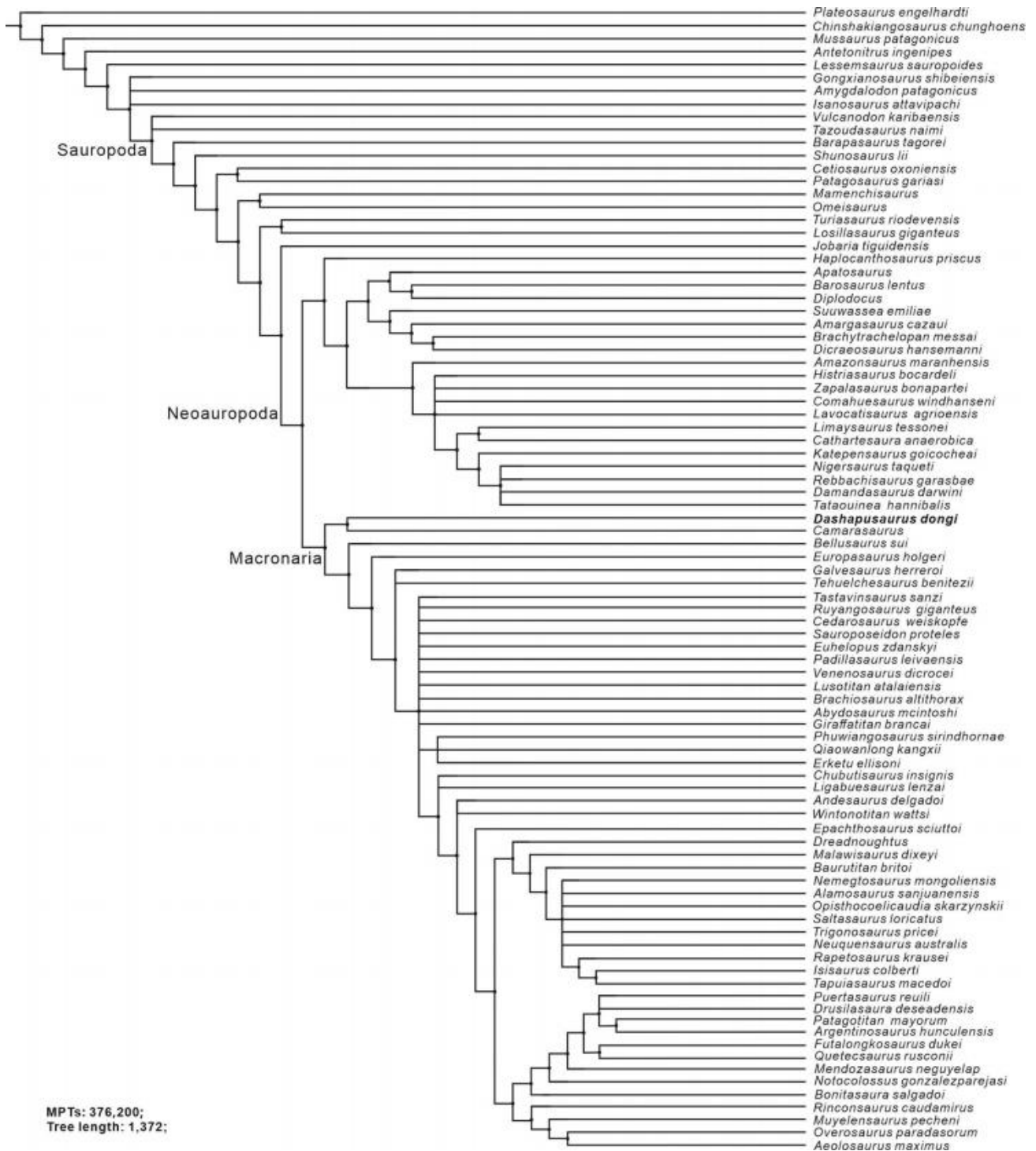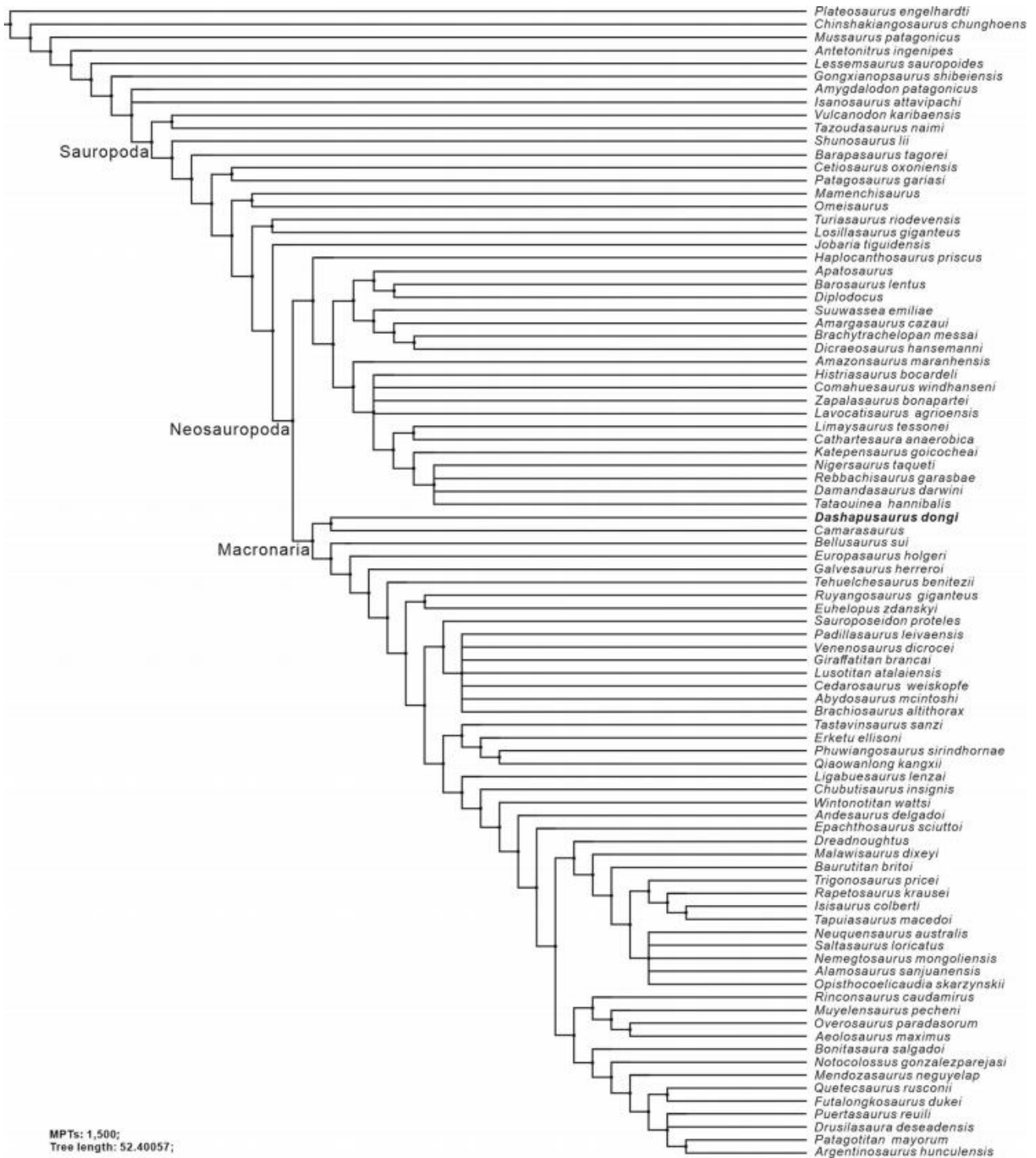
Figure 27. Strict consensus tree of the equal weights parsimony (EWP) analysis from the Carballido et al. (2020) data set depicting the phylogenetic position of Dashanpusaurus dongi.

margin of the distal femur is more prominently expanded than the lateral margin in Camarasaurus lewisi and Bellusaurus sui (McIntosh et al. 1996a, fig. 70; Mo 2013, pl. 59). The tibial condyle is anteroposteriorly larger than the fibular condyle in distal view. The two fibular and tibial condyles are medially separated by a pronounced intercondylar groove. This groove is much more concave on the posterior surface of the distal end.

Figure 28. Strict consensus tree of the extended implied weighting (EIW) analysis from the Carballido et al. (2020) data set depicting the phylogenetic position of Dashanpusaurus dongi.

The articular surface of the two condyles is slightly rough with irregular concavities. The distal articular surface is restricted on the distal portion of the femur, as occurred in other later-diverging taxa such as

Camarasaurus lewisi (McIntosh et al. 1996a, fig. 70). In distal view, the medial margin of the tibial condyle and lateral margins of the fibular condyle are smoothly curved. The tibial and fibular condyles are roughly

Tibia

The left tibia of the holotype is well preserved (Fig. 25G–L; see Table 4 for measurements). The total length of the tibia is about 0.6 the total length of the femur. This ratio is in the typical range for sauropods (McIntosh 1990; Upchurch 1998). The proximal end of the tibia is prominently expanded anteroposteriorly and transversely compared with the rest of the main shaft. The shaft is transversely wider than the anteroposterior length. This condition resembles that in Camarasaurus lewisi, Bellusaurus sui and many other sauropod taxa such as Mamenchisaurus youngi (McIntosh et al. 1996a, fig. 75; Ouyang & Ye 2002, fig. 41; Mo 2013, pl. 60). By contrast, some early-diverging sauropod taxa, such as Vulcanodon karibaensis, share an anteroposteriorly extended proximal surface of the tibia (Cooper 1984, fig. 23). The transverse width of this proximal surface is about 2.26 the anteroposterior length of the tibia. It differs from some taxa with a transversely compressed proximal end (e.g. Tazoudasaurus naimi) (Allain & Aquesbi 2008, fig. 28). The shape of the proximal tibia is sub-elliptical. The lateral and medial portions of the distal end are more expanded than the anterior and posterior portions. The articular surface of the proximal end is flat with irregular concavities. The articular surface is restricted to the dorsal end.

As in other eusauropods, the cnemial crest is robust (Wilson & Sereno 1998). It projects laterally and slightly posteriorly to articulate with the anteromedial surface of the fibula. The most prominent portion of the cnemial crest lies below the dorsal surface of the proximal end of the tibia with the dorsal and ventral regions connected by a rough ridge. The posterolaterally oriented fibular articular surface of tibia articulates with the anteromedial margin of the fibula. This condition resembles that of Camarasaurus lewisi, Bellusaurus sui, Omeisaurus tianfuensis, Mamenchisaurus youngi and most other eusauropods (He et al. 1988, fig. 52; McIntosh et al. 1996a, fig. 75; Ouyang & Ye 2002, fig. 41; Mo 2013, pl. 60). The cross-section of the midshaft is elliptical, as occurs in Camarasaurus lewisi and Bellusaurus sui. Additionally, the transverse width of the midshaft is about 0.18 of the dorsoventral length of the shaft.

The transverse width of the distal tibia is about 0.28 the dorsoventral length of the shaft, and the distal width is 1.54 that of the midshaft. These ratios are 0.28 and 1.38 in Bellusaurus sui, 0.29 and 2.20 in Camarasaurus lewisi, and 0.32 and 2.76 in Lourinhasaurus alenquerensis, respectively (McIntosh et al. 1996a; Mo 2013; Mocho et al. 2014). The distal expansion of the tibia is twisted about 10° relative to the proximal end. Distally, the anteroposterior length is greater than the transverse length, with a comma-shaped outline. This condition is similar to that in many sauropod taxa, such as Camarasaurus lewisi and Bellusaurus sui (McIntosh et al. 1996a, fig. 75; Mo 2013, pl. 60), whereas some taxa such as Apatosaurus ajax and some early-diverging sauropod taxa (e.g. Vulcanodon karibaensis, Cetiosaurus oxoniensis) have a more transversely extended distal end (Cooper 1984, fig. 23; Upchurch & Martin 2003, fig. 12; Upchurch et al. 2004a, fig. 12). The posterolateral surface terminates distally with a ventral concavity forming the groove that separates the lateral malleolus from the medial malleolus. The medial malleolus is much stouter than the lateral malleolus, as is the case in Camarasaurus lewisi and Bellusaurus sui (McIntosh et al. 1996a, fig. 75; Mo 2013, pl. 60). In posterior view, the medial malleolus is reduced to the point that the posterior fossa for the astragalus is exposed.

Phylogenetic analysis

To test the hypothesis that the two specimens of Dashanpusaurus dongi represent a monospecific assemblage, we have scored the two specimens (D. holotype; D. paratype) and 'Dashanpusaurus dongi total' separately and incorporated them as operational taxonomic units (OTUs) in the data matrix of Xu et al. (2018) (the main data matrix). We have chosen to use this matrix because it is a recently updated version of a series of data sets produced by Carballido and colleagues, and includes scores for many early-diverging neosauropods (e.g. the Middle Jurassic Lingwulong from China). Furthermore, this data set is suitable for our study because it samples a phylogenetically and spatiotemporally wide array of sauropodomorph taxa, and thus gives Dashanpusaurus the freedom to cluster anywhere within known sauropod diversity, especially among Asian diplodocids. The other four referred data sets are from Pol et al. (2020), Mannion et al. (2019), Carballido et al. (2020) and a revised version of González Riga et al. (GEA) (2018) from Moore et al. (2020). The data set from Pol et al. (2020) is one of the largest available for non-eusauropod sauropods that includes a broad sample of early-diverging sauropod diversity. This data set provides a suitable test of our hypothesis that Dashanpusaurus represents a neosauropod. The data set

of Carballido et al. (2020) is the most up-to-date version of the series of data sets produced by Carballido and colleagues; it could further potentially yield insights into the placement of Dashanpusaurus within Macronaria. Moreover, the data set of Mannion et al. (2019) is also one of the largest available for sauropods that includes a broad sample of eusauropod diversity. Furthermore, the sampling of neosauropods emphasized the inclusion and provides a suitable test for our hypothesis that this taxon represents a neosauropod. GEA from Moore et al. (2020) was also included as it is also a large data set available for sauropods that includes a broad sample of eusauropod diversity. Moreover, the sampling of some 'mamenchisaurids' emphasized the inclusion of single-specimen OTUs rather than at the genus-level in this data set. It therefore provides a suitable test of our hypothesis that Dashanpusaurus represents a macronarian, rather than a mamenchisaurid (Supplemental material).

To test the phylogenetic affinities of Dashanpusaurus dongi and other macronarians, we ran the analysis using EWP and EIW analyses (a concavity constant [K] of 12 was used) (Goloboff et al. 2003, 2008; Goloboff 2014; Goloboff & Catalano 2016). The EWP analysis of the main data set produced six MPTs with lengths of 1112 steps (consistency index = 0.397; retention index = 0.719) with limited resolution in some parts of the tree, although Dashanpusaurus was recovered within Neosauropoda, as a member of Macronaria (Fig. 26). The Neosauropoda clade is supported by three unambiguous synapomorphies ('0' to '1' for characters 96 and 225; '0' to '2' for character 106). The Macronaria clade is supported by three unambiguous synapomorphies ('0' to '1' for character 162; '1' to '0' for character 136; '1' to '2' for character 116). Dashanpusaurus dongi shares all three characters ('height divided by width between 0.7 and 0.9 in cervical vertebrae' [ch. 116]; 'transverse processes of dorsal vertebrae are directed laterally or slightly upwards' [ch. 136]; 'middle and posterior dorsal centrum in the transverse section are slightly dorsoventrally compressed' [ch. 162]).

Finally, we ran the EIW analysis using K = 12. This produced three MPTs with lengths of 43.10215 steps (consistency index = 0.397; retention index = 0.719) and a well-resolved strict consensus. In our EIW analysis, Dashanpusaurus dongi is situated as the basal-most macronarian, supported by three unambiguous character changes, the characters of which are similar to that in the EWP analysis.

EWP and EIW analyses were also run with the data sets of Carballido et al. (2020), Mannion et al. (2019) and Pol et al. (2020) and the revised version of GEA from Moore et al. (2020). The EWP analysis of Carballido et al. (2020) produced 376,200 MPTs with

tree lengths of 1372 steps. The strict consensus is generally well resolved (Fig. 27). Dashanpusaurus dongi was recovered within Neosauropoda as a basal member of Macronaria. Neosauropoda is supported by four unambiguous synapomorphies ('0' to '1' for characters 136 and 269; '0' to '2' for character 115; '1' to '0' for character 194). Dashanpusaurus dongi is situated in a basal position in Macronaria and shares a sister clade relationship with Camarasaurus, supported by three unambiguous synapomorphies ('0' to '1' for characters 138 and 152; '3' to '1' for character 277). The (Dashanpusaurus + Camarasaurus) and other macronarians are supported by 12 unambiguous synapomorphies ('0' to '1' for characters 93, 96, 195, 283, 320, 321, 337 and 342; '1' to '0' for characters 157 and 174; '2' to '0' for character 176; '1' to '2' for character 132). Dashanpusaurus shares five of these: height divided by the width of cervical vertebrae is between 0.9 and 0.7 (ch. 132); dorsal transverse processes are directed laterally or slightly upwards (ch. 157); anterior dorsal neural spine minimum width/length is 0.5 or greater (ch. 174); the dorsal edge of the anterior dorsal neural spine is flat (ch. 176); and the middle and posterior dorsal centrum in transverse section is slightly dorsoventrally compressed (ch. 195). EIW analysis was used with K = 12 and produced 1500 MPTs with lengths of 52.40057 steps (Fig. 28). The EIW resulted in Dashanpusaurus dongi being positioned within Neosauropoda. This result is supported by the characters similar to the EWP analysis. Macronaria is supported by 12 unambiguous synapomorphies, the same as the EWP analysis. Moreover, Dashanpusaurus dongi was situated at a basal position in Macronaria sharing a sister clade with Camarasaurus, which is supported by three unambiguous synapomorphic characters (the same as the EWP analysis).

The EWP analysis of the data set from Mannion et al. (2019) produced 500,000 MPTs with tree lengths of 2586 steps. The strict consensus of the EWP result is well-resolved (Fig. 29). Dashanpusaurus dongi was recovered within Neosauropoda, as a basal member of Macronaria. The Neosauropoda clade is supported by seven unambiguous synapomorphies ('0' to '1' for characters 48, 79, 108, 366, 407 and 519; '1' to '0' for character 208), and Dashanpusaurus dongi shares two of these seven characters within Neosauropoda: the ratio of the mediolateral width of distal end/anteroposterior width of the radius is <1.5 (ch. 48); and the humeral head forms a prominent sub-circular process on the posterior surface of the proximal end of the humerus (ch. 366). Macronaria is supported by two unambiguous synapomorphies ('1' to '0' for character 128; '1' to '2' for character 40), and Dashanpusaurus dongi shares epipophyses of cervical neural arches (post-Cv3) that do
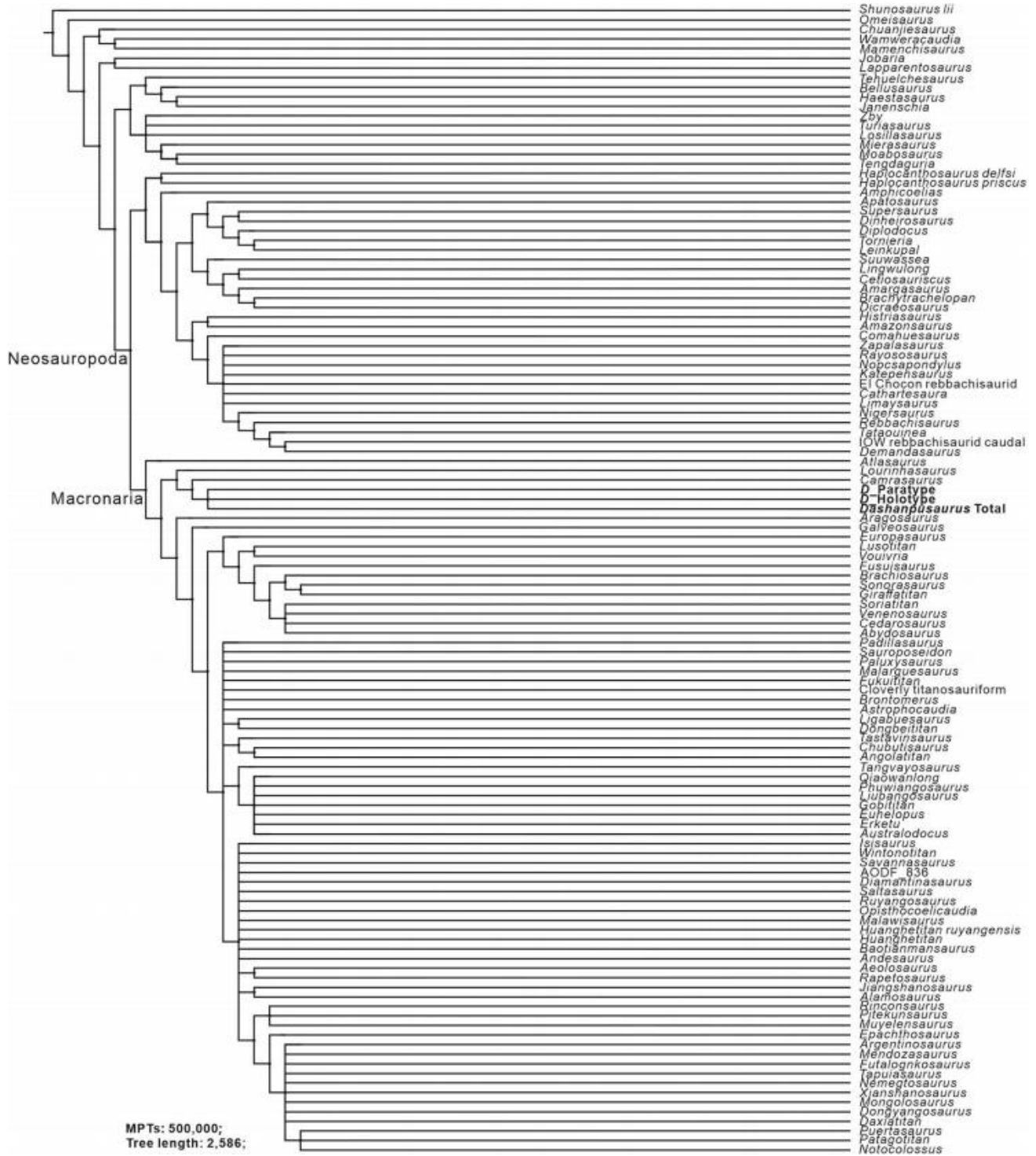
Figure 29. Strict consensus tree of the equal weights parsimony (EWP) analysis from the Mannion et al. (2019) data set depicting the phylogenetic position of Dashanpusaurus dongi.

not extend beyond the posterior margin of the postzyga-pophyses (ch. 128). Dashanpusaurus dongi is situated in a basal position in Macronaria and shares a sister clade with Camarasaurus. This is supported by four

unambiguous synapomorphies: dorsoventral height of ischial articulation of the pubis divided by pubis proxi-modistal length 0.4 or greater (ch. 59); the shape of the lateral margin of the humeral diaphysis (approximately
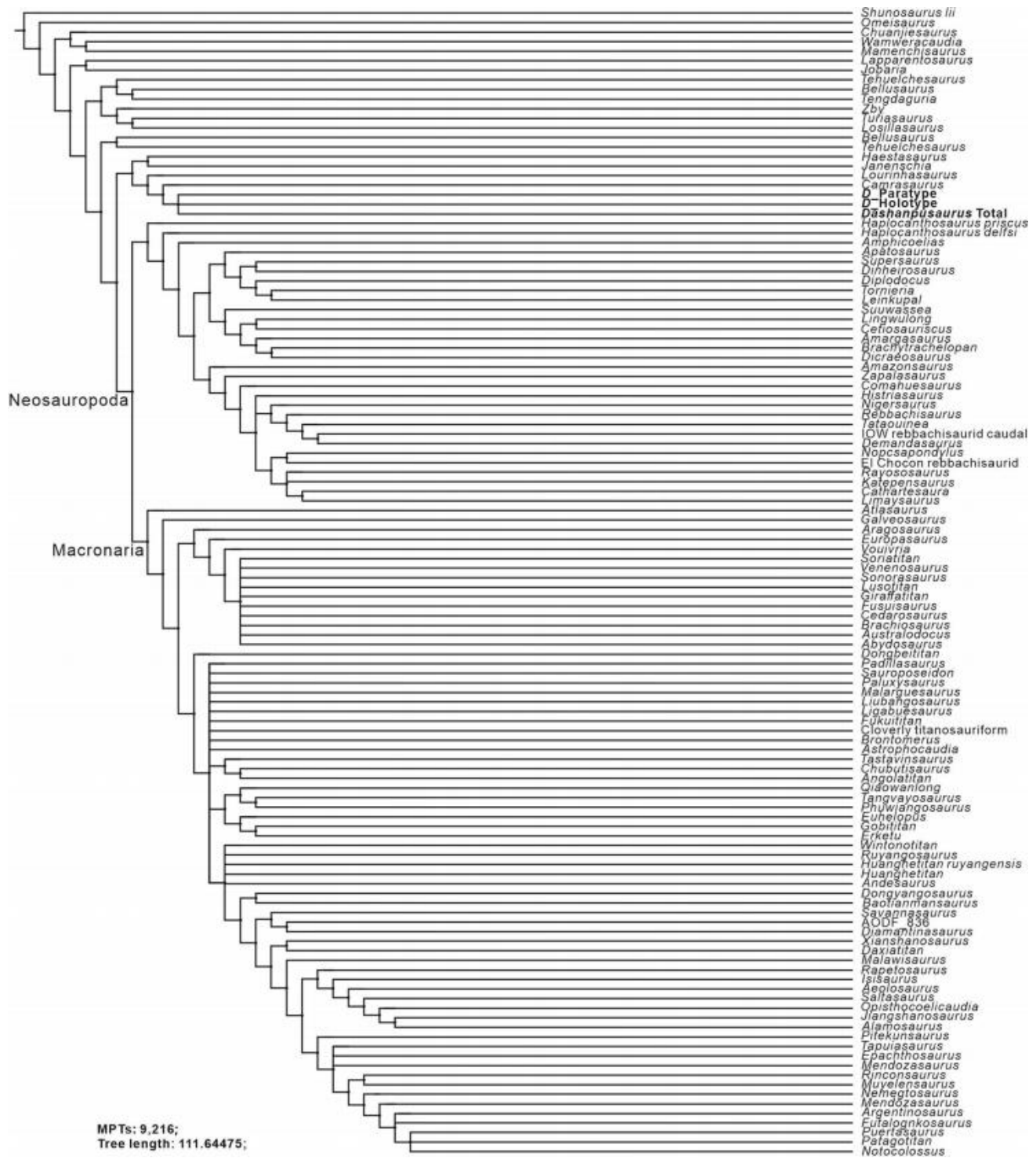
Figure 30. Strict consensus tree of the extended implied weighting (EIW) analysis from the Mannion et al. (2019) data set depicting the phylogenetic position of Dashanpusaurus dongi.

the middle third of the humerus) is concave in anterior view (ch. 224); the ratio of maximum mediolateral width of the distal end to the proximodistal length of the humerus is 0.3 or greater (ch. 370); and the profile of the iliac dorsal margin is strongly convex throughout its length and follows the arc of a circle in lateral view (ch. 520). These characters are more closely related to Lourinhasaurus than to the clade including all other

macronarians, by three characters: the EPRL is present in cervical neural arches (ch. 129); the middle dorsal neural spines are bifurcated (ch. 161); and the long axis of the ischial shaft, if projected upwards/proximally, passes through the lower part of the pubic articular surface (i.e. it is approximately horizontally oriented), such that the posterior margin of the iliac peduncle and the dorsal margin of the shaft form a right angle in lateral view (ch. 254). The EIW analysis (K = 12) produced 9216 MPTs with lengths of 111.64475 steps. The strict consensus of the EIW result is well resolved (Fig. 30). Neosauropoda is supported by eight unambiguous synapomorphies ('0' to '1' for characters 9, 59, 81, 106, 224 and 426; '1' to '0' for characters 49 and 72). However, Dashanpusaurus dongi was recovered outside of Neosauropoda, although the species shares one character (ch. 49). Dashanpusaurus dongi shares a sister clade with Camarasaurus and is supported by two unambiguous synapomorphies: the distal condyle is perpendicular or beveled with an angle of less than 20° to the long axis of the radial shaft (ch. 49); and the profile of the iliac dorsal margin is strongly convex throughout its length and follows the arc of a circle in lateral view (ch. 520). Dashanpusaurus dongi + Camarasaurus constitute a sister clade with Lourinhasaurus alenquerensis and are more closely related to Haestasaurus + Janenschia than to the clade including all other eusauropods.

An EWP analysis of the revised version of the GEA from Moore et al. (2020) produced 500,000 MPTs with tree lengths of 2183 steps. The strict consensus of the EWP results is limited in resolution, so we used 50% majority rule consensus (Fig. 31). Dashanpusaurus dongi was recovered within Neosauropoda as a basal member of Macronaria. Neosauropoda is supported by 13 unambiguous synapomorphies ('0' to '1' for characters 25, 52, 108, 133, 173, 266, 285 and 366; '1' to '0' for characters 41, 73 and 297; '1' to '2' for character 122; '2' to '3' for character 431), and Dashanpusaurus dongi shares three of the 13 characters within Neosauropoda: maximum mediolateral width of humeral proximal end divided by proximodistal length is 0.4 or greater (ch. 41); the posterior margin of radial distal end lacks condylar-like processes and fossa (ch. 285); and the humeral head forms a prominent sub-circular process on the posterior surface of the proximal end (ch. 366). Since Dashanpusaurus dongi is situated in the basal position of Macronaria, it shares a sister clade with Camarasaurus that is supported by four unambiguous synapomorphic characters: the EPRL is present along the cervical neural arch (ch. 129); the middle dorsal neural spines are bifurcated (ch. 161); the SPOL of the middle to posterior dorsal neural spines is divided into medial and lateral branches (ch. 165); and the ratio of the maximum mediolateral width of the distal end of the humerus to the proximodistal length of the humerus is 0.30 or greater (ch. 370). Together, they form a clade with later macronarians on the basis of five characters (chs. 22, 63, 212, 250 and 269), two of which are shared with Dashanpusaurus dongi: the ratio of the posterior articular face mediolateral width to dorsoventral height of middle to posterior dorsal centra is 1.0 or greater (ch. 22); and the obturator foramen of the pubis is oval or elliptical with the long axis oriented along the same plane as the long axis of the pubis in lateral view (ch. 250). This clade, together with Tehuelchesaurus + (Haestasaurus + Janenschia), constitutes the Macronaria clade ('0' to '1' for characters 155, 171, 267, 335 and 361); '1' to '0' for character 272; '1' to '2' for character 147). The EIW analysis (K = 12) produced 130,464 MPTs of lengths 96.19346 steps. The strict consensus of the EIW result is well resolved (Fig. 32). Dashanpusaurus dongi was positioned within Neosauropoda, as a basal member of Macronaria. Neosauropoda is supported by seven unambiguous synapomorphies ('0' to '1' for characters 16, 52, 133, 266, 285 and 366; '1' to '0' for character 73), two unambiguous synapomorphies more than the EWP analysis (ch. 16 and 52), but lacking seven characters (chs. 25, 41, 108, 122, 173, 297 and 431). Dashanpusaurus dongi is situated in the basal position of Macronaria and shares a sister clade with Camarasaurus that is supported by five unambiguous synapomorphic characters, which is more than the result of the EWP analysis with ch. 132 (the postaxial cervical and anterior dorsal neural spines are bifurcated). They together share the clade with other later macronarians by six characters, more than the result of EWP analysis. This clade, together with Tehuelchesaurus + (Haestasaurus + Janenschia), constitutes Macronaria. One more unambiguous synapomorphic character (ch. 125) further supports this clade, but lacks ch. 155 when compared with the result of the EWP analysis.

The EWP analysis of the data set from Pol et al. (2020) produced 9000 MPTs with tree lengths of 1926 steps. The strict consensus of EWP result is resolved (Fig. 33). Dashanpusaurus dongi was recovered within Neosauropoda as a basal member of Macronaria. Neosauropoda is supported by four unambiguous synapomorphies ('0' to '1' for characters 23 and 120; '0' to '2' for character 106; '1' to '0' for character 354). Dashanpusaurus dongi is situated in the basal position of Macronaria and shares a sister clade with Camarasaurus, supported by two unambiguous synapomorphies ('0' to '1' for ch. 132; '1' to '0' for ch. 142): the neural spines of the posterior cervical and anterior
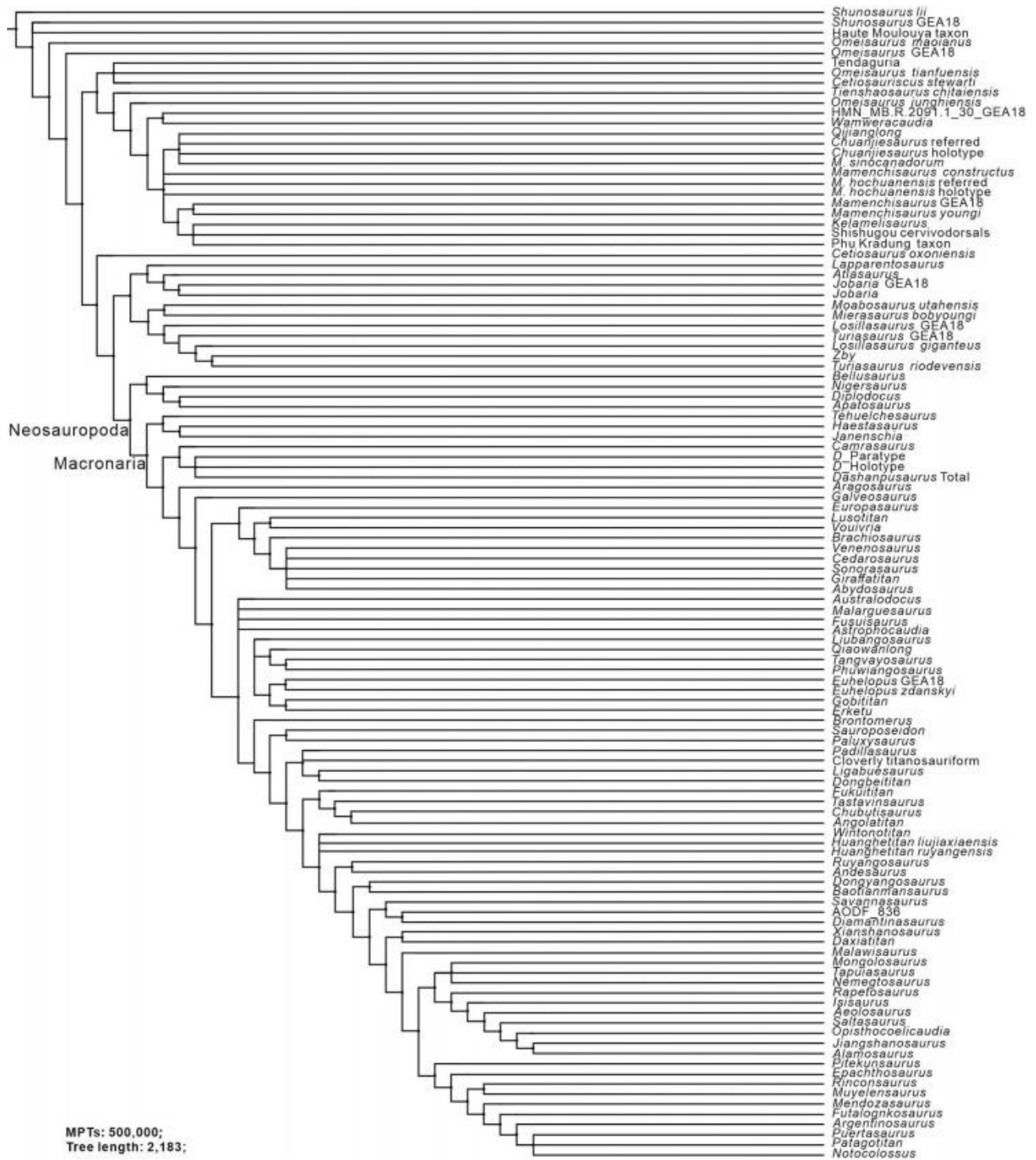
Figure 31. Reduced consensus (50% major consensus) tree of the equal weights parsimony (EWP) analysis from the González Riga et al. (GEA) (2018) data set of Moore et al. (2020) depicting the phylogenetic position of Dashanpusaurus dongi.

dorsal vertebrae are bifurcated (ch. 132); and a single PRSL is absent in single, not bifurcated, neural spines of dorsal vertebrae (ch. 142). The (Dashanpusaurus + Camarasaurus) clade shares nine unambiguous synapomorphies characters with Bellusaurus and other later macronarians ('0' to '1' for characters 143, 162, 238, 288 and 293; 1' to '0' for characters 136, 317 and 375; '1' to '2' for character 116). Dashanpusaurus
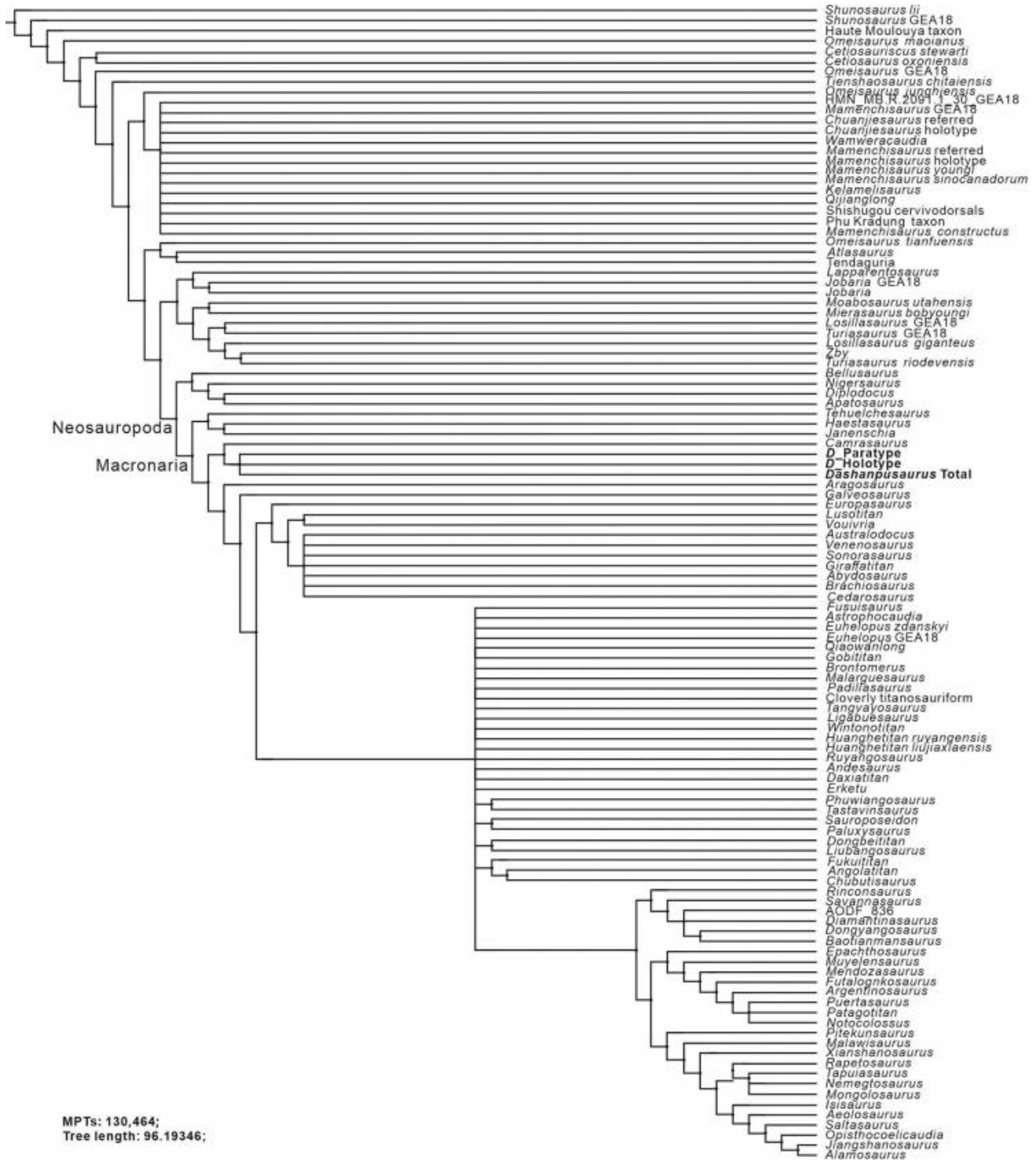
Figure 32. Strict consensus tree of the extended implied weighting (EIW) analysis from the González Riga et al. (GEA) (2018) data set of Moore et al. (2020) depicting the phylogenetic position of Dashanpusaurus dongi.

shares four of them: height divided by the width of the cervical posterior articular surface is between 0.9 and 0.7 (ch. 116); dorsal transverse processes are directed laterally or slightly upwards (ch. 136); middle and posterior dorsal centrum in the transverse section is slightly dorsoventrally compressed (ch. 163); and the cranial
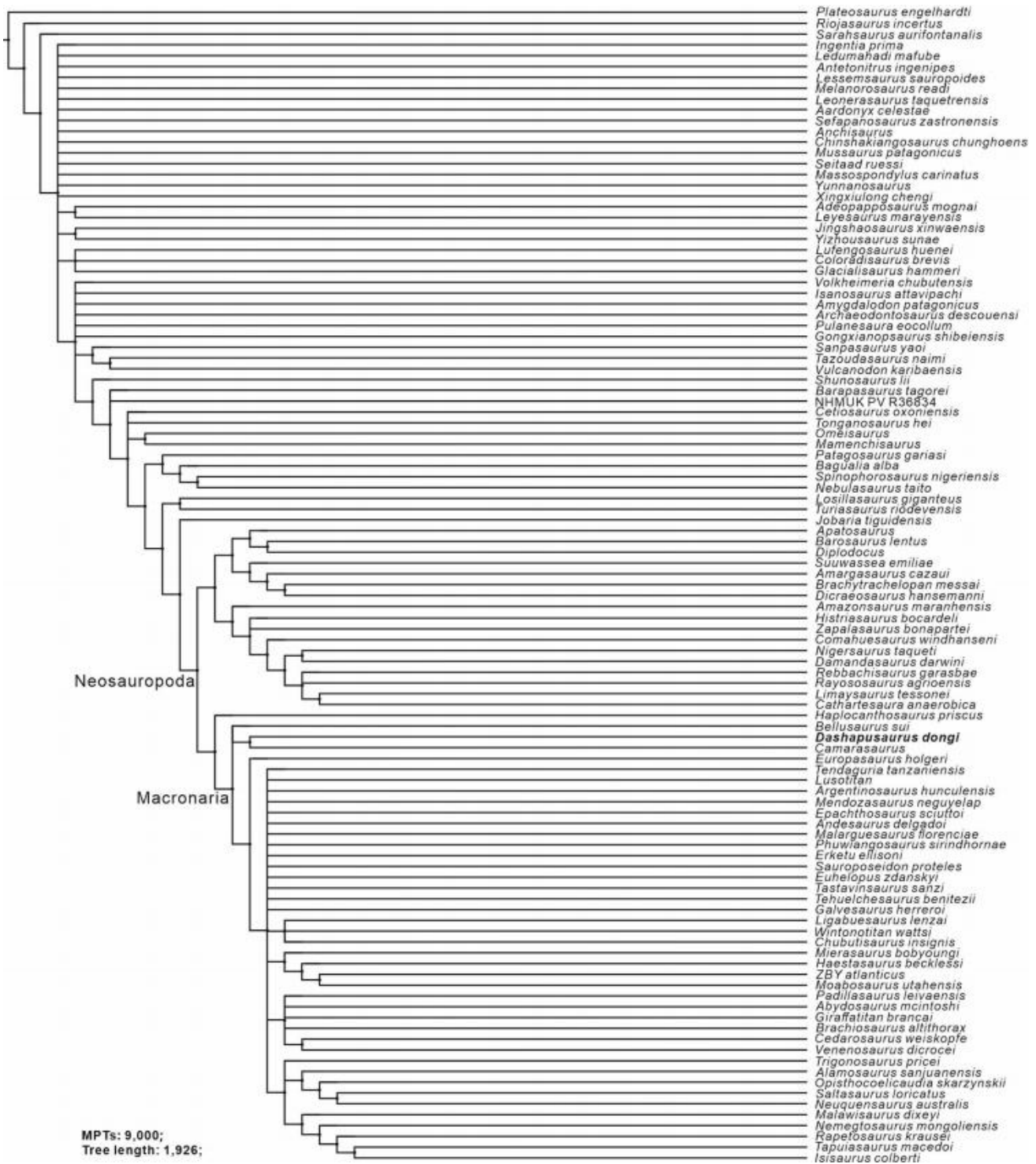
Figure 33. Strict consensus tree of the equal weights parsimony (EWP) analysis from the Pol et al. (2020) data set depicting the phylogenetic position of Dashanpusaurus dongi.

process of cervical prezygapophyses is not situated ventrolaterally to the articular surface (ch. 375). The EIW analysis (K = 12) produced 15 MPTs of lengths 80.99365 steps (consistency index = 0.306; retention index = 0.721). The strict consensus of the EIW result is well resolved (Fig. 34). Dashanpusaurus dongi was recovered within Neosauropoda as a basal member of Macronaria. Neosauropoda is supported by five

Figure 34. Strict consensus tree of the equal weights parsimony (EWP) analysis from the Pol et al. (2020) data set depicting the phylogenetic position of Dashanpusaurus dongi.

unambiguous synapomorphies ('0' to '1' for characters 23, 120 and 177; '0' to '1' for character 106; '1' to '0' for character 354), and Dashanpusaurus dongi shares two of these five characters within Neosauropoda: internal pneumaticity of cervical centra is present with single and wide cavities (ch. 120); and epipophyses on cervical vertebrae are stout, pillar-like expansions above postzygapophyses (ch. 354). Macronaria is supported by

= epipophysis

= attachment scars for mm. intercristales

= lamina of pneumatized spinodiapophyseal fossa

four unambiguous synapomorphies ('0' to '1' for characters 142, 186 and 236; '1' to '0' for character 161). Dashanpusaurus dongi shares two of these four characters within Macronaria: the PCPL of middle and posterior dorsal neural arches is absent (ch. 161); and the scapular length/minimum blade breadth ratio is 5.5 or more (ch. 236). Moreover, Dashanpusaurus dongi shares a sister clade with Camarasaurus, which is supported by two unambiguous synapomorphic characters: neural spine of posterior cervical and anterior dorsal vertebrae is bifid (ch. 132); and single PRSL of single, not bifid, dorsal neural spine is absent (ch. 142).

Discussion

Phylogenetic implications for macronarian evolution

In our EWP and EIW analyses (except for the EIW analysis using the data of Mannion et al. [2019]), Dashanpusaurus dongi is positioned as the basal-most member of Macronaria. This position is supported by many unambiguous synapomorphies (e.g. height divided by width is between 0.9 and 0.7 for cervical vertebrae; transverse processes of dorsal vertebrae are directed laterally or slightly upwards; middle and posterior dorsal centra in the transverse section are slightly dorsoventrally compressed) in the main data matrix. Dorsoventrally compressed cervical centra are widely observed in many later-diverging eusauropods (e.g. Mamenchisaurus [Ouyang & Ye 2002, table 4], Klamelisaurus gobiensis [Moore et al. 2020, table 1], Hudiesaurus sinojapanorum [Upchurch et al. 2021, fig. 2], Camarasaurus lewisi [McIntosh et al. 1996b, table 2]), and most of them are from the Late Jurassic or later. In the Middle Jurassic, only the Rutland Cetiosaurus (Upchurch & Martin 2002, table 2), Lingwulong shenqi (Xu et al. 2018, supplementary fig. 4) and Dashanpusaurus dongi are reported to share this character, especially among the other 'transversely compressed' sauropod taxa in Dashanpu quarry. The variation in cotyle shape in sauropod necks might arise from mechanical factors (Taylor 2022). Moreover, in the Middle Jurassic, the possession of bifurcated neural spines in the presacral vertebrae as seen in Lingwulong shenqi (posterior cervicals) and Dashanpusaurus dongi (preserved anterior to middle dorsals) is rare. The

bifurcated spines would increase the lateral leverage of the ligaments and muscles that attach to the metapophyses, thus enabling them to contribute to lateral stabilization and motion as well as vertical motion (Taylor & Wedel 2013). These cervical vertebral features may set them apart from the taxa with transversely compressed cervical centra and unsplit neural spines found at Dashanpu.

The length of the puboischial contact, reaching approximately one-half or greater of the total length of the pubis, is a plesiomorphic condition for Macronaria (e.g. Camarasaurus: Osborn & Mook 1921, fig. 88; Xu et al. 2018). By contrast, in non-neosauropod sauropod taxa (e.g. Shunosaurus lii: Zhang 1988, fig. 51), the ratio is less than one-third the length of the pubis. This ratio in Dashanpusaurus dongi is 0.4, which falls between the non-macronarian eusauropods and later-diverging macronarians. It further indicates the phylogenetic placement of Dashanpusaurus dongi in a basal position in Macronaria.

Conversely, Dashanpusaurus dongi lacks some characters that unite later-diverging macronarians, such as: a median tubercle that is present on the posterior cervical and anterior dorsal bifurcated neural spines; an articular surface of the posterior dorsal centra that is opisthocoelous; and the presence of pleurocoels along the lateral surfaces of the sacral centra (Xu et al. 2018). Furthermore, 12 or fewer dorsal vertebrae is a plesiomorphic condition for Omeisaurus + (Jobaria + Neosauropoda) (Wilson 2002). However, the number in Dashanpusaurus dongi is 13 (potentially 14) dorsal vertebrae, which is similar to the numbers in Shunosaurus lii and the neosauropod Haplocanthosaurus (probably 14 dorsals). Furthermore, the amphicoelous articular surfaces of the posterior dorsal vertebrae are a plesiomorphic condition for many Early–Middle Jurassic early-diverging sauropods, some diplodocoids (including the Middle Jurassic Lingwulong shenqi) and Dashanpusaurus dongi. Dashanpusaurus dongi still shares plesiomorphic features that may indicate its 'basal' position and possibly the species' mosaic morphological evolution.

The EPRL in early-diverging eusauropods

Epiphyses are common in saurischians and some lineages develop a lamina that crosses the SDF, connecting

Figure 35. Structures considered components of the epipophyseal-prezygapophyseal lamina (EPRL) feature exhibited in Dashanpusaurus dongi, Shunosaurus lii and Omeisaurus tianfuensis. A, B, Cv3 and D1 of Dashanpusaurus dongi (ZDM5028); C–G, Cv3, Cv7, Cv8, Cv9, Cv11 and Cv12 of Shunosaurus lii (ZDM5008); H–M, Cv3, Cv7, Cv8, Cv12, Cv15 and Cv17 of Omeisaurus tianfuensis (T5701 and T5705). Abbreviations: Cv, cervical; D, dorsal. Scale bar = 50 mm.
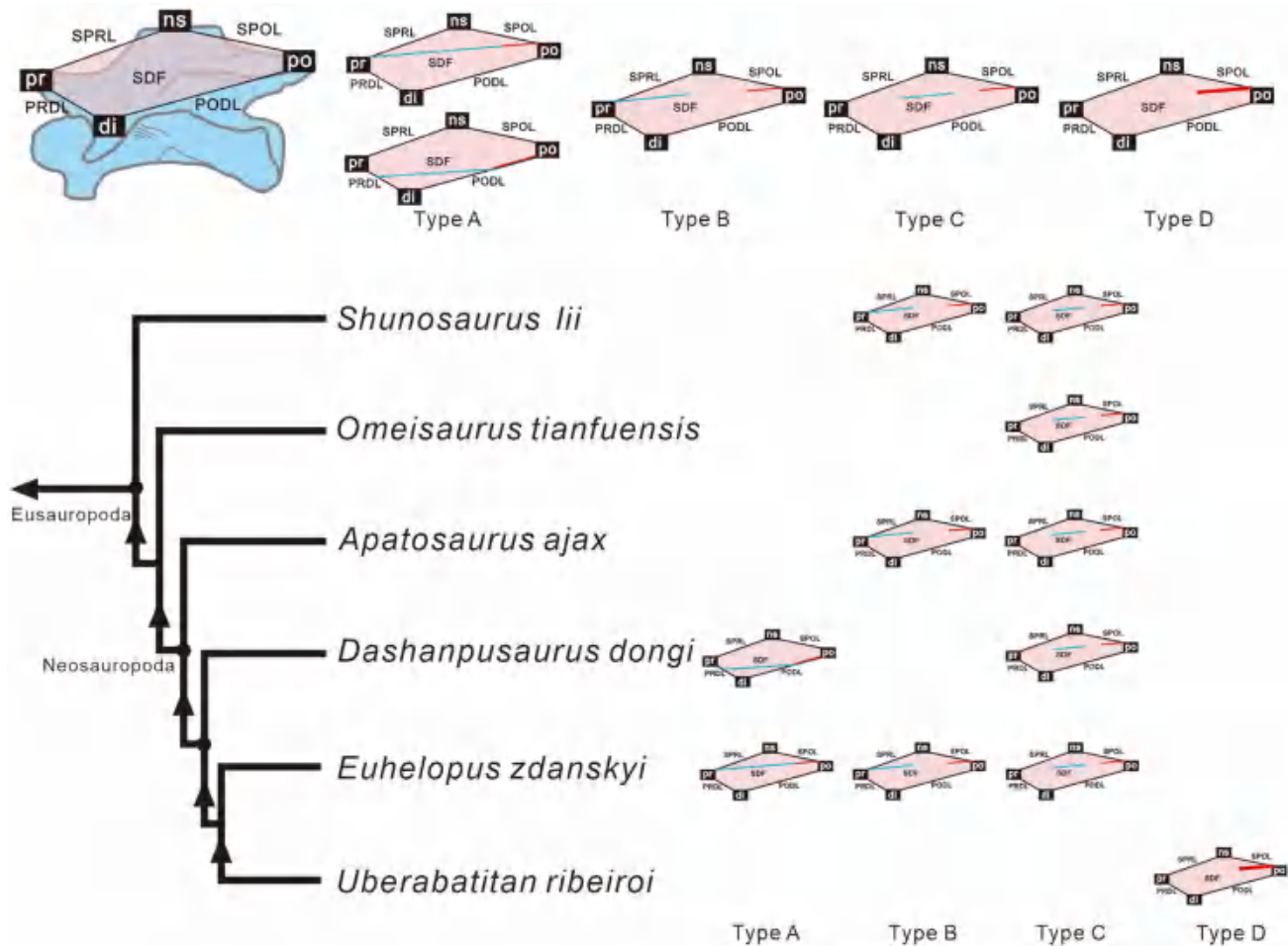
Figure 36. Types of the epipophyseal-prezygapophyseal lamina (EPRL) feature in cervical and anterior dorsal vertebrae of some eusauropod specimens representing several taxonomic groups. Shunosaurus lii, ZDM5008; Omeisaurus tianfuensis, ZDM T5701 and T5705; Apatosaurus ajax (after Upchurch et al. 2004a); Dashanpusaurus dongi, ZDM 5028; Euhelopus zdanskyi, PMU 233; Uberabatitan ribeiroi, CPP-1108-Urb. Abbreviations: di, diapophysis; ns, neural spine; po, postzygapophysis; PODL, postzygodiapophyseal lamina; pr, prezygapophysis; PRDL, prezygodiapophyseal lamina; SDF, spinodiapophyseal fossa; SPOL, spinopostzygapophyseal lamina; SPRL, spinoprezygapophyseal lamina.

them to the prezygapophyses in the cervical vertebrae (Wilson 2012) and sometimes the anterior dorsals (e.g. Wilson & Upchurch 2009, fig. 13). This feature was first recognized in the non-avian theropods Noasaurus and Carnotaurus (Bonaparte 1996b), then reported in many other theropods and later identified in many sauropods (Wilson 2012). This lamina was not named by Bonaparte (1996b) and has received many names and interpretations over the past few decades (e.g. Coria & Salgado 2000; O' Connor 2007; Sereno et al. 2007; Wilson & Upchurch 2009; Ezcurra et al. 2010; Dal Sasso & Maganuco 2011; Pol & Rauhut 2012; Wilson 2012; Moore et al. 2020). Among sauropods, this feature was first noted in Nigersaurus (Sereno et al. 2007, fig. 3). Wilson (2012) revised the existing definitions in accordance with the nomenclature devised by Wilson (1999) for sauropods, proposing the term 'epipophyseal-

prezygapophyseal lamina' (EPRL) (Wilson & Upchurch 2009) and distinguished two types: the lamina fully reaches and connects the prezygapophysis and epiphysis or connects the two landmarks via its union with the SPRL and PODL or prezygapophysis and epiphysis (we term this the 'standard' EPRL [Type A] in this study); or the 'stranded' EPRL where the lamina in the SDF contacts one of two landmarks (prezygapophysis or epiphysis), but in adjacent vertebrae its serial homologues contact two (Wilson 2012) (Type B in this study). Moore et al. (2020) argued against using the term EPRL and explicitly distinguished the pneumatic and muscular parts of the 'EPRL' from a truly segmented lamina in early-diverging sauropodomorphs that lack an SDF. Previously, a rugose anterior extension of the epiphysis (anterior epipophyseal muscle scar) and an unmoored lamina of the SDF (accessory strut of the
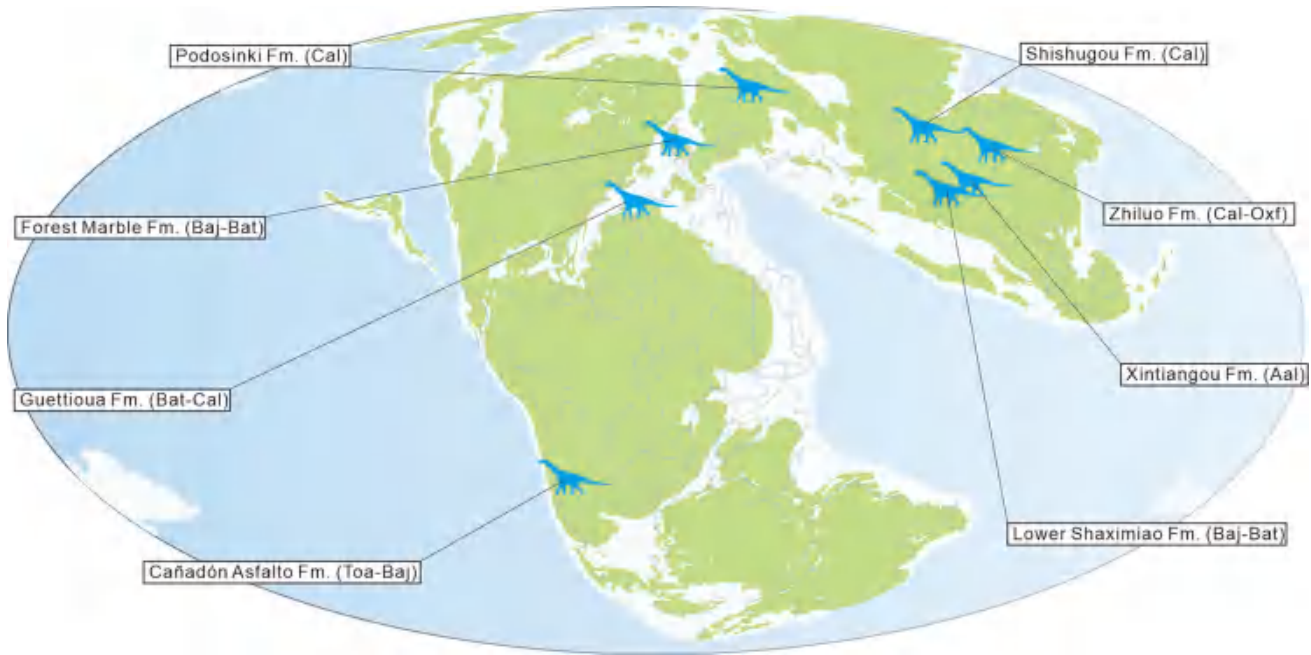
Figure 37. Palaeogeographic reconstruction showing the main Middle Jurassic neosauropod faunas discussed in this text. Palaeogeographic reconstruction of 170 Ma from PALEOMAP (Scotese 2014). Abbreviations: Aal, Aalenian; Baj, Bajocian; Bat, Bathonian; Cal, Callovian; Fm., formation.

SDF that is associated with pneumatized epithelium) were interpretable as the constituent elements of an EPRL. In Klamelisaurus gobiensis, the joint presence of these structures might indicate the EPRL is segmented. Moreover, these structures are more informatively considered distinct, rather than co-dependent (Moore et al. 2020). In particular, some vertebrae share more than one accessory strut across the SDF, with no convincing evidence for the one to be the constituent element of the EPRL feature. It is better to distinguish these struts from one constituent feature. Before better terms are applied, we advocate stating that the two structures are provisionally interpretable as an EPRL feature, rather than using the term EPRL, because these two terms are more accurate and descriptive of the actual morphology, and potentially more helpful for accurate homological analysis. Moreover, before the accurate homological interpretation of these two structures, intuitive morphological identification may be easier to operate for distinction – to identify this morphology easily, especially for usually partially preserved vertebral materials, and explore the potential synapomorphy for sauropod taxa. We distinguished four types of situations for this feature including the aforementioned 'Type A' and 'Type B', and added another two types of ERPL: a 'segmented' EPRL lamina where the laminae in the SDF are not attached directly to surrounding landmarks but extend past one another (Type C in this study), and a

pronounced anterior extension of the epipophysis that can be present in the absence of a strut of the SDF (we suggest 'partly' EPRL [Type D] in this study; e.g. Uberabatitan: Silva Junior et al. 2019, figs 3, 4). As Moore et al. (2020) mentioned, the osteological products of these soft tissues can often be distinguished and, when they can be identified, it is more anatomically informative to describe these structures separately in sauropods. Considering the lack of extensive evidence (e.g. the influence of morphogenetic soft tissues on some structures), it is still early to give hypotheses of the primary homology of the EPRL feature. We agree on the need to precisely describe these structures separately for the reason that they show the capacity for independent development in sauropods and that this can impact phylogenetic analyses (see Moore et al. 2020). Thus, we consider the structures of the EPRL feature from some early-diverging sauropods in the Dashanpu Dinosaur Fauna, to give more information on this feature as a homologous structure and to provide more information on it for a better understanding of these structures in future studies.

Dashanpusaurus dongi. In the preserved anterior cervical vertebrae (Cv4 and Cv6), rugose muscle scars extend from the epipophyseal ramus to the middle portion of the SDF. A robust strut crosses the SDF horizontally and disappears near the SPRL (Fig. 35A). This lamina morphologically approximates the 'accessory

strut of the SDF′ described in Cv5 of Camarasaurus lewisi (Moore et al. 2020). In the anterior dorsal vertebrae (D1 and D2) of Dashanpusaurus dongi, the morphologically distinct structures (Type A), on the lateral side of the neural arch are interpretable as the 'standard' EPRL as the anterior epipophyseal muscle scar extends from the epipophysis along the PODL, and the accessory strut distinctly extends from the PODL to the prezygapophysis. Each epipophysis is separated ventrally from its respective postzygapophysis by a shallow groove (D1: Fig 35B). The posterior portion of the muscle scar of the EPRL feature near the connection with the epipophysis is a low ridge above the SPOL. A weakly expressed line of rugosities is located dorsomedially to the smooth, rounded edge of the PODL. Anteriorly, a strut of the SDF is stout and extends as a combined ridge with the SPOL posteriorly near the anterior-most portion of the articular surface of the postzygapophysis. Then it crosses the neural spine to the base of the prezygapophysis, under the SPRL. This morphological condition is most similar to that of the preserved cervical of Zapalasaurus bonapartei, Cv10 of Nigersaurus taqueti and the middle cervical series of Euhelopus zdanskyi (Salgado et al. 2006, fig. 4; Sereno et al. 2007, fig. 3; Wilson & Upchurch 2009, fig. 10; Wilson 2012, fig. 3). By contrast, it is a stout element on the anterior dorsal vertebrae of Dashanpusaurus dongi, and the combination of the EPRL and PODL is much more robust compared with those on Cv10 of Euhelopus zdanskyi. However, it differs from the condition on the anterior dorsal vertebrae of Euhelopus zdanskyi with the remnant of SDF connecting the two landmarks directly (Wilson & Upchurch 2009).

Shunosaurus lii. A similar correspondence between an anterior epipophyseal muscle scar and an accessory strut of the SDF lamina of the SDF is apparent in Shunosaurus lii (ZDM5008) (Fig. 25C–G). In Cv3 of Shunosaurus lii (Fig. 35C), a rugose ridge (muscle scar) tops the posterior end of the postzygapophysis anteroposteriorly and a weak lamina (accessory strut) anteriorly crosses the SDF. The anterior and posterior margins of this lamina disappear near SPRL and PODL, respectively. These structures are interpreted as the 'segmented' EPRL (Type C). In Cv6 and Cv7 (Fig. 35D), the rugose muscle scars are much more prominently expanded than in Cv3 (blue arrows in Fig. 35C, D). The muscle scar on the dorsal surface of the postzygapophyseal ramus, along the PODL, extends further into the SDF. The SDFs of Cv6 and Cv7 contain a weak, smooth-edged accessory lamina (accessory strut of the SDF), as in Cv3. It disappears near the PODL posteriorly. This lamina is prominently elongated compared with that in Cv3. In contrast to the aforementioned cervical vertebrae, the accessory strut of Cv8 is prominent (Fig. 35E) and situated at the middle portion of the SDF. The rugose muscle scar further extending to the SDF from the epipophysis seems displaced by the horizontal lamina distally in SDF (yellow arrow in Fig. 35E). In this cervical, the segmented lamina (accessory strut) of the SDF and rugose ridge (anterior epipophyseal muscle scar) extending from the epipophyseal ramus are generally continuous, but still belong to the two structures that constituted the 'segmented' EPRL (Type C). On the other hand, the anterior portion of the rugose ridge from the epipophysis is more prominent than the posterior portion near the epipophysis. This condition is opposite to that in the anterior cervicals. In Cv10 and Cv11 (Fig. 35F), the rugose ridge, situated inwards near the base of the neural spine, extends further from the epipophysis into the middle portion of the SDF. The anterior portion of this ridge is robust and more prominent than the posterior portion, as occurred in the middle cervical vertebrae (e.g. Cv8). A horizontal lamina (accessory strut) is situated in a secondary pneumatic fossa (situated at the base of SDF, much deeper than other regions of SDF) that crosses the SDF. This sharp ridge ends at the anterior and posterior margins of the secondary pneumatic fossa. The rugose ridge (muscle scar) from the epipophysis and the horizontal lamina of SDF is not continuous, and these two segmented structures constitute the 'segmented' EPRL (Type C). It is worth noting that the horizontal lamina of SDF in Cv12 (Fig. 35G) extends from the PODL, which seems to connect to the anterior epipophyseal muscle scar, and disappears anteriorly in SDF, projecting to the prezygapophysis. This structure closely aligns with the rugose 'stranded' lamina (Type B).

The EPRL featured in the cervical neural arch of Shunosaurus lii bears two distinct types: the 'segmented' EPRL (Type C, which consists of the anterior epipophyseal muscle scar and the 'segmented' accessory strut of the SDF in most of the cervical vertebrae except the last one) and the 'stranded' EPRL (Type B, which includes the anterior epipophyseal muscle scar and 'stranded' horizontal lamina of the SDF that extend from PODL and project to the prezygapophysis in Cv12). In contrast to the 'segmented' lamina of SDF in Omeisaurus tianfuensis, this lamina is much more weakly and solely extended in the SDF of Shunosaurus lii.

Omeisaurus tianfuensis. Slight variation in the morphology of the cervical neural arches in Omeisaurus tianfuensis (Cv3, 15 and 17 of T5701 and Cv7 and 8 of T5705) provides strong evidence that the anterior epipophyseal muscle scars and pneumatic laminae of the SDF

constitute the EPRL feature in this lineage (Fig. 35H–M).

In Cv3 of Omeisaurus tianfuensis (Fig. 35H), the epipophysis is slightly expanded. A low rugose ridge extends anteriorly from the epipophysis and crosses the posterior portion of the SDF. This muscle scar then disappears in the middle portion of the SDF. Anteriorly, a stout lamina anteriorly extends that crosses the SDF but fades near the SPRL. This latter structure approximates the 'segmented' lamina of the EPRL (Type C) described in Camarasaurus lewisi and Klamelisaurus gobiensis (Moore et al. 2020). Cv6 shares a relatively stout nodule on the dorsal surface of the postzygapophyseal ramus and extends beyond the distal end of the postzygapophysis posteriorly. The anterior projection of the muscle scar is sub-parallel with the PODL and extends farther anteriorly towards the SDF. A stout but short lamina (accessory strut) crosses the SDF anteroposteriorly. This accessory lamina is situated at the anterior portion of the SDF and is dissolved near the SPRL. This condition resembles that found in Cv3. A similar arrangement is present in Cv7 of Omeisaurus tianfuensis (Fig. 35I). In contrast to Cv3, the epipophysis is weakly projected whereas the muscle scars are prominent ridges that do not extend to the junction area of the SDF. Interestingly, the SDF of Cv7 contains two robust, smooth-edged accessory laminae on the middle portion. These two laminae are generally parallel and anteroventrally extended. The lower lamina is dissolved on the dorsal portion of the diapophysis. These structures of the EPRL feature in Cv7 can be classified as Type C. In Cv8 of Omeisaurus tianfuensis (Fig. 35J), the accessory laminae of the SDF are more prominent than any other cervical vertebrae noted above. At least five struts occupy the anterior portion of the SDF: two of these project anteroventrally under the anterior portion of the neural spine and three project anteroposteriorly toward the prezygapophysis. It is worth noting that the lower anteroventrally oriented and dorsal-most anteriorly extended laminae are serially segmented from the epipophysis towards the SPRL, and possibly belong to the accessory strut. In addition to the soft tissue attached to muscle scars for the epipophysis, conspicuous pneumatic structures were preserved in the SDF in sauropods (Wilson et al. 2011). In Cv12 (Fig. 35K) and Cv14, the epipophysis extends beyond the postzygapophysis and the posterior portion of the epaxial musculature is more prominent than the anterior segments. A thin lamina crosses the middle portion of the SDF and projects anteroventrally. The rugose ridge is robust along the PODL and anteriorly extended in Cv15 (Fig. 35L), as occurs in other cervical vertebrae. An accessory lamina is situated at the anterior portion of the SDF (yellow arrow in Fig. 35L), similar to that in many other cervical vertebrae (e.g. Cv7). In Cv16 and 17 (Fig. 35M), the posterior portions of the muscle scars are more extended than the anterior portion, similar to those in Cv12 and Cv14. The segmented lamina crosses in a secondary pneumatic fossa and is situated at the anterior portion of the SDF.

In short, the ridge extending anteriorly from the epipophysis and a (or several) lamina(e) of the SDF constitute the structures of the EPRL feature. The lamina(e) of SDF is (or are) situated at the anterior portion of the SDF and horizontally or slightly ventrally. This entity could be considered to have a 'segmented EPRL', belonging to type C, in the cervical vertebrae of Omeisaurus tianfuensis.

Our observation shows the two structures (rugose muscle scar extended from epipophyseal ramus and accessory strut(s) usually horizontally crossing the SDF), constitute the features of the ERPL and are universally found in some early-diverging eusauropods (especially in Asian lineages at present). These two structures could vary in appearance (e.g. 'segmented' or 'stranded') in a single cervical series of a species. Limited by observation and referred specimens, we cannot establish a paradigm at present, but the EPRL feature exists widely in some early-diverging eusauropods (Fig. 36). Although there are different types of this feature, these widespread morphologies might indicate an important function for the EPRL feature. However, more anatomical information needs to be collected before further homological analysis of these structures can be conducted.

Spatiotemporal distribution of eusauropod materials in the Middle Jurassic

The presence of a new macronarian sauropod from China provides further evidence of the diversity and biogeography of the clade during the Middle Jurassic. Early putative macronarians are typically represented in the fossil record as fragmentary bones (Moser et al. 2006) or teeth (Bindellini & Dal Sasso 2019), making the specimens described here some of the best-preserved evidence of a basal macronarian sauropod to date. The sauropod fossils preserved within the lower Shaximiao Formation provide the first information to suggest that individual variation or sexual dimorphism may have been present among populations of Dashanpusaurus dongi during the Middle Jurassic (e.g. the orientation of anterior caudal neural spines between the holotype and paratype), though the extent of individual variation still needs to be analysed. The lack of globally distributed macronarians in the Middle Jurassic suggests that the clade was able to disperse rapidly during, or just prior to, the Middle Jurassic before diversifying into the Late

Jurassic basal macronarian and titanosauriform taxa present in Asia (e.g. Mo 2013), Europe (e.g. Royo-Torres et al. 2014), North America (e.g. McIntosh et al. 1996a), South America (e.g. Carballido et al. 2011b) and Africa (e.g. Fraas 1908). Additionally, the sauropods from the Late Jurassic Tendaguru Formation of Tanzania further indicate a more widespread diversification of many sauropod clades than realized previously (Mannion et al. 2019). Previous studies have proposed that a shallow marine barrier isolated Asia via the western margin of the continent starting in the Late Jurassic and receding in the Early Cretaceous (Russell 1993; Upchurch et al. 2002). Dubbed the ʹEast Asian Isolation Hypothesisʹ (EAIH), it suggested that terrestrial faunas would have been isolated in Central and East Asia, leading to endemism within the continent (e.g. mamenchisaurids: Xing et al. 2015b). Here, we propose that the basal-most macronarian, D. dongi, provides more evidence that conflicts with the interpretation of a permanent marine barrier during at least the Jurassic that would support the EAIH. If D. dongi is the basal-most macronarian, then it is probable that any marine barrier that existed during the Middle Jurassic would have been intermittent based on the global distribution of other basal macronarians (e.g. camarasaurids) and titanosauriforms in the Late Jurassic. This hypothesis is further supported if the African sauropod Atlasaurus imelakei is retrieved as a basal macronarian, although the placement of A. imelakei is still uncertain (e.g. Upchurch et al. 2015; Mannion et al. 2019; Moore et al. 2020; this study). Several other geographical regions preserved diverse eusauropod faunas, including some potential Middle Jurassic neosauropods (Fig. 37), and brief comparisons are made below.

1. Africa. Four areas with Middle Jurassic sauropod material have been reported (Nicholl et al. 2018; Mannion et al. 2019): Morocco (Atlasaurus and ʹCetiosaurusʹ mogrebiensis), Algeria (Chebsaurus), Niger (Spinophorosaurus and Jobaria) and Madagascar (Lapparentosaurus, Archaeodontosaurus and ʹBothriospondylus madagascariensisʹ) (Lapparent 1955; Bonaparte 1986a; Monbaron et al. 1999; Sereno et al. 1999; Upchurch & Martin 2003; Buffetaut 2005; Mahammed et al. 2005; Rauhut & López-Arbarello 2009; Remes et al. 2009; Läng and Mahammed 2010; Mannion 2010; Raveloson et al. 2019). Many African sauropod remains are poorly preserved and they have seldom been included in phylogenetic analyses due to a lack of useful anatomical detail. For example, the initial report on Archaeodontosaurus indicated that it had a similar morphology to the Chinese species Protognathosaurus oxyodon (Buffetaut 2005).

However, it was later recovered as a non-eusauropod sauropod (Pol et al. 2020), and the morphology of Chebsaurus shows more affinities with Lapparentosaurus and Cetiosaurus (Mahammed et al. 2005). New information on Lapparentosaurus suggests that the relatively fragmentary elements provide information on the autapomorphies shared with Cetiosaurus (Raveloson et al. 2019), which lies outside the Neosauropoda (Mannion et al. 2013). Spinophorosaurus nigerensis was reported from the Irhazer Group (Bajocian–Bathonian) of Niger (Remes et al. 2009). Some studies phylogenetically supported it as a non-eusauropod sauropod (Remes et al. 2009; Holwerda et al. 2021), while another recovered it as a non-neosauropod eusauropod (Pol et al. 2020). Moreover, Jobaria tiguidensis was the other sauropod taxon excavated from the Irhazer Group (Bathonian–Callovian) in Niger (Sereno et al. 1999; Rauhut & López-Arbarello 2009). Phylogenetically, it was situated outside of Neosauropoda (e.g. Mannion et al. 2019; Moore et al. 2020; Pol et al. 2020), but it was also supported as a basal neosauropod (e.g. Carballido et al. 2020). Atlasaurus imelakei was excavated from the Guettioua Formation (Bathonian–Callovian) in Morocco (Monbaron et al. 1999). In some phylogenetic analyses Atlasaurus imelakei is positioned as an early-diverging macronarian, while others find it as a non-neosauropod eusauropod (e.g. Mannion et al. 2017; Moore et al. 2020). Our phylogenetic analyses support it as either a basal-most member of Diplodocoidea or as a macronarian (e.g. Mannion et al. 2019; Liao et al. 2021).

2. South America. Late Early–Middle Jurassic sauropods from South America are restricted to a small number of localities in southern Argentina. Most of the remains belong to Patagosaurus fariasi, Volkheimeria chubutensis and Bagualia alba, which were excavated in the upper sections of the Cañadón Asfalto Formation (Toarcian–Aalenian or Bajocian) (Bonaparte 1986b; Rauhut 2003; Cúneo et al. 2013; Hauser et al. 2017; Pol et al. 2020). Phylogenetically, these three taxa are found outside of Neosauropoda (Pol et al. 2020). Patagosaurus fariasi is often recovered as the sister clade to Cetiosaurus (e.g. Xu et al. 2018; Carballido et al. 2020) and Volkheimeria chubutensis was found as a non-sauropod sauropodomorph or non-eusauropod sauropod (Pol et al. 2020; Holwerda et al. 2021). Some fragmentary remains indicate more diversity among the sauropod taxa (Rauhut 2003; Holwerda et al. 2015), including some with putative

neosauropod affinities in the latest Early–Middle Jurassic Patagonia (Carballido et al. 2017).

3. Europe. The most common Middle Jurassic sauropod from the United Kingdom is the non-neosauropod eusauropod Cetiosaurus, which has been recovered from several Bajocian–Bathonian localities (Upchurch & Martin 2002, 2003). The Callovian Cetiosauriscus stewarti from the Oxford Clay Formation (Charig 1980, 1993) was recovered as a dicraeosaurid in this study. Holwerda et al. (2019) reported four isolated sauropod axial elements from the Middle Jurassic (Callovian) Oxford Clay Formation of Peterborough in the UK which includes possible neosauropod affinities. Many other Middle Jurassic materials from the UK are fragmentary and can only be regarded as indeterminate eusauropods rather than referring them to particular taxa (Mannion et al. 2019). In Russia, the Middle Jurassic (Callovian) marine deposits of the Podosinki Formation have produced two anterior caudal vertebrae from a single individual referred to Diplodocoidea (Averianov & Zverkov 2020).

4. India. Moser et al. (2006) reported fragmentary camarasaurid-like material from the Middle Jurassic (Bajocian) Khadir Formation of Khadir Island. However, these materials have never been assessed phylogenetically.

5. Eastern Asia. Middle Jurassic Eastern Asia is generally dominated by non-neosauropod eusauropods, particularly in south-west China, including well-known taxa such as Shunosaurus and Omeisaurus spp. and others like Yuanmousaurus and Nebulasaurus. The recently reported diplodocoid Lingwulong, from the Middle Jurassic (Callovian) Zhiluo Formation (Ningxia, north-west China), is the only valid neosauropod taxon in Middle Jurassic Asia (Xu et al. 2018; You et al. 2019). Its bone-bearing stratum was first suggested to be from the Yan'an Formation (Xu et al. 2018), but a systematic sedimentary analysis showed that the bone-bearing horizon was in the upper portion of the Zhiluo Formation (the Zhiluo Formation overlies the Yan'an Formation) (You et al. 2019). Bellusaurus sui is reported from the upper part of the Shishugou Formation (Dong 1990) with the age of the horizon being late Middle Jurassic (Mo 2013). However, this unit has since been re-assigned to the Late Jurassic (Oxfordian: Moore et al. 2020). Recent phylogenetic analyses have positioned Bellusaurus sui as an early-diverging macronarian or lying just outside of Neosauropoda (e.g. Mannion et al. 2019; Carballido et al. 2020; Moore et al. 2020; Pol et al. 2020). Our phylogenetic analyses place the species near the base of Macronaria. Woodruff & Fowler (2012) suggested that immature dinosaurs may occupy more basal positions in phylogenetic analyses because their morphologies are often similar to their ancestral states. It is possible that the early ontogenetic stage of this sauropod is the reason that its position is unstable in phylogenetic analyses. Additionally, Bashunosaurus kaijiangensis is reported as a macronarian from the lower Shaximiao Formation (the specific horizon is unknown) of Kaijiang, Sichuan. However, this taxon has not been described in detail or included in a phylogenetical analysis. The potential macronarian position for this taxon should be treated with caution. Furthermore, Tan et al. (in preparation) reported two isolated sauropod dorsal vertebrae from the lower Shaximiao Formation of Chongqing, south-west China, and phylogenetic analyses support these as possible diplodocid materials.

6. Summary. Middle Jurassic deposits have yielded evidence of neosauropods from at least four continents (Asia, South America, Europe and Africa). Phylogenetic analysis shows that most of the taxa from this era are non-neosauropod eusauropods. It is seldom that neosauropod specimens from the Middle Jurassic are taxonomically valid. Middle Jurassic eusauropods display a great range of diversity and geographic distribution. This indicates that basal members of the leading eusauropod lineages appeared earlier than previously realized. The record of Middle Jurassic neosauropods consists of fragmentary materials that could also be considered to represent an early radiation of Neosauropoda. Differentiated dental morphology and teeth with wear facets have been reported from the basal layer of the Cañadón Asfalto Formation (late Early Jurassic–Middle Jurassic). This variety indicates different food-gathering strategies and implies potentially separate lineages (Upchurch & Barrett 2000). In that sense, the placement of phylogenetically distinct lineages of eusauropods further pushes the initial diversification event of the neosauropod clade to an earlier age than expected. Neosauropods were already highly diverse during the Middle Jurassic (Fig. 37).

Conclusions

Our comprehensive description and re-assessment of Dashanpusaurus dongi indicates that it is a valid taxon that can be distinguished from other Middle Jurassic sauropods. Moreover, morphological comparisons to

other macronarians reveal many synapomorphic similar-
ities. The comparative anatomical data presented here
provides an opportunity for not only re-visiting the
phylogenetic relationships within Neosauropoda but also
carrying out a revision of the taxonomy and systematics
of sauropods from the Middle Jurassic of China.
Anatomical comparisons of the cervical vertebrae of
several other Middle Jurassic early-diverging eusauro-
pod lineages in the Dashanpu quarry indicate that con-
stituent structures of the ʹEPRL featureʹ are prevalent
among early-diverging eusauropods, and it is better to
use this term separately from ʹEPRLʹ. However, more
anatomical comparisons are needed for establishing
homologies. As an early-diverging macronarian, a better
understanding of Dashanpusaurus dongi allows for a
better understanding of the origin, early evolution and
palaeogeographic distribution of neosauropods.
Moreover, we demonstrate that sauropods had greater
morphological diversity in the Middle Jurassic of Asia
than previously thought. This study also suggests that
the increase in diversity of the neosauropod clade
occurred much earlier than previously realized.

Acknowledgements

Supplemental material

Supplemental material for this article can be accessed
here: https://dx.doi.org/10.1080/14772019.2022.2132886.

ORCID

Shan Jiang http://orcid.org/0000-0001-7766-222X
Xu-Ri Wang http://orcid.org/0000-0003-2947-0439
Hai-Lu You http://orcid.org/0000-0003-2203-6461

References

Allain, R. & Aquesbi, N. 2008. Anatomy and phylogenetic
relationships of Tazoudasaurus naimi (Dinosauria,
Sauropoda) from the late Early Jurassic of Morocco.
Geodiversitas, 30, 345–424.

Averianov, A. O. & Zverkov, N. G. 2020. New diplodocoid
sauropod dinosaur material from the Middle Jurassic of
European Russia. Acta Palaeontologica Polonica, 65,
499–509. doi:10.4202/app.00724.2020

Bandyopadhyay, S., Gillette, D. D., Ray, S. & Sengupta,
D. P. 2010. Osteology of Barapasaurus tagorei
(Dinosauria: Sauropoda) from the Early Jurassic of India.
Palaeontology, 53, 533–569. doi:10.1111/j.1475-4983.
2010.00933.x

Barco, J. L., Canudo, J. I. & Cuenca-Bescós, G. 2006.
Descripción de las vértebras cervicales de Galvesaurus
herreroi Barco, Canudo, Cuenca-Bescós & Ruiz-Omeñaca,
2005 (Dinosauria, Sauropoda) del tránsito Jurásico
Cretácico en Galve (Teruel, España). Revista Española de
Paleontología, 21, 189–205. doi:10.7203/sjp.21.2.20490

Barrett, P. M., Butler, R. J. & Knoll, F. 2005. Small-bodied
ornithischian dinosaurs from the Middle Jurassic of
Sichuan, China. Journal of Vertebrate Paleontology, 25,
823–834.

Bindellini, G. & Dal Sasso, C. 2019. Sauropod teeth from the
Middle Jurassic of Madagascar, and the oldest record of
Titanosauriforms. Papers in Palaeontology, 7, 137–161.
doi:10.1002/spp2.1282

Bonaparte, J. F. 1986a. The early radiation and phylogenetic
relationships of the Jurassic sauropod dinosaurs, based on
vertebral anatomy. Pp. 247–258 in Padian, K. (ed.) The
beginning of the age of dinosaurs. Cambridge University
Press, Cambridge.

Bonaparte, J. F. 1986b. Les Dinosaures (Carnosaures,
Allosauridés, Sauropodes, Cétiosauridés) du
Jurassiquemoyen de Cerro Condor (Chubut, Argentine)
(Dinosaurs (carnosaurs, allosaurids, sauropods,
cetiosaurids) of the Middle Jurassic of Cerro Cóndor,
Chubut, Argentina). Annales de Paléontologie, 72,
325–386.

Borsuk-Bialynicka, M. 1977. A new camarasaurid sauropod
Opisthocoelicaudia skarzynskii, gen. n., sp. n., from the
Upper Cretaceous of Mongolia. Palaeontologia Polonica,
37, 5–64.

Britt, B. B., Scheetz, R. D., Whiting, M. F. & Wilhite,
D. R. 2017. Moabosaurus utahensis, n. gen., n. sp., a new
sauropod from the Early Cretaceous (Aptian) of North
America. Contributions from the Museum of Paleontology,
University of Michigan, 32, 189–243. doi:10.1671/0272-
4634(2008)28[712:ANSTSG]2.0.CO;2

Buffetaut, E. 2005. A new sauropod dinosaur with
prosauropod-like teeth from the Middle Jurassic of
Madagascar. Bulletin de la Societe Geologique de France,
176, 467–473.

Canudo, J. I., Royo-Torres, R. & Cuenca-Bescós, G. 2008.
A new sauropod: Tastavinsaurus sanzi gen. et sp. nov.
from the Early Cretaceous (Aptian) of Spain. Journal of
Vertebrate Paleontology, 28, 712–731. doi:10.1671/0272-
4634(2008)28[712:ANSTSG]2.0.CO;2

Carballido, J. L., Pol, D., Cerda, I. & Salgado, L. 2011a.
The osteology of Chubutisaurus insignis del Corro, 1975
(Dinosauria: Neosauropoda) from the ʹmiddleʹ Cretaceous

of central Patagonia, Argentina. Journal of Vertebrate Paleontology, 31, 93–110. doi:10.1080/02724634.2011.539651

Carballido, J. L., Rauhut, O. W. M., Pol, D. & Salgado, L. 2011b. Osteology and phylogenetic relationships of Tehuelchesaurus benitezii (Dinosauria, Sauropoda) from the Upper Jurassic of Patagonia. Zoological Journal of the Linnean Society, 163, 605–662. doi:10.1111/j.1096-3642.2011.00723.x

Carballido, J. L. & Sander, P. M. 2014. Postcranial axial skeleton of Europasaurus holgeriholgeri (Dinosauria, Sauropoda) from the Upper Jurassic of Germany: implications for sauropod ontogeny and phylogenetic relationships of basal Macronaria. Journal of Systematic Palaeontology, 12, 335–387. doi:10.1080/14772019.2013.764935

Carballido, J. L., Holwerda, F. M., Pol, D. & Rauhut, O. W. M. 2017. An Early Jurassic sauropod tooth from Patagonia (Cañadón Asfalto Formation): implications for sauropod diversity. Publicación Electrónica de la Asociación Paleontológica Argentina, 17, 50–57.

Carballido, J. L., Scheil, M., Knötschke, N. & Sander, M. 2020. The appendicular skeleton of the dwarf macronarian sauropod Europasaurus holgeri from the Late Jurassic of Germany and a re-evaluation of its systematic affinities. Journal of Systematic Palaeontology, 18, 739–781. doi:10.1080/14772019.2019.1683770

Charig, A. J. 1980. A diplodocid sauropod from the lower cretaceous of England. Pp. 231–244 in Jacobs, L. L. (ed.) Aspects of vertebrate history. Museum of Northern Arizona Press, Flagstaff.

Charig, A. J. 1993. Case 1876 Cetiosauriscus von Huene, 1927 (Reptilia, Sauropodomorpha): proposed designation of C. stewarti (Charig, 1980) as the type species. Bulletin of Zoological Nomenclature, 50, 282–283.

Chen, P.-J., Li, W.-B., Chen, J.-H., Ye, C.-H., Wang, Z., Shen, Y.-B. & Sun, D.-L. 1982. Sequence of fossil biotic groups and stratigraphical classification of Jurassic and Cretaceous in China. Scientia Sinica B, 25, 1011–1020.

Chure, D., Britt, B. B., Whitlock, J. A. & Wilson, J. A. 2010. First complete sauropod dinosaur skull from the Cretaceous of the Americas and the evolution of sauropod dentition. Naturwissenschaften, 97, 379–391.

Cooper, M. R. 1984. A reassessement of Vulcanodon karibaensis raath (Dinosauria: Saurischia) and the origin of the Sauropoda. Palaeontologia africana, 25, 203–231. doi:10.1007/s00114-010-0650-6

Coria, R. A. & Salgado, L. 2000. A basal Abelisauria Novas, 1992 (Theropoda–Ceratosauria) from the Cretaceous of Patagonia, Argentina. GAIA – Ecological Perspectives on Science and Society, 15, 89–102.

Cúneo, R., Ramezani, J., Scasso, R., Pol, D., Escapa, I., Zavattieri, A. M. & Bowring, S. A. 2013. High-precision U-Pb geochronology and a new chronostratigraphy for the Cañadón Asfalto Basin, Chubut, central Patagonia: Implications for terrestrial faunal and floral evolution in Jurassic. Gondwana Research, 24, 1267–1275. doi:10.1016/j.gr.2013.01.010

Curry Rogers, K. A. 2009. The postcranial osteology of Rapetosaurus krausei (Sauropoda: Titanosauria) from the Late Cretaceous of Madagascar. Journal of Vertebrate Paleontology, 29, 1046–1086.

D'Emic, M. D. 2012. The early evolution of titanosauriform sauropod dinosaurs. Zoological Journal of the Linnean Society, 166, 624–671. doi:10.1111/j.1096-3642.2012.00853.x

Dai, H., Ma, Q. Y., Hu, X. F., Zhou, Y. X., Tan, C. & Li, N. 2020. A new dinosaur fauna is discovered in Yunyang, Chongqing, China. Acta Geologica Sinica (English Edition), 94, 216–217.

Dal Sasso, C. & Maganuco, S. 2011. Scipionyx samniticus (Theropoda: Compsognathidae) from the Lower Cretaceous of Italy. Osteology, ontogenetic assessment, phylogeny, soft tissue anatomy, taphonomy, and palaeobiology. Memorie della Società Italiana di Scienze Naturali e del Museo Civico di Storia Naturale di Milano, 37, 1–282.

Deng, S.-H., Lu, Y.-Z., Zhao, Y., Fan, R., Wang, Y.-D., Yang, X.-J., Li, X. & Sun, B.-N. 2017. The Jurassic palaeoclimate regionalization and evolution of China. Earth Science Frontiers, 24, 106–142. doi:10.13745/j.esf.2017.0l.007

Dong, Z.-M. 1990. On remains of the sauropods from Kelamaili Region, Junggar Basin, Xinjiang, China. Vertebrata PalAsiatica, 28, 43–58.

Dong, Z.-M., Zhou, S.-W. & Zhang, Y.-Z. 1983. The Jurassic dinosaurs of the Sichuan Basin. Palaeontologica Sinica, Series C, 23, 1–136.

Dong, Z.-M. & Tang, Z.-L. 1984. Note on a new Mid-Jurassic sauropod (Datousaurus bashanensis gen. et sp. nov.) from Sichuan Basin, China. Vertebrata PalAsiatica, 22, 69–75.

Dong, Z.-M. & Tang, Z.-L. 1985. A new Mid-Jurassic theropod (Gasosaurus constructus gen, et sp. nov.) from Dashanpu, Zigong, Sichuan Province, China. Vertebrata PalAsiatica, 23, 77–83.

Du, C.-Q. & Wang, Q.-L. 2009. Characteristics of sporo-pollen assemblages near the boundary of the Upper and Lower Shaximiao Formations of the Middle Jurassic in Jinsha, Guizhou. Proceedings of Guizhou Geological Science and Technology and Prospecting Breakthrough Forum, 26, 12–14.

Ezcurra, M. D., Agnolin, F. L. & Novas, F. E. 2010. An abelisauroid dinosaur with a non-atrophied manus from the Late Cretaceous Pari Aike Formation of southern Patagonia. Zootaxa, 2450, 1–25. doi:10.11646/zootaxa.2450.1.1

Fang, X.-S., Pang, Q.-Q., Lu, L.-W., Zhang, Z.-X., Pan, S.-G., Wang, Y.-M., Li, X.-K. & Cheng, Z.-W. 2000. Lower, Middle, and Upper Jurassic subdivision in the Lufeng region, Yunnan Province. Pp. 208–214 in Anonymous (ed.) Proceedings of the Third National Stratigraphical Conference of China. Geological Publishing House, Beijing.

Fraas, E. 1908. Ostafrikanische Dinosaurier. Palaeontographica, 55, 105–144.

Gao, Y.-H. 1993. A new species of Szechuanosaurus from the Middle Jurassic of Dashanpu, Zigong, Sichuan. Vertebrata PalAsiatica, 33, 308–314.

Gauthier, J. 1986. Saurischian monophyly and the origin of birds. Memoirs of the California Academy of Sciences, 8, 1–55.

Gilmore, C. W. 1936. Osteology of Apatosaurus with special reference to specimens in the Carnegie Museum. Memoirs of the Carnegie Museum, 11, 175–300.

Gilmore, C. W. 1946. Reptilian fauna of the north Horn Formation of central Utah. US Geological Survey Professional Paper, 210, 29–53.

Goloboff, P. A. 2014. Extended implied weighting. Cladistics, 30, 260–272. doi:10.1111/cla.12047

Goloboff, P. A., Farris, J. S., Källersjö, M., Oxelman, B., Ramıacuterez, M. J. & Szumik, C. A. 2003. Improvements to resampling measures of group support. Cladistics, 19, 324–332. doi:10.1111/j.1096-0031.2003.tb00376.x

Goloboff, P., Farris, J. S. & Nixon, K. C. 2008. TNT, a free program for phylogenetic analysis. Cladistics, 24, 774–786. doi:10.1111/j.1096-0031.2008.00217.x

Goloboff, P. A. & Catalano, S. A. 2016. TNT version 1.5, including a full implementation of phylogenetic morphometrics. Cladistics, 32, 221–238. doi:10.1111/cla.12160

González Riga, B. J., Mannion, P. D., Poropat, S. F., David, O. D. L. & Coria, J. P. 2018. Osteology of the Late Cretaceous Argentinean sauropod dinosaur Mendozasaurus neguyelap: implications for basal titanosaur relationships. Zoological Journal of the Linnean Society, 184, 136–181. doi:10.1093/zoolinnean/zlx103/4816851

Harris, J. D. 2006. Cranial osteology of Suuwassea emilieae (Sauropoda: Diplodocoidea: Flagellicaudata) from the Upper Jurassic Morrison Formation of Montana, USA. Journal of Vertebrate Paleontology, 26, 88–102.

Hatcher, J. B. 1903. Osteology of Haplocanthosaurus. Memoirs of the Carnegie Museum, 2, 1–75.

Hauser, N., Cabaleri, N. G., Gallefo, O. F., Monferran, M. D., Nieto, D. S., Armella, C., Matteini, M., González, P. A., Pimentei, M. M., Volkheimer, W. & Reimold, W. U. 2017. U-Pb and Lu-Hf zircon geochronology of the Cañadón Asfalto Basin, Chubut, Argentina: implications for the magmatic evolution in central Patagonia. Journal of South American Earth Sciences, 78, 190–212.

He, X.-L., Li, K., Cai, K.-J. & Gao, Y.-H. 1984. Omeisaurus tianfuensis – a new species of Omeisaurus from Dashanpu, Zigong, Sichuan. Journal of the Chengdu College of Geology (Supplement), 2, 13–32.

He, X.-L., Li, C. & Cai, K.-J. 1988. Omeisaurus tianfuensis. The Middle Jurassic dinosaur fauna from Dashanpu, Zigong, Sichuan: sauropod dinosaurs. Volume 4. Sichuan Publishing House of Science and Technology, Chengdu, 143 pp.

Holwerda, F. M., Pol, D. & Rauhut, O. W. 2015. Using dental enamel wrinkling to define sauropod tooth morphotypes from the Cañadón Asfalto Formation, Patagonia, Argentina. PLoS ONE, 10, e0118100. doi:10.1371/journal.pone.0118100

Holwerda, F. M., Evans, M. & Liston, J. J. 2019. Additional sauropod dinosaur material from the Callovian Oxford Clay Formation, Peterborough, UK: evidence for higher sauropod diversity. PeerJ, 7, e6404. doi:10.7717/peerj.6404

Holwerda, F. M., Rauhut, O. W. M. & Pol, D. 2021. Osteological revision of the holotype of the Middle Jurassic sauropod dinosaur Patagosaurus fariasi Bonaparte, 1979 (Sauropoda: Cetiosauridae). Geodiversitas, 43, 575–643. doi:10.5252/geodiversitas2021v43a16

Huang, D.-Y. 2019. Jurassic integrative stratigraphy and timescale of China. Science China Earth Science, 62, 223–255. doi:10.1007/s11430-017-9268-7

Huene, F. von. 1932. Die Fossile Reptil-ordnung Saurischia: Ihre Entwicklung und Geschichte. Gebruder Borntraeger. Monographien Geologie und Palaontologie, 1, 1–361.

Jiang, S., Li, F., Peng, G.-Z. & Ye, Y. 2011. A new species of Omeisaurus from the Middle Jurassic of Zigong, Sichuan. Vertebrata PalAsiatica, 49, 185–194.

Kuang, X.-W. 2004. A new Sauropoda from Kaijiang dinosaur fauna in Middle Jurassic beds of North-Eastern Sichuan. P. 40 in Sun, J.-W. (ed.) Collection of the 90th anniversary of Tianjin Museum of Natural History. Tianjin Science and Technology Press, Tianjin.

Läng, E. & Mahammed, F. 2010. New anatomical data and phylogenetic relationships of Chebsaurus algeriensis (Dinosauria, Sauropoda) from the Middle Jurassic of Algeria. Historical Biology, 22, 142–164. doi:10.1080/08912960903515570

de Lapparent, A. F.. 1955. Étude paléontologique des vertébrés du Jurassique d′El Mers. Notes et Mémoires du Service Géologique du Maroc, 124, 1–36.

Li, N., Dai, H., Tan, C., Hu, X.-F., Wei, Z.-Y., Lin, Y., Wei, G.-B., Li, D.-L., Meng, L., Hao, B.-Q., You, H.-L. & Peng, G.-Z. 2021. A neornithischian dinosaur from the Middle Jurassic Xintiangou Formation of Yunyang, Chongqing, China: the earliest record in Asia. Historical Biology, 33, 1089–1102. doi:10.1080/08912963.2019.1679129.

Li, R.-B., Pei, X.-Z., Liu, Z.-Q., Li, Z.-C. & Wang, X.-L. 2010. Basin-mountain coupling relationship of foreland basins between Dabashan and northeastern Sichuan – the evidence from LA-ICP-MS U-Pb dating of the detrital zircons. Acta Geologica Sinica, 84, 1118–1134.

Liao, C.-C., Moore, A., Jin, C., Yang, T.-R., Shibata, M., Jin, F., Wang, B., Jin, D., Guo, Y. & Xu, X. 2021. A possible brachiosaurid (Dinosauria, Sauropoda) from the mid-Cretaceous of northeastern China. PeerJ, 9, e11957. doi:10.7717/peerj.11957

Liao, H.-Y., Shen, Y.-B. & Huang, D.-Y. 2014. Micro-ornamentations on the carapaces of Euestheria jingyuanensis (Crustacea: Spinicaudata) and its biostratigraphic significance. Acta Palaeontologica Sinica, 53, 210–216. doi:10.19800/j.cnki.aps.2014.02.007

Lü, J.-C., Li, S.-X., Ji, Q., Wang, G.-F., Zhang, J.-H. & Dong, Z.-M. 2006. New eusauropod dinosaur from Yuanmou of Yunnan Province. Acta Geologica Sinica, 80, 1–10.

Luo, L., Qi, J.-F., Zhang, M.-Z., Wang, K. & Han, Y.-Z. 2014. Detrital zircon U-Pb ages of Late Triassic–Late Jurassic deposits in the western and northern Sichuan Basin margin: constraints on the foreland basin provenance and tectonic implications. International Journal of Earth Science, 103, 1553–1568. doi:10.1007/s00531-014-1032-7

Maddison, W. P. & Maddison, D. R. 2011. Mesquite: a modular system for evolutionary analysis. Version 2.75. https://www.mesquiteproject.org/

Mahammed, F., Läng, E., Mami, L., Mekahli, L., Benhamou, M., Bouterfa, B., Kacemi, A., Chérief, S-A., Chaouati, H. & Taquet, P. 2005. The ′Giant of Ksour′, a Middle Jurassic sauropod dinosaur from Algeria. Comptes Rendus Palevol, 4, 707–714.

Mannion, P. D. 2010. A revision of the sauropod dinosaur genus ′Bothriospondylus′ with a redescription of the type material of the Middle Jurassic form ′B.

madagascariensis′. Palaeontology, 53, 277296. doi:10.1111/j.1475-4983.2009.00919.x

Mannion, P. D., Upchurch, P., Barnes, R. N. & Mateus, O. 2013. Osteology of the Late Jurassic Portuguese sauropod dinosaur Lusotitan atalaiensis (Macronaria) and the evolutionary history of basal titanosauriforms. Zoological Journal of the Linnean Society, 168, 98–206. doi:10.1111/zoj.12029

Mannion, P. D., Allain, R. & Moine, O. 2017. The earliest known titanosauriform sauropod dinosaur and the evolution of Brachiosauridae. PeerJ, 5, 1–82. doi:10.7717/peerj.3217

Mannion, P. D., Upchurch, P., Schwarz, D. A. & Wings, O. 2019. Taxonomic affinities of the putative titanosaurs from the Late Jurassic Tendaguru Formation of Tanzania: phylogenetic and biogeographic implications for eusauropod dinosaur evolution. Zoological Journal of the Linnean Society, 9, 1–126. doi:10.1093/zoolinnean/zly068

Marsh, O. C. 1878. Principal characters of American Jurassic dinosaurs. American Journal of Science, Series 3, 16, 411–416.

McIntosh, J. S. 1990. Species determination in sauropod dinosaurs. Pp. 53–69 in Carpenter, K. & Currie, P. J. (eds) Dinosaur systematics: approaches and perspective. Cambridge University Press, Cambridge.

McIntosh, J. S., Miles, C. A., Cloward, K. C. & Parker, J. R. 1996a. A new nearly complete skeleton of Camarasaurus. Bulletin of the Gunma Museum of Natural History, 1, 1–87.

McIntosh, J. S., Miller, W. E., Stadtman, K. L. & Gillette, D. D. 1996b. The osteology of Camarasaurus lewisi (Jensen, 1988). Brigham Young University Geology Studies, 41, 73–95.

Mo, J. 2013. Bellusaurus sui. Henan Science and Technology Press, Zhengzhou, 231 pp.

Mocho, P., Royo-Torres, R. & Ortega, F. 2014. Phylogenetic reassessment of Lourinhasaurus alenquerensis, a basal Macronaria (Sauropoda) from the Upper Jurassic of Portugal. Zoological Journal of the Linnean Society, 170, 875–916. doi:10.1111/zoj.12113

Monbaron, M., Russell, D. A. & Taquet, P. 1999. Atlasaurus imelakei n.g., n.sp., a brachiosaurid-like sauropod from the Middle Jurassic of Morocco. Comptes Rendus de l'Académie des Sciences, Series IIA, 329, 519–526.

Moore, A. J., Upchurch, P., Barrett, P. M., Clark, J. M. & Xu, X. 2020. Osteology of Klamelisaurus gobiensis (Dinosauria, Eusauropoda) and the evolutionary history of Middle–Late Jurassic Chinese sauropods. Journal of Systematic Palaeontology, 18, 1299–1393. doi:10.1080/14772019.2020.1759706.

Moser, M., Mathur, U. B., Fürsich, F. T., Pandey, D. K. & Mathur, N. 2006. Oldest camarasauromorph sauropod (Dinosauria) discovered in the Middle Jurassic (Bajocian) of the Khadir Island, Kachchh, western India. Paläontologische Zeitschrift, 80, 34–51.

Nicholl, C. S. C., Mannion, P. D. & Barrett, P. M. 2018. Sauropod dinosaur remains from a new Early Jurassic locality in the Central High Atlas of Morocco. Acta Palaeontologica Polonica, 63, 147–157.

O′Connor, P. M. 2007. Postcranial axial skeleton of Majungasaurus crenatissimus (Theropoda: Abelisauridae) from the Late Cretaceous of Madagascar. Journal of Vertebrate Paleontology, 8, 127–162. doi:10.1671/0272-4634(2007)27[127:TPASOM]2.0.CO;2

Osborn, H. F. & Mook, C. C. 1921. Camarasaurus, Amphicoelias, and other sauropods of Cope. Memoirs of the American Museum of Natural History, New Series, 3, 249–387.

Ouyang, H. 1989. A new sauropod from Dashanpu, Zigong Co., Sichuan Province (Abrosaurus dongpoensis gen. et sp. nov.). Zigong Dinosaur Museum Newsletter, 2, 10–14.

Ouyang, H. & Ye, Y. 2002. Mamenchisaurus youngi. The first mamenchisaurid skeleton with complete skull. Sichuan Publishing House of Science and Technology, Chengdu, 111 pp.

Owen, R. 1842. Report on British fossil reptiles. Part II. Report of the British Association for the Advancement of Science, 11, 60–204.

Peng, G.-Z. 1992. Jurassic ornithopod Agilisaurus louderbachi (Ornithopoda: Fabrosauridae) from Zigong, Sichuan, China. Vertebrata PalAsiatica. 30, 39–53.

Peng, G.-Z., Ye, Y., Gao, Y.-H., Shu, C.-K. & Jiang, S. 2005. Jurassic dinosaur faunas in Zigong. Sichuan People′s Publishing House, Chengdu, 236 pp.

Peng, G.-Z., Qin, G., Ye, Y., Zhu, T.-X., Hao, B. Q., Jiang, S., Tang, W. & Li, S.-J. 2019. Discovery and research of dinosaur fossils in Sichuan. Journal of Sichuan Geology, 39, 215–223.

Pi, L.-Z., Ouyang, H. & Ye, Y. 1996. A new species of sauropod from Zigong, Sichuan: Mamenchisaurus youngi. Pp. 87–91 in Department of Spatial Planning and Regional Economy (ed.) Papers on geosciences from the 30th International Geological Congress. China Economic Publishing House, Beijing.

Pol, D. & Rauhut, O. W. M. 2012. A Middle Jurassic abelisaurid from Patagonia and the early diversification of theropod dinosaurs. Proceedings of the Royal Society B, 279, 3070–3175. doi:10.1098/rspb.2012.0660

Pol, D., Ramezani, J., Gomez, K., Carballido, J. L., Carabajal, A. P., Rauhut, O. W. M., Escapa, I. H. & Cúneo, N. R. 2020. Extinction of herbivorous dinosaurs linked to Early Jurassic global warming event. Proceedings of the Royal Society B, 287, 20202310. doi:10.1098/rspb.2020.2310

Poropat, S. F., Mannion, P. D., Upchurch, P., Hocknull, S. A., Kear, B. P., Kundrát, M., Tischler, T. T., Sloan, T., Sinapius, G. H. K., Elliott, J. A. & Elliott, D. A. 2016. New Australian sauropods shed light on Cretaceous dinosaur palaeobiogeography. Scientific Reports, 6, 34467. doi:10.1038/srep34467

Powell, J. E. 1992. Osteologia de Saltasaurus loricatus loricatus (Sauropoda – Titanosauridae) del Cretácico Superior del noroeste Argentino. Pp. 165–230 in Sanz, J. L. & Buscalioni, A. D. (eds) Los dinosaurios y su entorno biotico: actas del Segundo Curso de Paleontologia in Cuenca. Institutio ′Juan de Valdes′, Cuenca, Argentina.

Qian, T., Liu, S.-F., Wang, Z.-X., Li, W.-P. & Chen, X.-L. 2016. A detrital record of continent-continent collision in the Early–Middle Jurassic foreland sequence in the northern Yangtze foreland basin, South China. Journal of Asian Earth Sciences, 131, 123–137. doi:10.1016/j.jseaes.2016.09.016

Rauhut, O. W. M. 2003. Revision of Amygdalodon patagonicus Cabrera, 1947 (Dinosauria, Sauropoda). Fossil Record, 6, 173–181.

Rauhut, O. W. M. & Lopez-Arbarello, A. 2009. Considerations on the age of the Tiouaren Formation (Iullemmeden Basin, Niger, Africa): implications for Gondwanan Mesozoic terrestrial vertebrate faunas. Palaeogeography, Palaeoclimatology, Palaeoecology, 271, 259–267. doi:10.1016/j.palaeo.2008.10.019

Raveloson, M. L. T., Clark, N. D. L. & Rasoamiaramana, A. H. 2019. New information on the Madagascan Middle Jurassic sauropod Lapparentosaurus madagascariensis. Geosciences, 9, 498. doi:10.3390/geosciences9120498

Remes, K. 2006. Revision of the Tendaguru sauropod Tornieria africana (Fraas) and its relevance for sauropod paleobiogeography. Journal of Vertebrate Paleontology, 26, 651–669. doi:10.1671/0272-634(2006)26[651:ROTTSD]2.0.CO;2

Remes, K., Ortega, F., Fierro, I., Joger, U., Kosma, R. & Ferrer, J. M. M. 2009. A new basal sauropod dinosaur from the Middle Jurassic of Niger and the early evolution of Sauropoda. PLoS ONE, 4, e6924. doi:10.1371/journal.pone.0006924

Ren, X.-X., Huang, J.-D. & You, H.-L. 2020. The second mamenchisaurid dinosaur from the Middle Jurassic of Eastern China. Historical Biology, 32, 602–610. doi:10.1080/08912963.2018.1515935

Ren, X.-X., Sekiya, Y., Wang, T., Yang, Z.-W. & You, H.-L. 2021. A revision of the referred specimen of Chuanjiesaurus anaensis Fang et al., 2000: a new early branching mamenchisaurid sauropod from the Middle Jurassic of China, Historical Biology, 33, 1872–1887. doi:10.1080/08912963.2020.1747450

Rich, T. H., Vickers-Rich, P., Gimenez, O., Cúneo, R., Puerta, P. & Vacca, R. 1999. A new sauropod dinosaur from Chubut Province, Argentina. National Science Museum Monographs, 15, 61–84.

Royo-Torres, R., Upchurch, P., Mannion, P. D., Mas, R., Cobos, A., Gascó, F., Alcalá, L. & Sanz, J. L. 2014. The anatomy, phylogenetic relationships, and stratigraphic position of the Tithonian–Berriasian Spanish sauropod dinosaur Aragosaurus ischiaticus. Zoological Journal of the Linnean Society, 171, 623–655. doi:10.1111/zoj.12144

Russell, D. A. 1993. The role of Central Asia in dinosaurian biogeography. Canadian Journal of Earth Sciences, 30, 2002–2012.

Salgado, L. & Bonaparte, J. F. 1991. A new dicraeosaurid sauropod, Amargasaurus cazaui gen. et sp. nov., from the La Amarga Formation, Neocomian of Neuquen Province, Argentina. Ameghiniana, 28, 333–346.

Salgado, L., Coria, R. A. & Calvo, J. O. 1997. Evolution of titanosaurid sauropods. I: Phylogenetic analysis based on the postcranial evidence. Ameghiniana, 34, 3–32.

Salgado, L., Carvalho, I. S. & Garrido, A. C. 2006. Zapalasaurus bonapartei, a new sauropod dinosaur from La Amarga Formation (Lower Cretaceous), northwestern Patagonia, Neuquén Province, Argentina. Geobios, 39, 695–707. doi:10.1016/j.geobios.2005.06.001

Sánchez-Hernández, B. 2005. Galveosaurus herreroi, a new sauropod dinosaur from Villar del Arzobispo Formation (Tithonian-Berriasian) of Spain. Zootaxa, 1034, 1–20.

Scotese, C. R. 2014. Atlas of Jurassic Paleogeographic Maps, PALEOMAP Atlas for ArcGIS, Volume 4, The Jurassic and Triassic, Maps 32–42, Mollweide Projection, PALEOMAP Project, Evanston, IL.

Seeley, H. G. 1887. On the classification of the fossil animals commonly named Dinosauria. Proceedings of the Royal Society of London, 43, 165–171.

Sekiya, T. 2011. Re-examination of Chuanjiesaurus anaensis (Dinosauria: Sauropoda) from the Middle Jurassic Chuanjie Formation, Lufeng County, Yunnan Province, southwest China. Memoir of the Fukui Prefectural Dinosaur Museum, 10, 1–54.

Sereno, P. C., Beck, A. L., Dutheil, D. A., Larsson, H. C. E., Lyon, G. H., Moussa, B., Sadleir, R. W., Sidor, C. A., Varricchio, D. J., Wilson, G. P. & Wilson, J. A. 1999. Cretaceous sauropods from the Sahara and the uneven rate of skeletal evolution across dinosaurs. Science, 286, 1342–1347.

Sereno, P. C., Wilson, J. A., Witmer, L. M., Whitlock, J. A., Maga, A., Lde, O. & Rowe, T.A. 2007. Structural extremes in a Cretaceous dinosaur. PLoS ONE, 11, e1230. doi:10.1371/journal.pone.0001230

Shen, Y.-B. 2003. Conchostracan faunas of Jurassic. Pp 50–58. in Deng, S.-H., Yao, Y. M. & Ye, D.-Q. (eds), Jurassic system in the north of China, Volume I, stratum introduction. Petroleum Industry Press, Beijing.

Shen, Y.-B. 2004. Conchostraca. Pp 54–55 in Yumen Oilfield Company, PetroChina Co. Ltd. & Nanjing Institute of Geology and Palaeontology and Chinese Academy of Sciences (eds), Cretaceous and Jurassic stratigraphy and environment of the Chaoshui and Yabulai basins, NW China. University of Science and Technology of China Press, Beijing.

Shen, Y.-B. 2010. Conchostraca fauna. Pp 179–184 in Deng, S.-H. (ed.), The Jurassic system of northern Xinjiang, China. Contributions to the 8th international congress on the Jurassic system. University of Science and Technology of China Press, Beijing.

Silva Junior, J. C. G., Marinho, T. S., Martinelli, A. G. & Langer, M. C. 2019. Osteology and systematics of Uberabatitan ribeiroi (Dinosauria; Sauropoda): a Late Cretaceous titanosaur from Minas Gerais, Brazil. Zootaxa, 4577, 401–438. doi:10.11646/zootaxa.4577.3.1

Suteethorn, S., Le Loeuff, J., Buffetaut, E., Suteethorn, V. & Wongko, K. 2013. First evidence of a mamenchisaurid dinosaur from the Upper Jurassic–Lower Cretaceous Phu Kradung Formation of Thailand. Acta Palaeontologica Polonica, 58, 459–469. doi:10.4202/app.2009.0155

Tan, C., Xiao, M., Dai, H., Hu, X.-F., Li, N., Ma, Q.-Y., Wei, Z.-Y., Yu, H.-D, Xiong, C., Peng, G.-Z., Jiang, S., Ren, X.-X. & You, H.-L. 2021. A new species of Omeisaurus (Dinosauria: Sauropoda) from the Middle Jurassic of Yunyang, Chongqing, China. Historical Biology, 33, 1817–1829. doi:10.1080/08912963.2020.1743286

Tang, F., Jing, X., Kang, X. & Zhang, G. 2001. A complete sauropod from Jingyuan, Sichuan: Omeisaurus maoianus. China Ocean Press, Beijing, 128 pp.

Taylor, M. P. 2022. Almost all known sauropod necks are incomplete and distorted. PeerJ, 10, e12810. doi:10.7717/peerj.12810

Taylor, M. P. & Wedel, M. J. 2013. Why sauropods had long necks and why giraffes have short necks. PeerJ, 1, e36. doi:10.7717/peerj.36

Tschopp, E., Mateus, O. & Benson, R. B. J. 2015. A specimen-level phylogenetic analysis and taxonomic revision of Diplodocidae (Dinosauria, Sauropoda). PeerJ, 3, e857. doi:10.7717/peerj.857

Upchurch, P. 1998. The phylogenetic relationships of sauropod dinosaurs. Zoological Journal of the Linnean Society, 124, 43–103.

Upchurch, P. & Barrett, P. M. 2000. The evolution of sauropod feeding. Pp. 79–122 in Sues, H.-D. (eds) Evolution of herbivory in terrestrial vertebrates. Cambridge University Press, Cambridge.

Upchurch, P., Hunn, C. A. & Norman, D. B. 2002. An analysis of dinosaurian biogeography: evidence for the existence of vicariance and dispersal patterns caused by geological events. Proceedings of the Royal Society of London. Series B, 269, 613–621. doi:10.1098/rspb.2001.1921

Upchurch, P. & Martin, J. 2002. The Rutland Cetiosaurus: the anatomy and relationships of a Middle Jurassic British sauropod dinosaur. Palaeontology, 45, 1049–1074. doi:10.1111/1475-4983.00275

Upchurch, P. & Martin, J. 2003. The anatomy and taxonomy of Cetiosaurus (Saurischia, Sauropoda) from the Middle Jurassic of England. Journal of Vertebrate Paleontology, 23, 208–231.

Upchurch, P., Tomida, Y. & Barrett, P. M. 2004a. A new specimen of Apatosaurus ajax (Sauropoda: Diplodocidae) from the Morrison Formation (Upper Jurassic) of Wyoming, USA. National Science Museum Monographs, 26, 1–108.

Upchurch, P., Barrett, P. M. & Dodson, P. 2004b. Sauropoda. Pp. 259–322 in Weishampel, D. B., Dodson, P. & Osmolska, H. (eds) The Dinosauria. Second edition. University of California Press, Berkeley.

Upchurch, P., Mannion, P. D. & Taylor, M. P. 2015. The anatomy and phylogenetic relationships of 'Pelorosaurus' becklesii (Neosauropoda, Macronaria) from the Early Cretaceous of England. PLoS ONE, 10, e0125819. doi:10.1371/journal.pone.0125819

Upchurch, P., Mannion, P. D., Xu, X. & Barrett, P. M. 2021. Reassessment of the Late Jurassic eusauropod dinosaur Hudiesaurus sinojapanorum Dong, 1997, from the Turpan Basin, China, and the evolution of hyper-robust antebrachia in sauropods. Journal of Vertebrate Paleontology, 41, e1994414. doi:10.1080/02724634.2021.1994414

Vidal, D., Mocho, P., Aberasturi, A., Sanz, J. L. & Ortega, F. 2020. High browsing skeletal adaptations in Spinophorosaurus reveal an evolutionary innovation in sauropod dinosaurs. Scientific Reports, 10, 6638. doi:10.1038/s41598-020-63439-0.

Wang, J., Ye, Y., Pei, R., Tian, Y.-M., Feng, C.-Q., Zheng, D.-R. & Chang, S.-C. 2018. Age of Jurassic basal sauropods in Sichuan, China: a reappraisal of basal sauropod evolution. Geological Society of America Bulletin,130, 1493–1500. doi:10.1130/B31910.1

Wedel, M. J. 2005. Postcranial skeletal pneumaticity in sauropods and its implication for mass estimates. Pp. 201–228 in Wilson, J. A. & Curry-Rogers, K. (eds), The sauropods: evolution and paleobiology. University of California Press, Berkeley.

Wedel, M. J., Cifelli, R. L. & Sanders, R. K. 2000. Osteology, paleobiology, and relationships of the sauropod dinosaur Sauroposeidon. Acta Palaeontologica Polonica, 45, 343–388.

Wilson, J. A. 1999. A nomenclature for vertebral laminae in sauropods and other saurischian dinosaurs. Journal of Vertebrate Paleontology, 19, 639–653.

Wilson, J. A. 2002. Sauropod dinosaur phylogeny: critique and cladistic analysis. Zoological Journal of the Linnean Society, 136, 217–276.

Wilson, J. A. 2012. New vertebral laminae and patterns of serial variation in vertebral laminae of sauropod dinosaurs. Contributions from the Museum of Paleontology, University of Michigan, 32, 91–110.

Wilson, J. A. & Sereno, P. C. 1998. Early evolution and higher-level phylogeny of sauropod dinosaurs. Memoirs of the Society of Vertebrate Paleontology, 5, 1–68.

Wilson, J. A. & Upchurch, P. 2009. Redescription and reassessment of the phylogenetic affinities of Euhelopus zdanskyi zdanskyi (Dinosauria: Sauropoda) from the Early Cretaceous of China. Journal of Systematic Palaeontology, 7, 199–239. doi:10.1017/S1477201908002691

Wilson, J. A., D′Emic, M. D., Ikejirl, T., Moacdieh, E. M. & Whitlock, J. A. 2011. A nomenclature for vertebral fossae in sauropods and other saurischian dinosaurs. PLoS ONE, 6, e17114. doi:10.1371/journal.pone.0017114

Wilson, J. A. & Allain, R. 2015. Osteology of Rebbachisaurus garasbae Lavocat, 1954, a diplodocoid (Dinosauria, Sauropoda) from the early Late Cretaceous–aged Kem Kem beds of southeastern Morocco. Journal of Vertebrate Paleontology, 35, e1000701. doi:10.1080/02724634.2014.1000701

Woodruff, D. C. & Fowler, D. W. 2012. Ontogenetic influence on neural spine bifurcation in Diplodocoidea (Dinosauria: Sauropoda): a critical phylogenetic character. Journal of Morphology, 273, 754–764. doi:10.1002/jmor.20021

Woodruff, D. C. & Foster, J. R. 2017. The first specimen of Camarasaurus (Dinosauria: Sauropoda) from Montana: the northernmost occurrence of the genus. PLoS ONE, 12, e177423. doi:10.1371/journal.pone.0177423

Wu, W., Zhou, C., Wings, O., Sekiya, T. & Dong, Z. 2013. A new gigantic sauropod dinosaur from the Middle Jurassic of Shanshan, Xinjiang. Global Geology, 32, 437–446.

Xing, L.-D., Miyashita, T., Currie, P. J., You, H.-L., Zhang, J.-P. & Dong, Z.-M. 2015a. A new basal eusauropod from the Middle Jurassic of Yunnan, China, and faunal compositions and transitions of Asian sauropodomorph dinosaurs. Acta Palaeontologica Polonica, 60, 145–154.

Xing, L.-D., Miyashita, T., Zhang, J.-P., Li, D.-Q., Ye, Y., Sekiya, T., Wang, F.-P. & Currie, P. J. 2015b. A new sauropod dinosaur from the Late Jurassic of China and the diversity, distribution, and relationships of mamenchisaurids. Journal of Vertebrate Paleontology, 35, e889701. doi:10.1080/02724634.2014.889701

Xu, X., Upchurch, P., Mannion, P. D., Barrett, P. M., Regalado-Fernandez, O. R., Mo, J.-Y., Ma, J.-F. & Liu, H.-G. 2018. A new Middle Jurassic diplodocoid suggests an earlier dispersal and diversification of sauropod dinosaurs. Nature Communications, 9, 2700. doi:10.1038/s41467-018-05128-1

Yang, C.-Y. 2003. The research and quantitative phylogenetic analysis of a new sauropod from the Lower Jurassic of Huili Sichuan, China. Unpublished Master′s thesis, Chengdu University of Technology, 92 pp.

Yang, X.-H. 1987. Jurassic plants from the Lower Shaximiao Formation of Rongxian, Sichuan. Bulletin Chengdu Institute of Geology and Mineral Resource, Chinese Academy of Geological Sciences, 8, 1–13.

Ye, Y., Gao, Y.-H. & Jiang, S. 2005. A new genus of sauropod from Zigong, Sichuan. Vertebrata PalAsiatica, 43, 175–181.

You, S.-S., Li, Z.-J. & Li, Y.-B. 2019. The stratigraphical characteristics and sedimentary environment of dinosaurs in Lingwu, Ningxia. Acta Geolgica Sichuan, 39, 31–35.

Young, C.-C. 1937. A new dinosaurian from Sinkiang. Palaeontologia Sinica (series C), 2, 1–25.

Young, C.-C. 1939. On a new Sauropoda, with notes on other fragmentary reptiles from Szechuan. Bulletin of the Geological Society of China, 19, 279–316.

Young, C.-C. 1958. New sauropods from China. Vertebrata PalAsiatica, 2, 1–27.

Young, C.-C. & Zhao, X.-J. 1972. Mamenchisaurus hochuanensis, sp. nov. Institute of Vertebrate Paleontology and Paleoanthropology Monographs (Series A), 8, 1–30.

Zhang, W.-T., Cheng, P.-J. & Shen, Y.-B. 1976. Fossil conchostracans of China. Science Press, Beijing, 325 pp.

Zhang, X.-Q., Li, D.-Q., Xie, Y. & You, H.-L. 2020. Redescription of the cervical vertebrae of the mamenchisaurid sauropod Xinjiangtitan shanshanesis Wu et al. 2013. Historical Biology, 32, 803–822. doi:10.1080/08912963.2018.1539970

Zhang, Y.-H. 1988. Shunosaurus lii. The Middle Jurassic Dinosaur Fauna from Dashanpu, Zigong, Sichuan: Sauropod Dinosaurs, Volume 3. Sichuan Publishing House of Science and Technology, Chengdu, 89 pp.

Zhao, X.-J. 1993. A new Middle Jurassic sauropod subfamily (Klamelisaurinae subfam. nov.) from Xinjiang Autonomous Region, China. Vertebrata PalAsiatica, 31, 132–138.

Zhou, S.-W. 1984. Stegosaurs. The Middle Jurassic dinosaurian fauna from Dashanpu, Zigong, Sichuan. Volume II. Sichuan Scientific and Technological Publishing House, Chengdu, 52 pp.

Zhou, Y., Dai, H., Yu, H., Ma, Q., Tan, C., Li, N., Lin, Y. & Li, D. 2021. Zircon geochronology of the new dinosaur fauna in the Middle Jurassic lower Shaximiao Formation in Chongqing, SW China. Palaeogeography, Palaeoclimatology, Palaeoecology, 592, 110894. doi:10.1016/j.palaeo.2022.110894

Associate Editor: Paul Barrett